Technische Universiteit
Eindhoven
University of Technology

NMR/MRI for imaging plastic in a hamburger

Dr.ir. Leo Pel
Ing. Jef Noijen

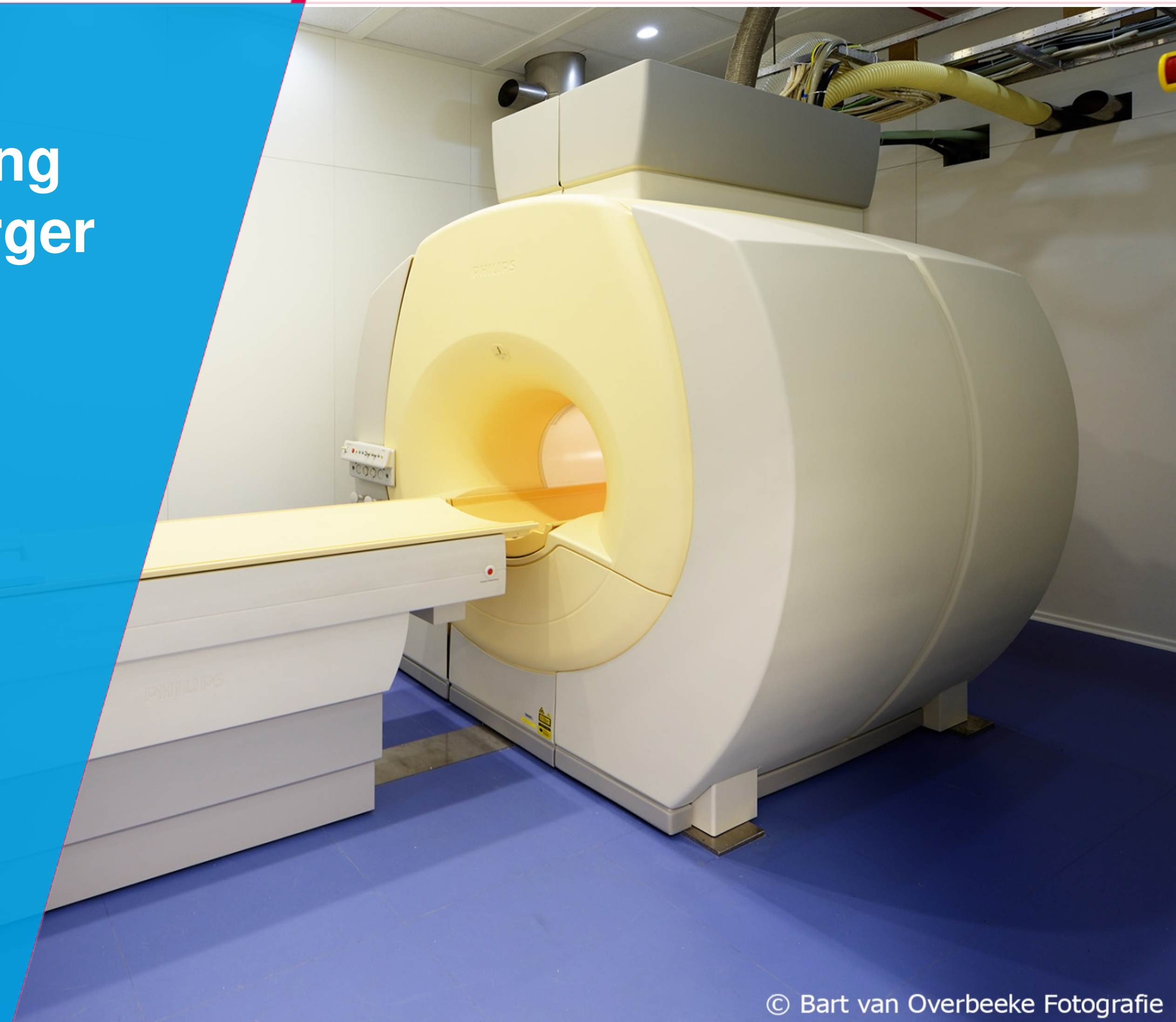

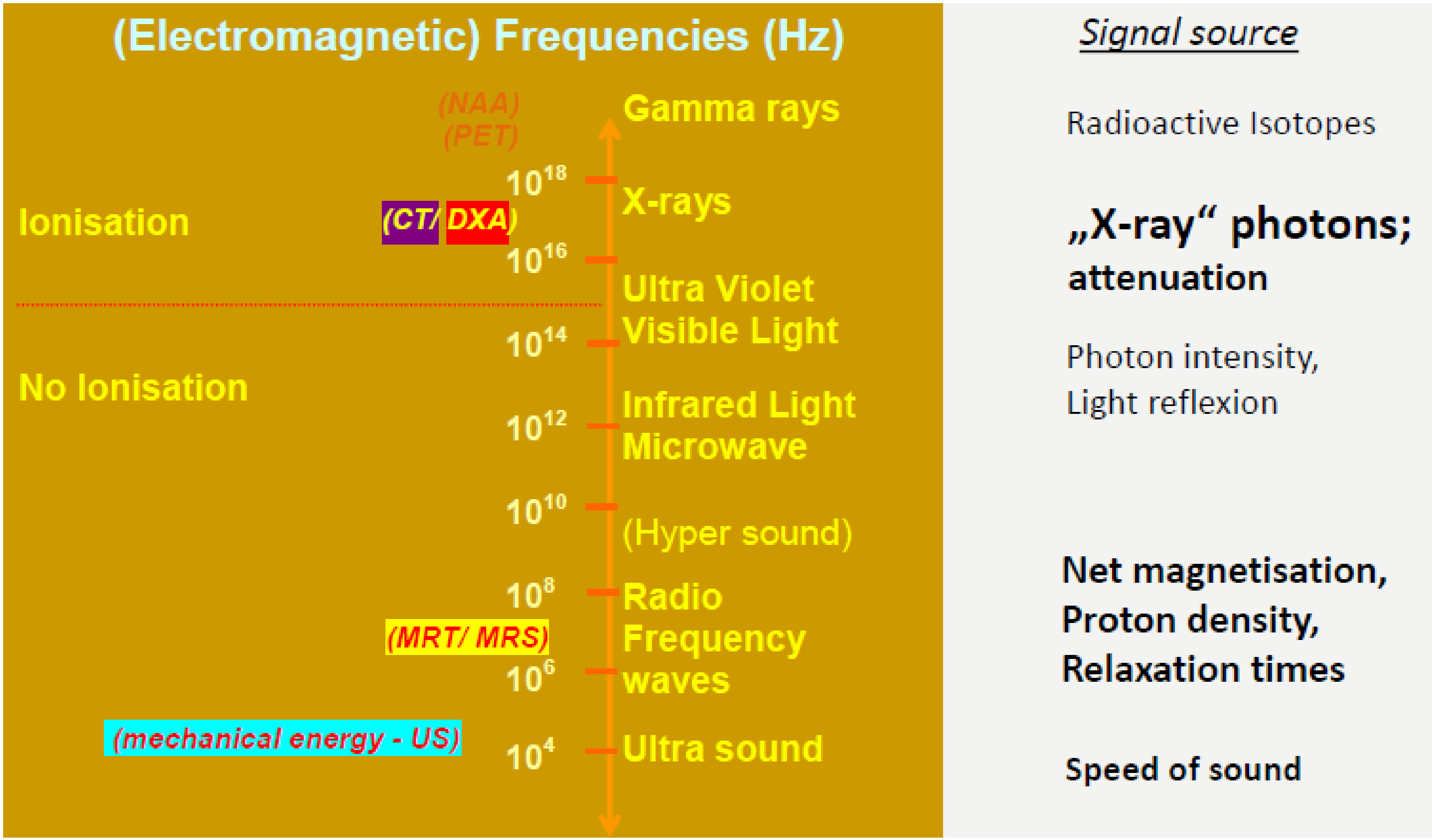
(Electromagnetic) Frequencies (Hz)
(NAA)
(PET)
Gamma rays
10^{18}
X-rays
Ionisation
(CT/ DXA)
10^{16}
Ultra Violet
Visible Light
10^{14}
No Ionisation
Infrared Light
10^{12}
Microwave
10^{10}
(Hyper sound)
10^{8}
Radio Frequency waves
(MRT/ MRS)
10^{6}
(mechanical energy - US)
10^{4}
Ultra sound
Signal source
Radioactive Isotopes
„X-ray“ photons; attenuation
Photon intensity, Light reflexion
Net magnetisation, Proton density, Relaxation times
Speed of sound

Measurement moisture/plastic ?

Example x-ray images


PHILIPS

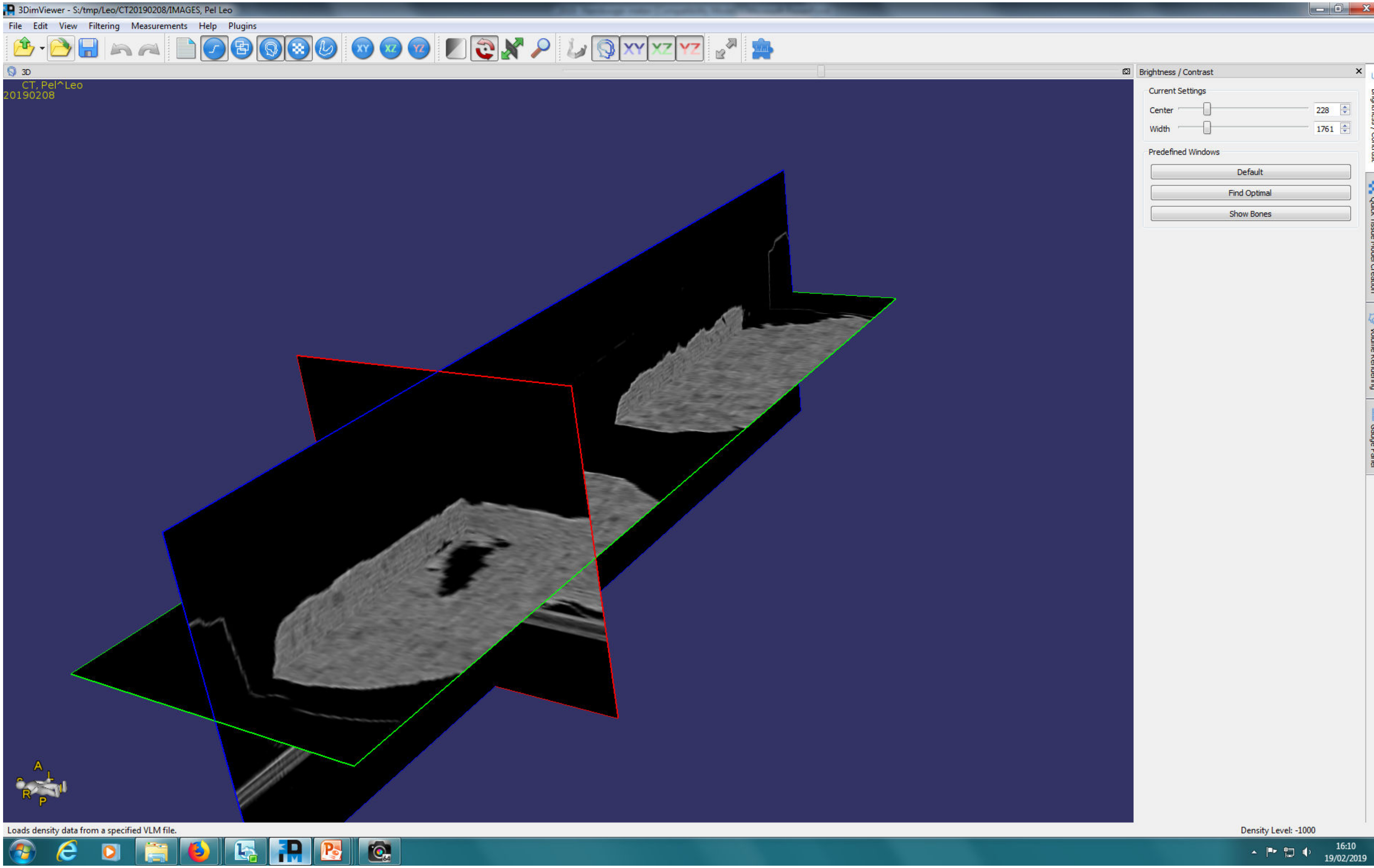

No direct measurements > contrast due to not seeing plastic

- problem air voids

NMR/MRI

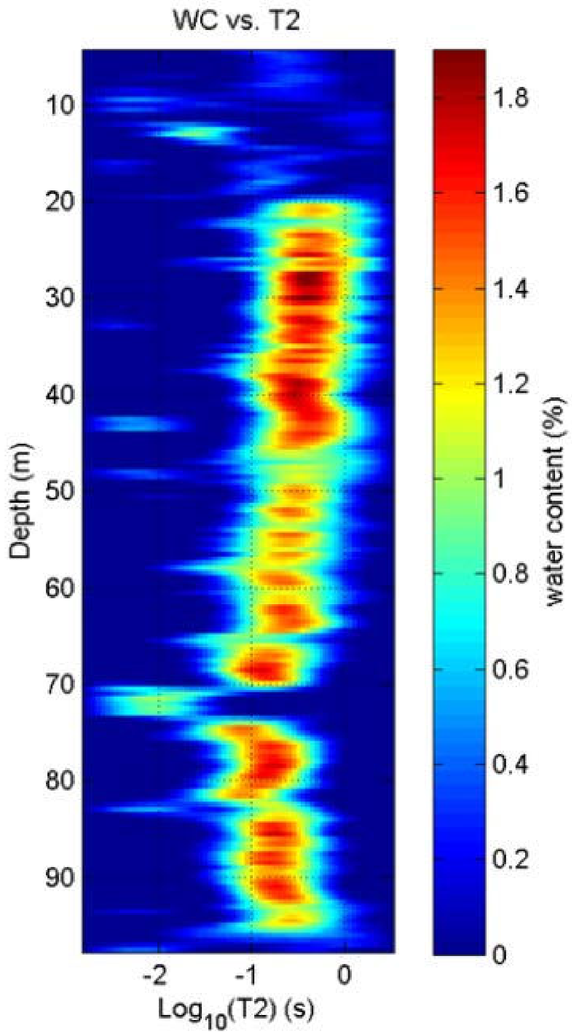

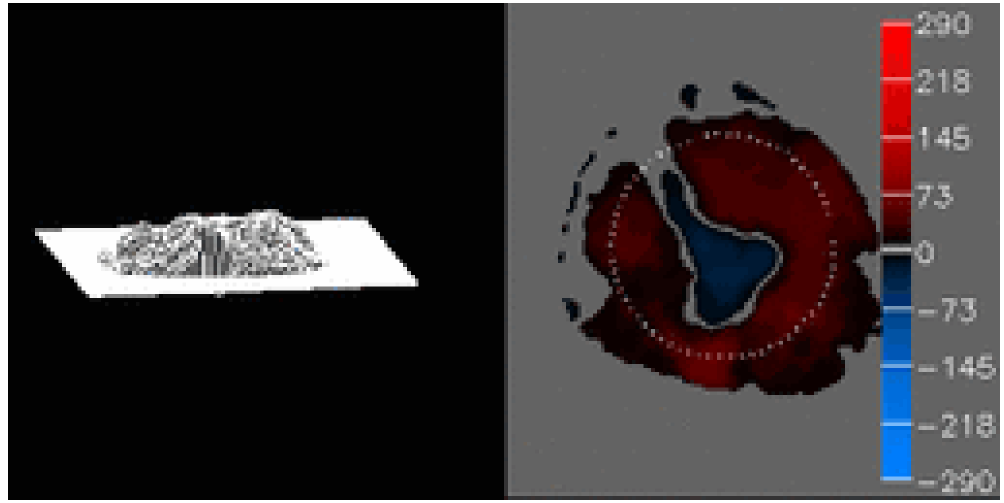

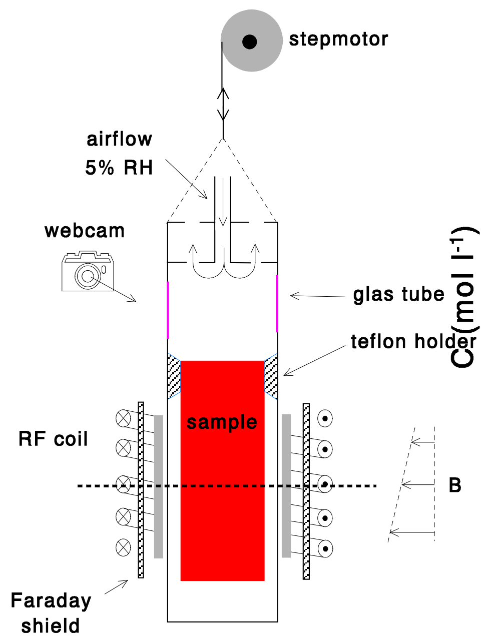

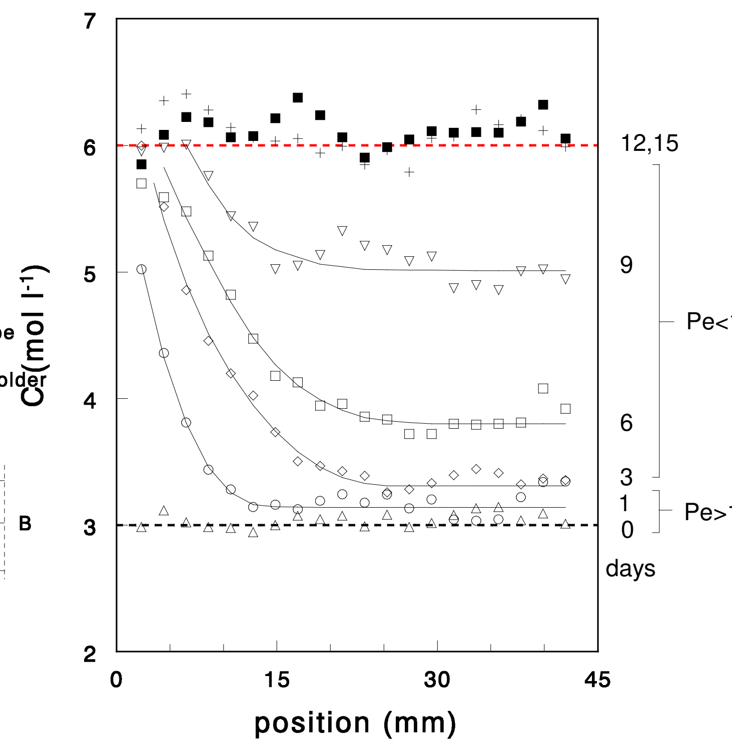

One of the *MOST* Routinely used Analytical Techniques

Introduction

NMR signal

Spectroscopy

T1-T2 relaxation

Diffusion

Imaging

Plastics

Conclusions

Introduction

NMR signal

Spectroscopy

T1-T2 relaxation

Diffusion

Imaging

Plastics

Conclusions

NMR - timeline

1922
Stern-Gerlach
Electron spin

1952 Nobel prize
Felix Bloch, Edward Purcell
NMR in solids

1985
Wüthrich .
Protein stucture

1902
Pieter Zeeman
Radiation in a magnetic field

1937
Isidor Rabi
Nuclear magnetic resonance

1973
Paul Lauterbur, Peter Mansfield
NMR imaging

1936
Linus Pauling
Deoxyhemoglobin electronic structure

NMR History

First NMR Spectra on Water

^1H NMR spectra of water

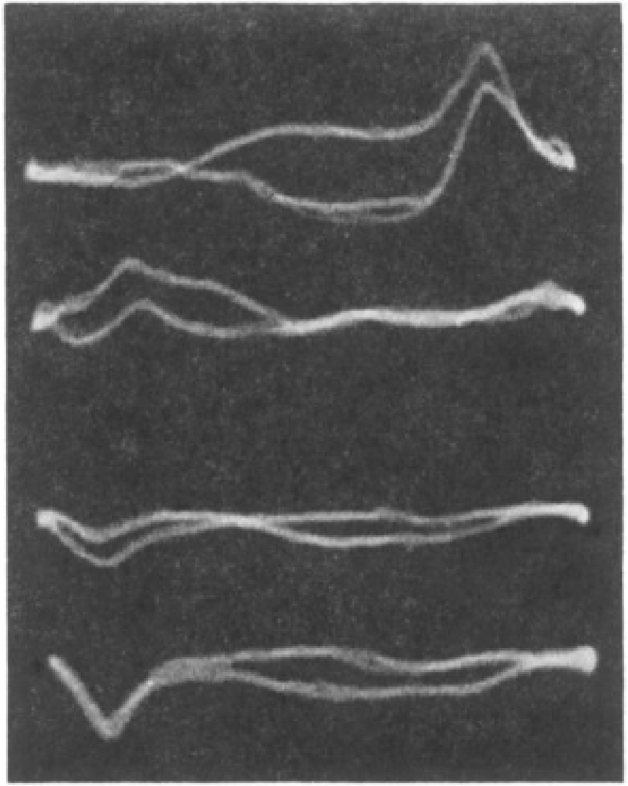

FIG. 10. Photographic record of the proton signal in water. The four traces from top to bottom correspond to the times t_1, t_2, t_3, t_4 of Fig. 9. In the text they are referred to as a, b, c, d, respectively.

Bloch, F.; Hansen, W. W.; Packard, M. The nuclear induction experiment. Physical Review (1946), 70 474-85.

NMR History

First Observation of the Chemical Shift

^{1}H NMR spectra ethanol

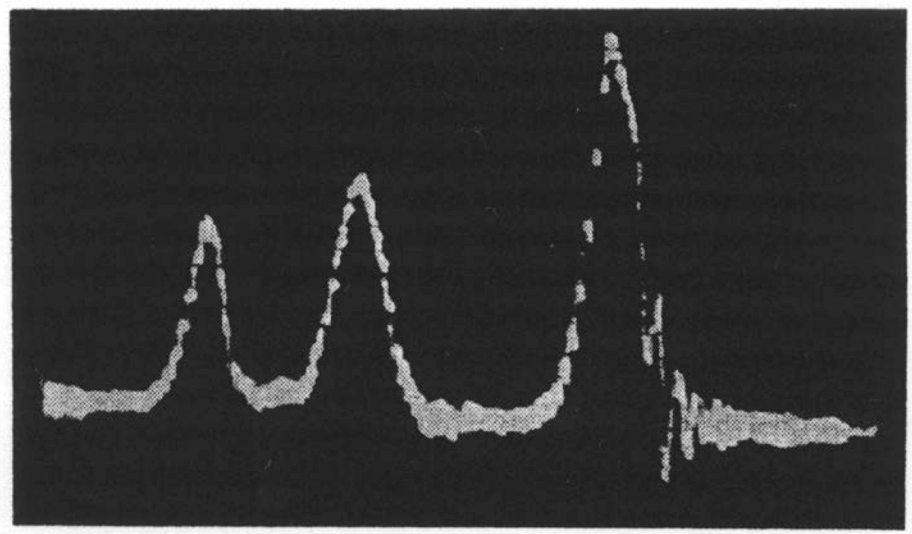

Modern ethanol spectra

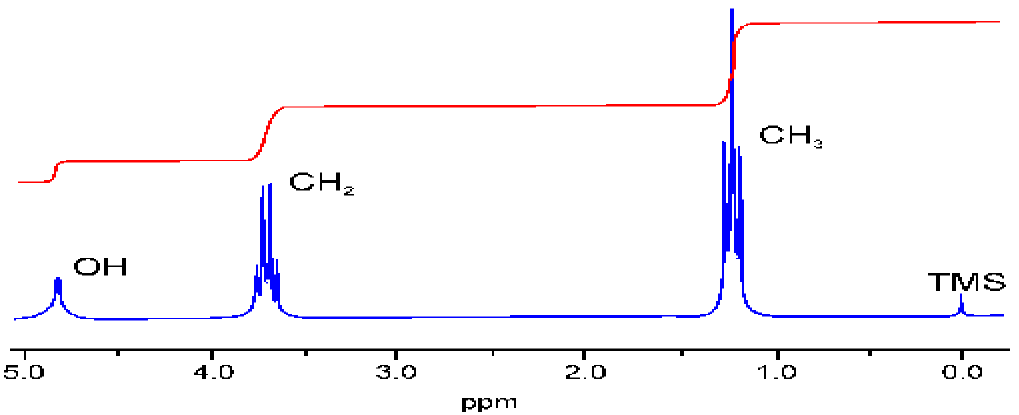

Arnold, J.T., S.S. Dharmatti, and M.E. Packard, J. Chem. Phys., 1951. **19**: p. 507.

Nobel prizes

1944 *Physics* Rabi (Columbia)

"for his resonance method for recording the magnetic properties of atomic nuclei"

1991 *Chemistry* Ernst (ETH)

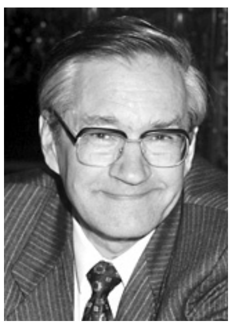

"for his contributions to the development of the methodology of high resolution nuclear magnetic resonance (NMR) spectroscopy"

2002 *Chemistry* Wüthrich (ETH)

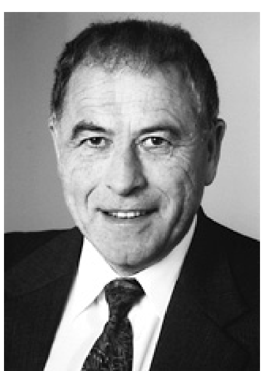

"for his development of nuclear magnetic resonance spectroscopy for determining the three-dimensional structure of biological macromolecules in solution"

1952 *Physics* Bloch (Stanford), Purcell (Harvard)

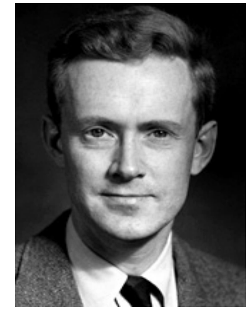

"for their development of new methods for nuclear magnetic precision measurements and discoveries in connection therewith"

2003 *Medicine* Lauterbur (University of Illinois in Urbana), Mansfield (University of Nottingham)

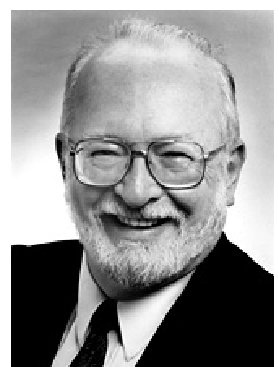

"for their discoveries concerning magnetic resonance imaging"

History of MRI

1971: Raymond Damadian uses NMR for tumor detection
1972: Lauterbur suggests NMR could be used to form images using gradients
1977: Peter Mansfield proposes echo-planar imaging (EPI) to acquire images faster
1977: first MRI scanner (0.05 T) created by Damadian's FONAR corporation, named "Indomitable"

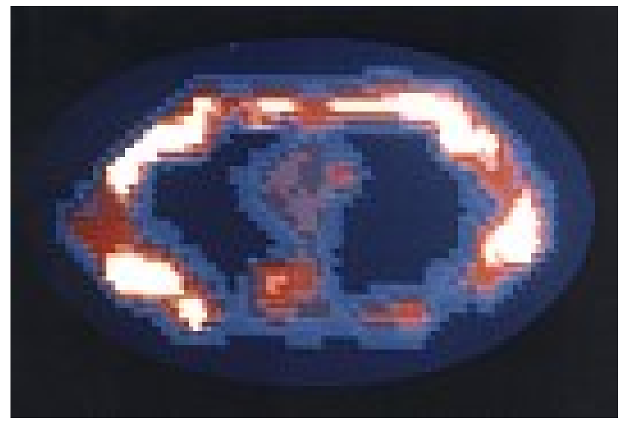

1977: First MR image of human body
- Didn't use EPI
- Each voxel took 2 min; 106 voxels
- 4 hours to get one slice

Introduction

NMR signal

Spectroscopy

T1-T2 relaxation

Diffusion

Imaging

Plastics

Conclusions

The Basics of MRI

Joseph P. Hornak, Ph.D.

Language: English, Italiano, Spanish, Russian

XVII

Chapter 6 to 8

Nuclear Magnetic Resonance

Nuclear spin

$$\mu = \gamma I \hbar$$

μ - magnetic moment

γ - gyromagnetic ratio

I - spin quantum number

$\hbar$ - Planck's constant

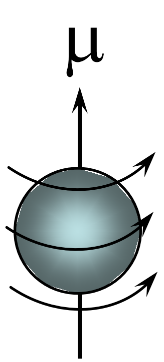

I is a property of the nucleus

Mass #	Atomic #	I
Odd	Even or odd	1/2, 3/2, 5/2,…
Even	Even	0
Even	Odd	1, 2, 3

NMR Periodic Table

NMR "active" Nuclear Spin (I) = ½:

^{1}H, ^{13}C, ^{15}N, ^{19}F, ^{31}P

biological and chemical relevance

Odd atomic mass

I = +½ & -½

NMR "inactive" Nuclear Spin (I) = 0:

^{12}C, ^{16}O

Even atomic mass & number

Quadrupole Nuclei Nuclear Spin (I) > ½:

^{14}N, ^{2}H, ^{10}B

Even atomic mass & odd number

I = +1, 0 & -1

Element	*Atomic mass*	*Spin I*	*Natural abundance (%)*	*Receptivity (^{13}C = 1.00)*	*Quadrupole moment (10^{30} m^2)*	*Resonant frequency (MHz) at 2.348 T*
Hydrogen	1	1/2	99.985	5670	None	100.00
Deuterium	2	1	0.015	0.0082	0.287	15.35
Tritium	3	1/2	Radioactive	–	None	106.66
Helium	3	1/2	0.00014	0.0035	None	76.18
Lithium	6	1	7.42	3.58	–0.064	14.72
Lithium	7	3/2	92.58	1540	–3.7	38.87
Beryllium	9	3/2	100	78.8	5.3	15.06
Boron	10	3	19.58	22.1	7.4	10.75
Boron	11	3/2	80.42	754	4.1	32.08
Carbon	13	1/2	1.108	1.00	None	25.15
Nitrogen	14	1	99.63	5.70	1.67	7.23
Nitrogen	15	1/2	0.37	0.022	None	10.14
Oxygen	17	5/2	0.037	0.061	–2.6	13.56
Fluorine	19	1/2	100	4730	None	94.09
Neon	21	3/2	0.257	0.0036	9	7.90
Sodium	23	3/2	100	524	10	26.43
Magnesium	25	5/2	10.13	1.54	22	6.13
Aluminium	27	5/2	100	1170	14	26.08
Silicon	29	1/2	4.7	2.1	None	19.87
Phosphorus	31	1/2	100	377	None	40.48
Sulfur	33	3/2	0.76	0.098	–6.4	7.67
Chlorine	35(37)	3/2	75.53	20.2	–8.2	9.81
Potassium	39	3/2	93.1	2.69	5.5	4.67
Calcium	43	7/2	0.145	0.053	–5	6.74
Scandium	45	7/2	100	1720	–22	24.33
Titanium	49(47)	7/2	5.51	1.18	24	5.64
Vanadium	51(50)	7/2	99.76	2170	–5.2	26.35
Chromium	53	3/2	9.55	0.49	–15	5.64
Manganese	55	5/2	100	1014	40	24.84
Iron	57	1/2	2.19	0.00425	None	3.24
Cobalt	59	7/2	100	1560	42	23.73
Nickel	61	3/2	1.19	0.24	16	8.93
Copper	63(65)	3/2	69.09	368	–22	26.51
Zinc	67	5/2	4.11	0.67	15	6.25
Gallium	71(69)	3/2	39.6	322	11	30.58
Germanium	73	9/2	7.76	0.62	–17	3.48
Arsenic	75	3/2	100	144	29	17.18
Selenium	77	1/2	7.58	3.02	None	19.07
Bromine	81(79)	3/2	49.46	279	27	27.10
Krypton	83	9/2	11.55	1.24	27	3.86
Rubidium	87(85)	3/2	27.85	280	13	32.84
Strontium	87	9/2	7.02	1.08	16	4.35
Yttrium	89	1/2	100	0.676	None	4.92
Zirconium	91	5/2	11.23	6.05	–21	9.34
Niobium	93	9/2	100	2770	–32	24.55
Molybdenum	95(97)	5/2	15.72	2.92	–1.5	6.55
Technetium	99	9/2	Radioactive	–	–0.13	22.51
Ruthenium	99(101)	5/2	12.72	0.815	7.6	4.61
Rhodium	103	1/2	100	0.18	None	3.16
Palladium	105	5/2	22.23	1.43	65	4.58
Silver	109(107)	1/2	48.18	0.28	None	4.65
Cadmium	113(111)	1/2	12.26	7.69	None	22.18

Apply an external magnetic field

(i.e., put your sample in the magnet)

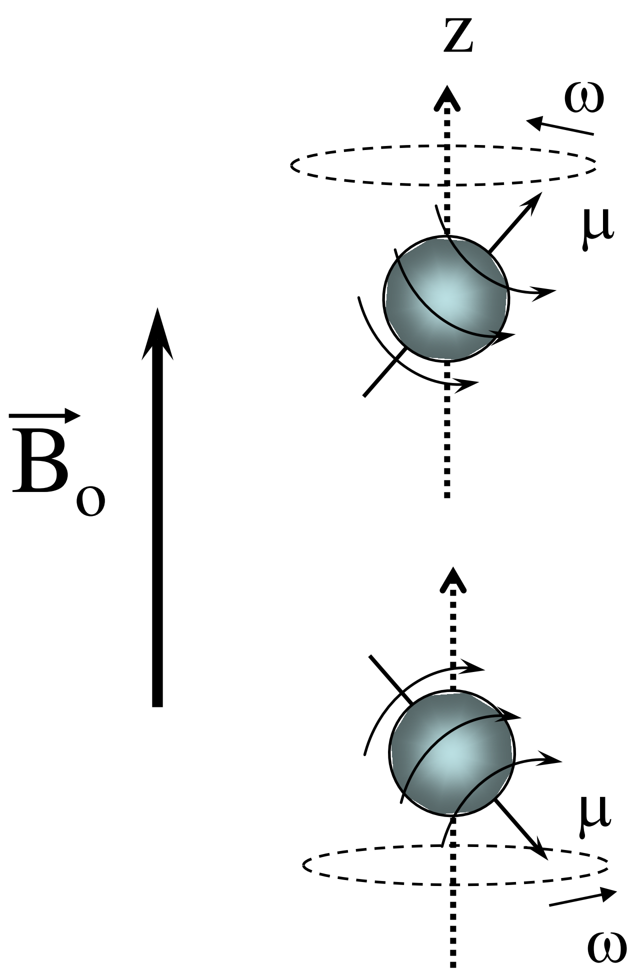

$$\omega = \gamma B_o = \nu/2\pi$$

ω - resonance frequency in radians per second, also called Larmor frequency

ν - resonance frequency in cycles per second, Hz

γ - gyromagnetic ratio

B_o - external magnetic field (the magnet)

Spin 1/2 nuclei will have two orientations in a magnetic field +1/2 and -1/2.

Net magnetic moment

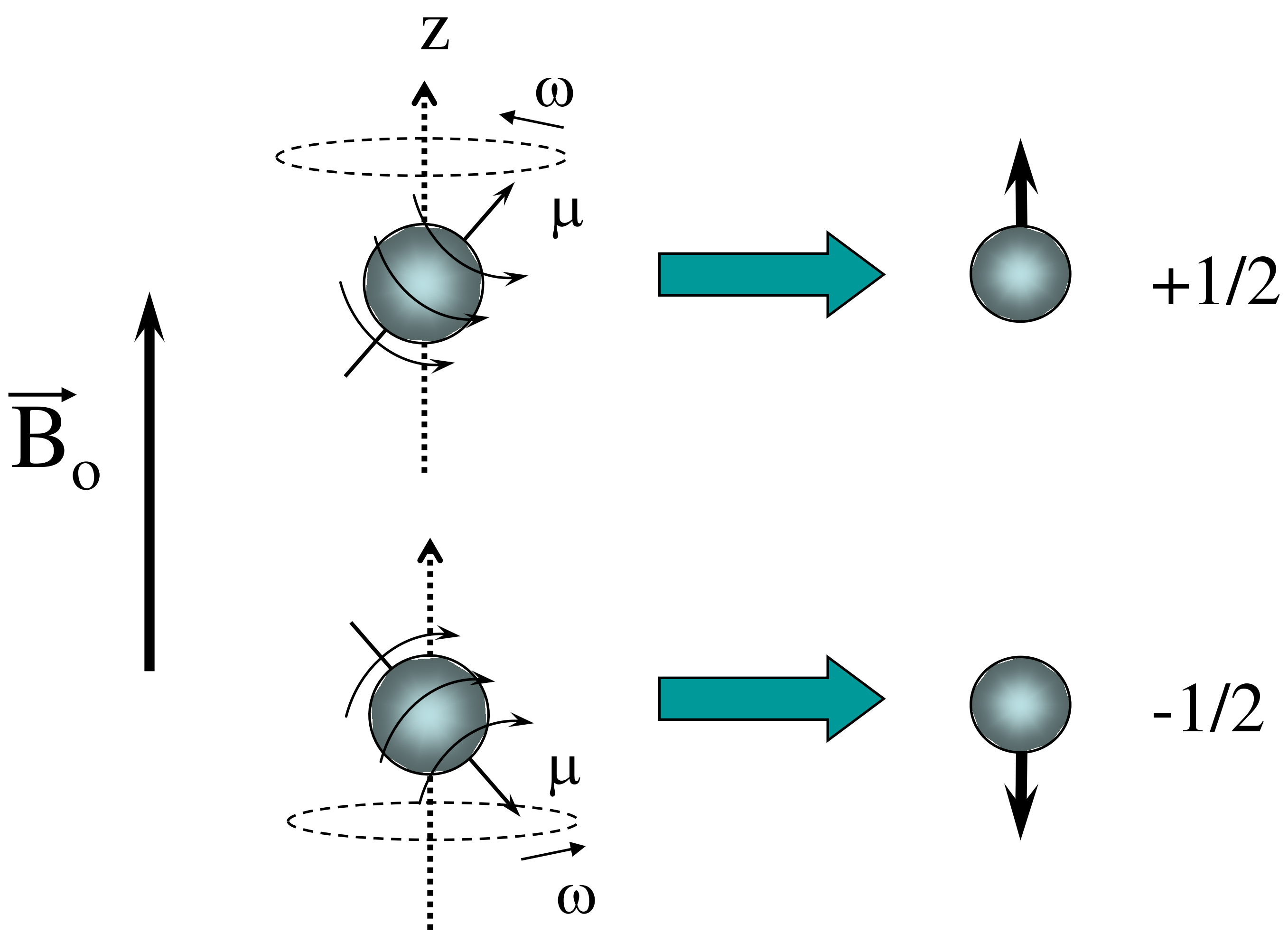

Ensemble of Nuclear Spins

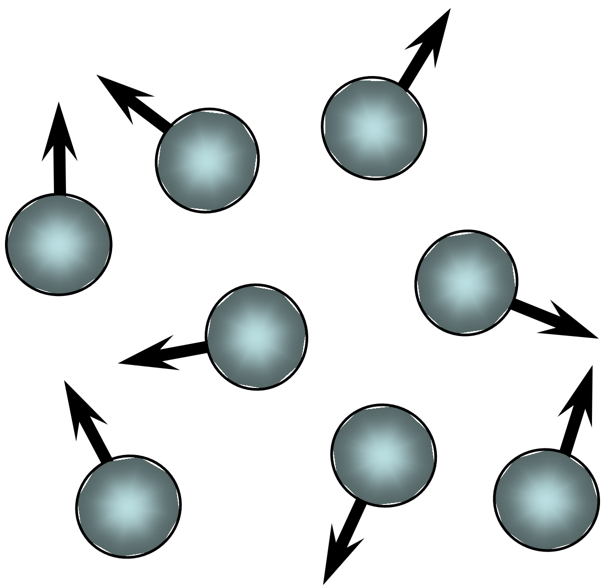

$\vec{B}_o = 0$

Randomly oriented

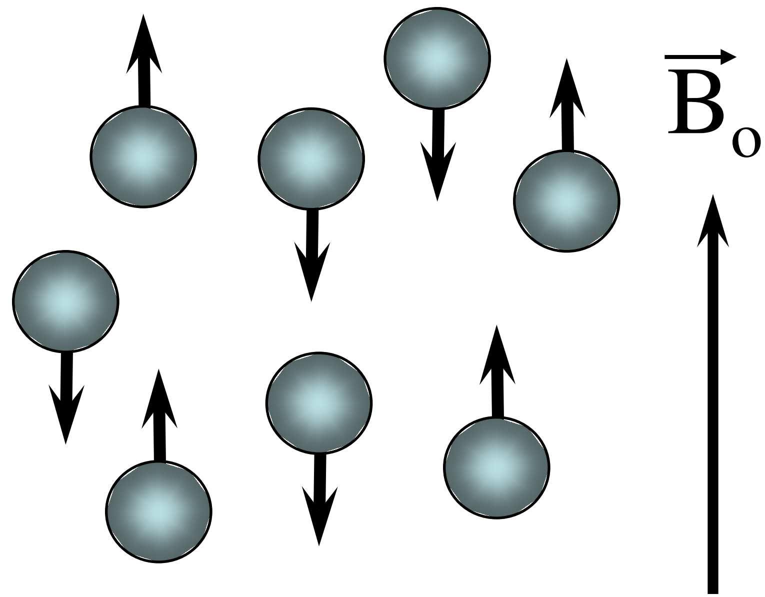

$\vec{B}_o > 0$

Highly oriented

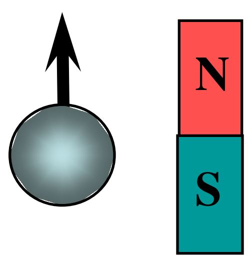

Each nucleus behaves like a bar magnet.

Allowed Energy States for a Spin 1/2 System

$$\Delta E = \gamma \hbar \overrightarrow{B_o} = \hbar \nu$$

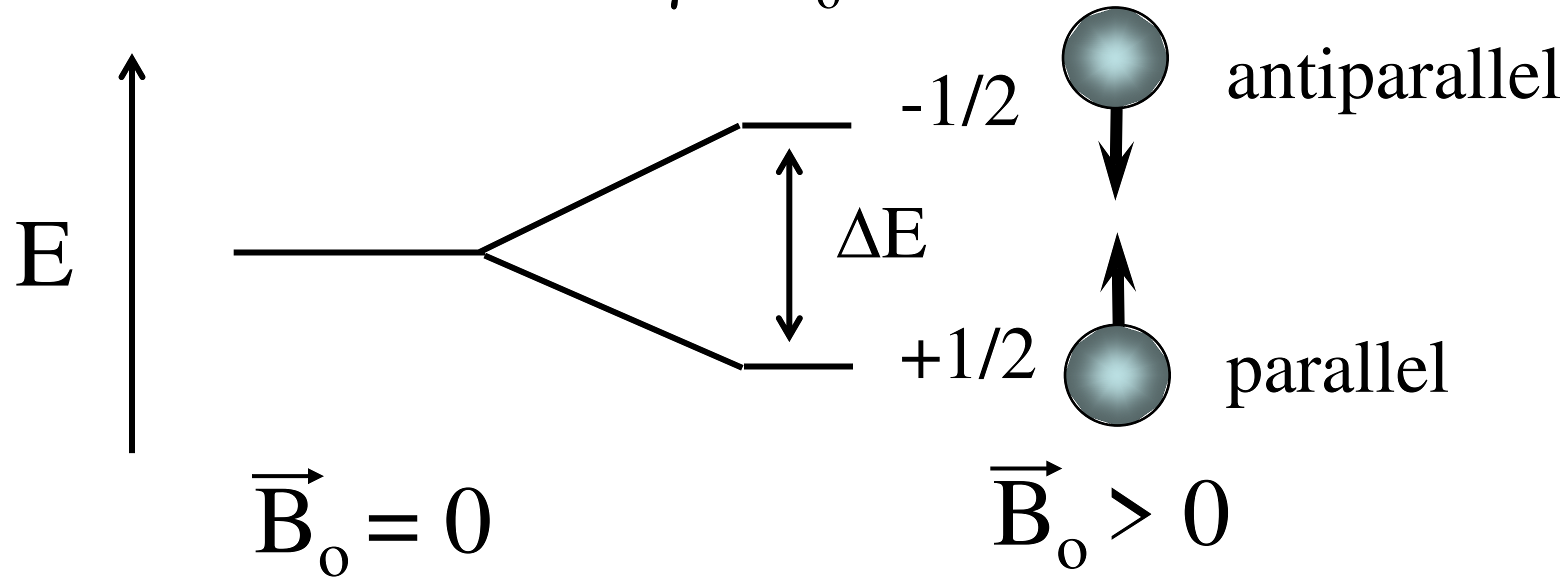

Therefore, the nuclei will absorb radiation with energy ΔE resulting in a change of the spin states.

Spins Orientation in a Magnetic Field (Energy Levels)

- Transition from the low energy to high energy spin state occurs through an absorption of a photon of radio-frequency (RF) energy

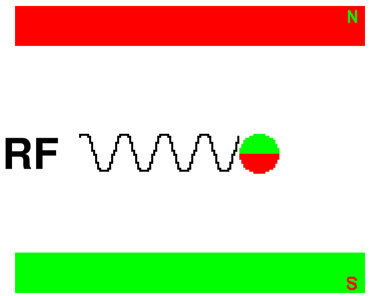

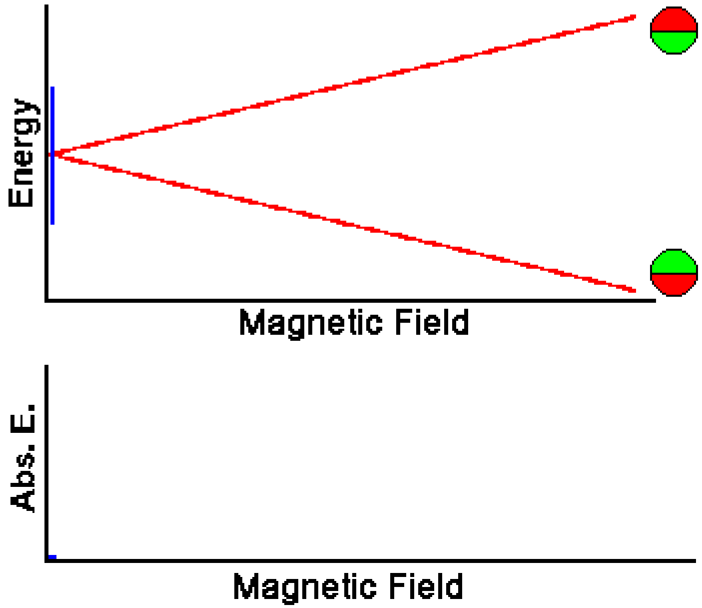

Frequency of absorption: $\nu = \gamma B_o / 2\pi$

Resonance technique

The NMR Experiment
Continuous Wave

- Sample is dissolved in suitable solvent
- Solvent is generally $CDCl_3$ (no protons)
- Placed in thin glass tube (highly purified glass is used)
- Tube is placed in magnetic field
- Radiofrequency is used to excite nuclei and to spin flip

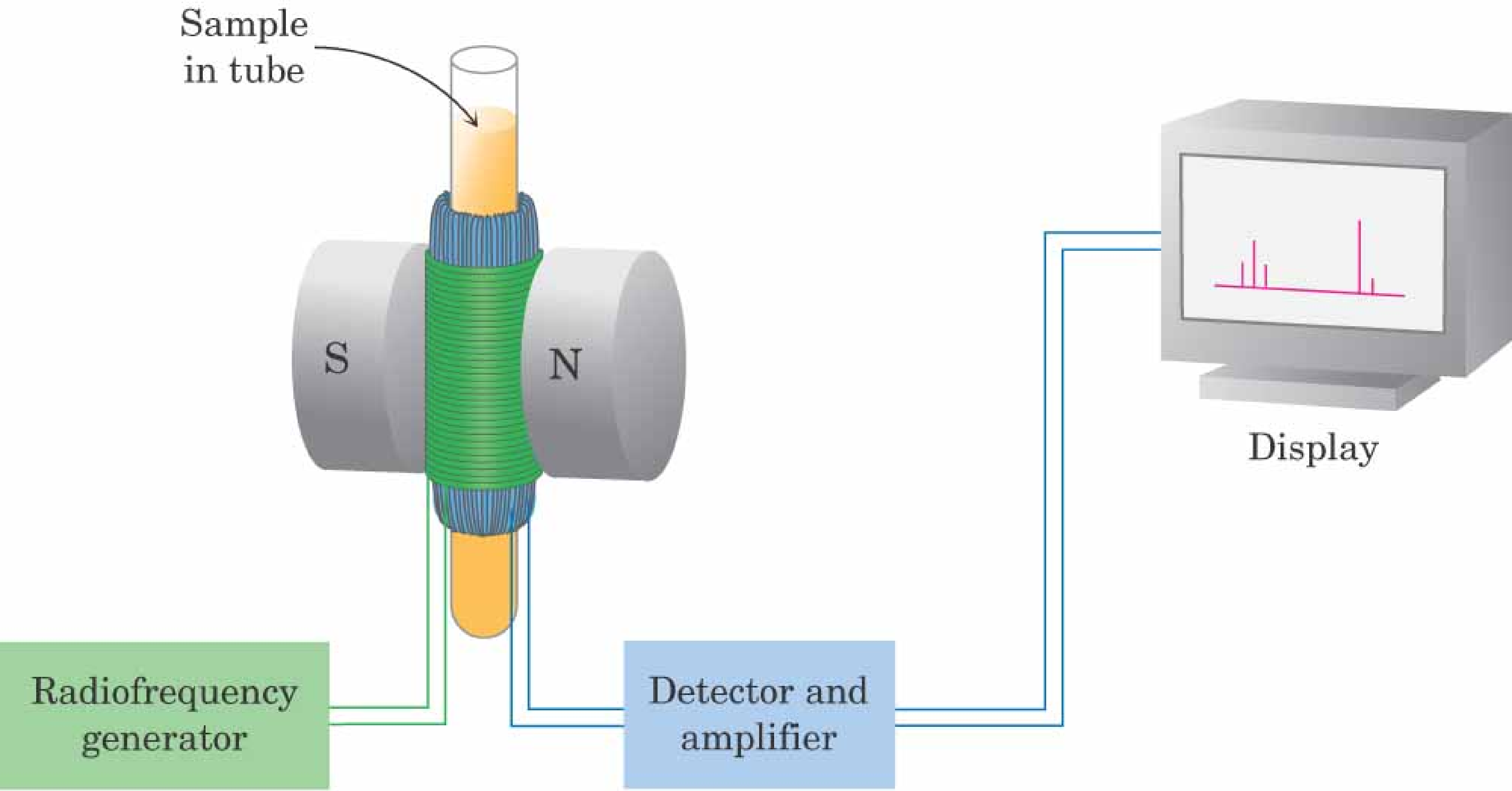
Sample
in tube
S
N
Display
Radiofrequency
generator
Detector and
amplifier

CW NMR 40MHz
(1960)

Magnetization

Boltzmann

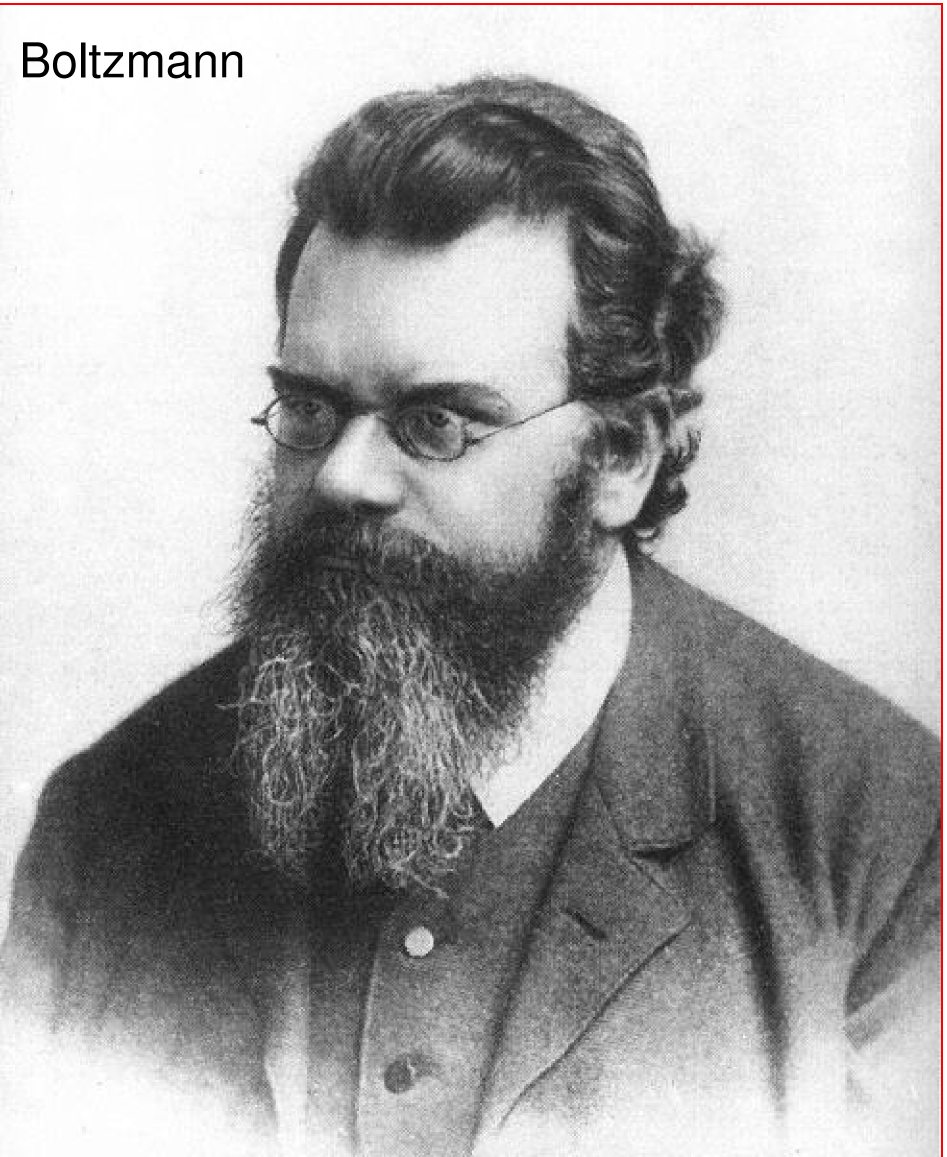

$$\frac{N_{+1/2}}{N_{-1/2}} = \exp\left(+\Delta E/k_B T\right)$$

$$\Delta E \equiv E_{-1/2} - E_{+1/2} = \hbar\omega_L$$

$$N = N_{+1/2} + N_{-1/2}$$

Magnetization

$$M \propto N_{+1/2} - N_{-1/2}$$

NMR Signal (sensitivity)

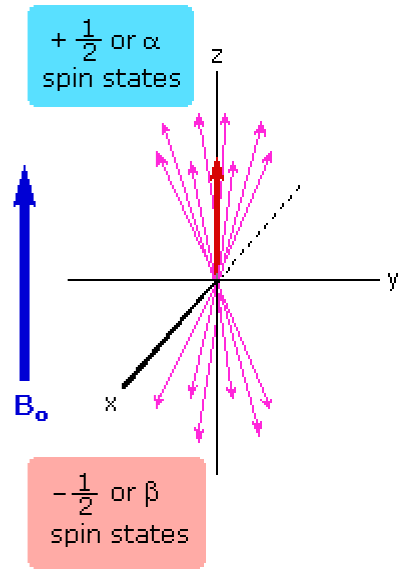

Since:

$$\Delta E = h\nu$$

and

$$\nu = \gamma\, B_o / 2\pi$$

then:

$$N_\alpha / N_\beta = e^{\Delta E / kT} \quad \Rightarrow \quad N_\alpha / N_\beta = e^{(\gamma h B_o / 2\pi k T)}$$

The ΔE for ^1H at 400 MHz (**B_o** = 9.39 T) is 6 x 10^{-5} Kcal / mol

$$N_\alpha / N_\beta = 1.000060$$

Very Small !
~ 60 excess spins per million in lower state

Energy vs Field strength

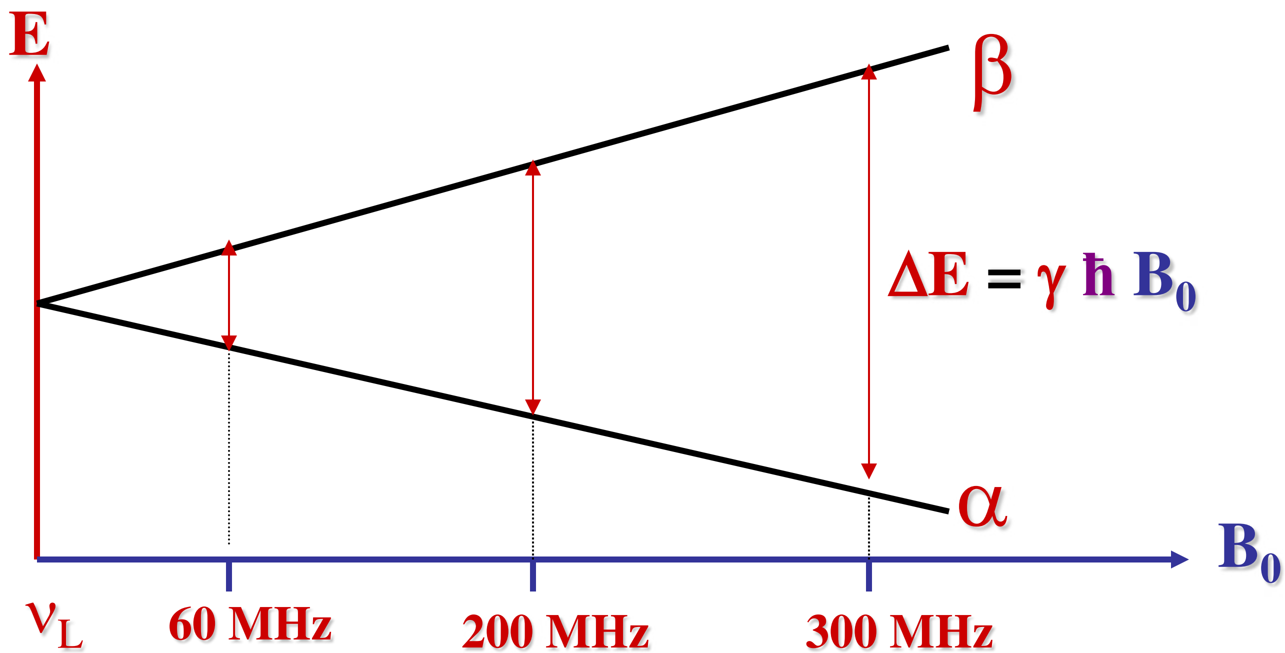

Boltzmann Equation

$$\frac{N_\beta}{N_\alpha} = e^{(\Delta E/kT)} \sim 1 - \Delta E/kT$$

Where **k=1.3805 x 10^{-23} J K^{-1}**

T is the temperature

e.g. with **B_0=1.4 T** (ν_L=60 MHz)

ΔE_H ~2.4 J/mol **At T=300K**

N_β = .9999904 N_α

with **B_0=7.05 T** (ν_L=300 MHz)

N_β = .99995 N_α

Sensitivity of NMR Experiments

The sensitivity of pulsed FT-NMR is given by the signal to noise ratio:

$$\left(\frac{S}{N}\right) = N\,T_2\,\frac{\sqrt[3]{B_o \gamma_{\mathrm{det}}}\sqrt{Ns}}{T}$$

N = number of spins in the system-sample concentration
T_2 = transverse relaxation time
γ_{det} = magnetogyric ratio of detected nucleus
Ns = number of scans
B_o = external field strength
T = sample temperature

NMR Sensitivity

Increase in Magnet Strength is a Major Means to Increase Sensitivity

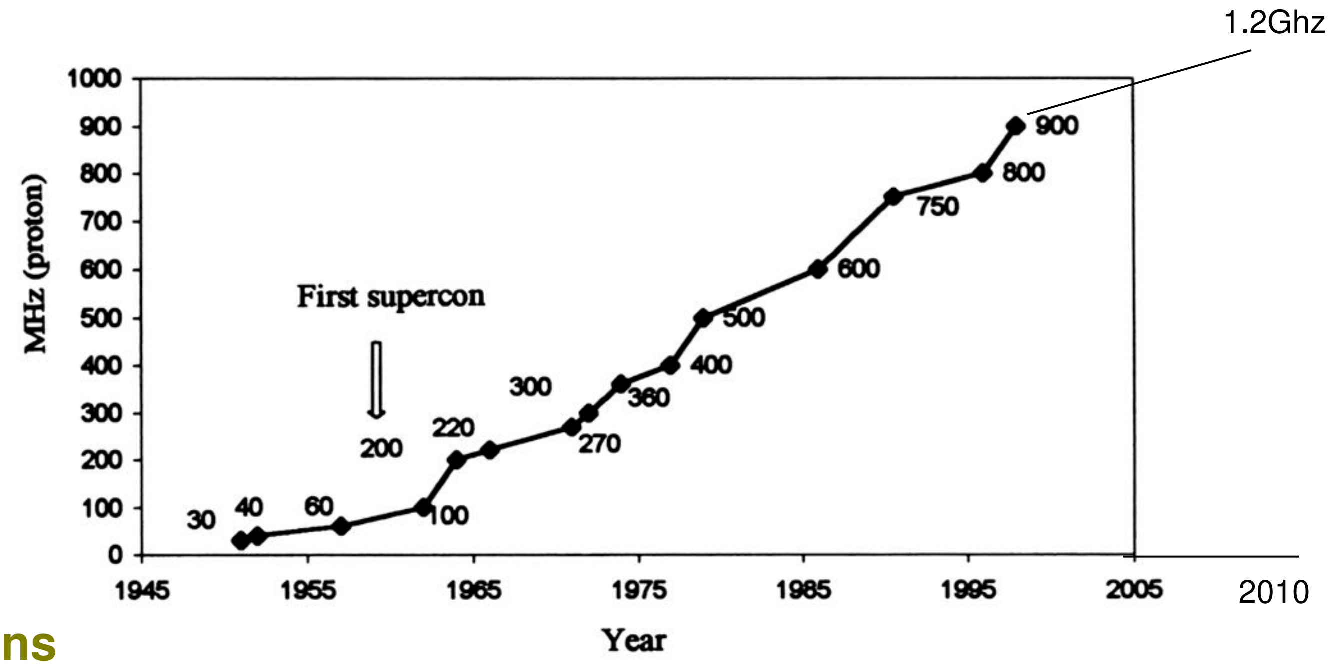

Signal to noise improvement with magnetic field (sensitivity)

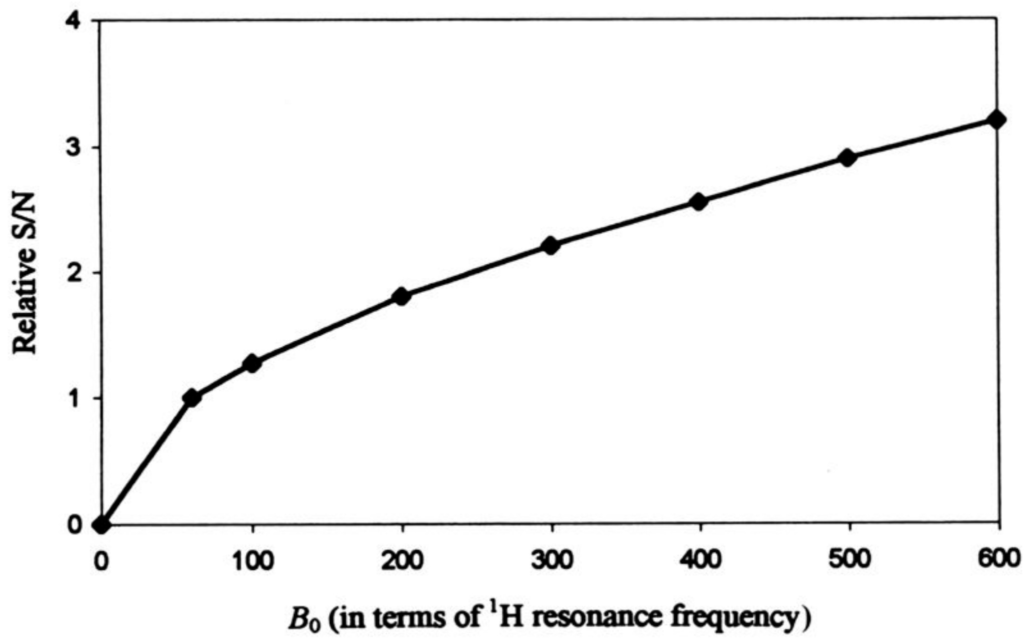

NMR Sensitivity

But at a significant cost!

~ $800,000

~ $2,00,000

~ $4,500,000

Comparison of 1.5 and 3T performance

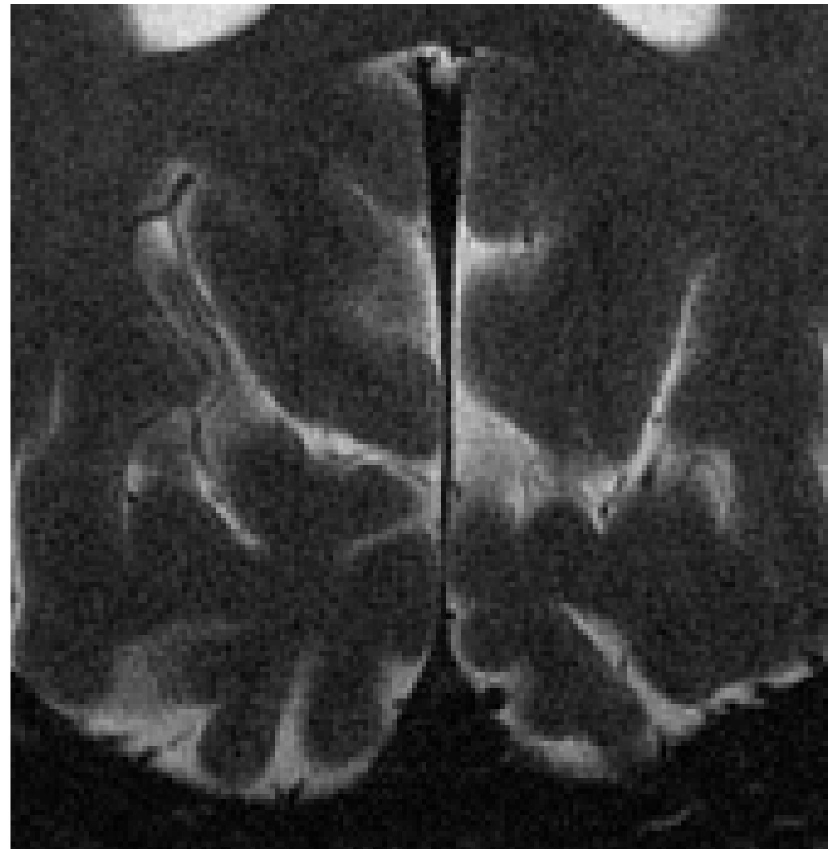

1.5T Image courtesy of MGH **3T**

Magnet Safety

The whopping strength of the magnet makes safety essential.
Things fly – Even big things!

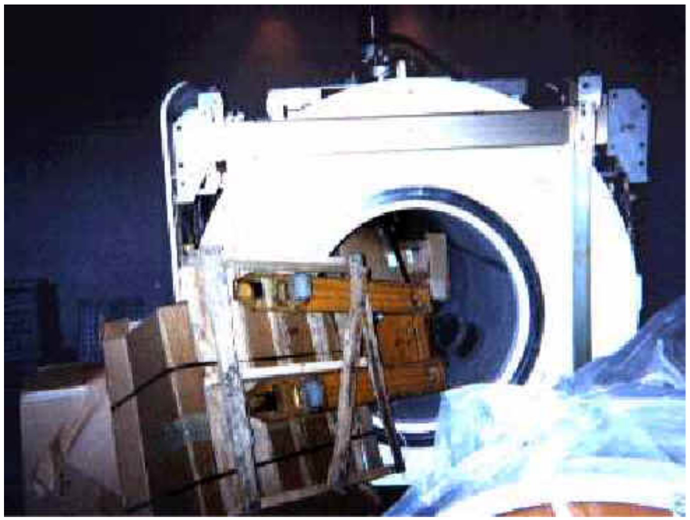

Source: www.howstuffworks.com

Source: http://www.simplyphysics.com/flying_objects.html

Source: Jody Culham's fMRI for Dummies web site

Introduction

NMR signal

Spectroscopy

T1-T2 relaxation

Diffusion

Imaging

Plastics

Conclusions

Quantum

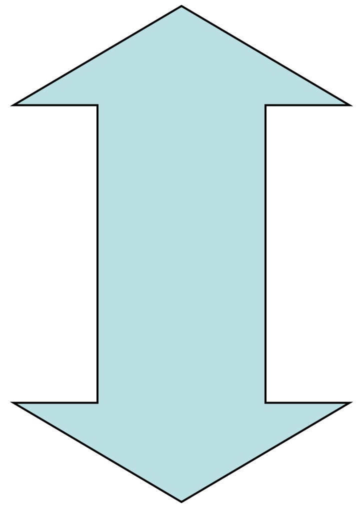

Classical

Classical Description

- *Spinning particle precesses around an applied magnetic field*

A Spinning Gyroscope in a Gravity Field

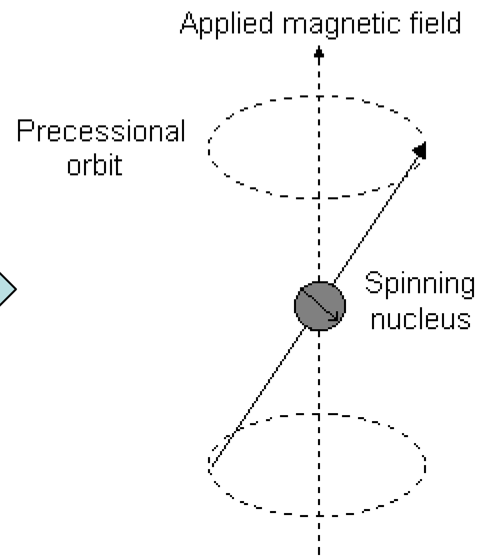

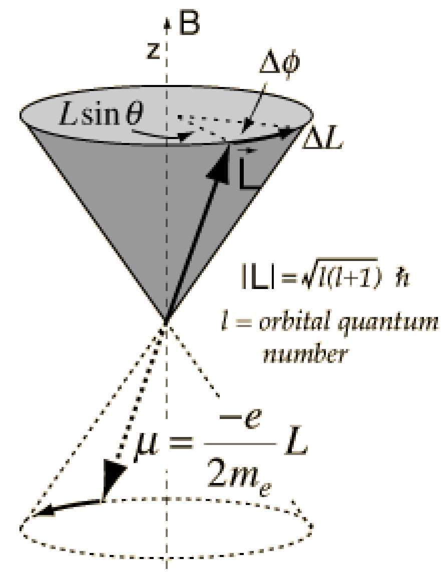

Simplified Bloch equations

The return to equilibrium is generally (mono) exponential

$$\frac{dM_z}{dt} = \frac{M_0 - M_z}{T_1}$$

T_1 is the spin-lattice relaxation time constant

$$\frac{dM_{xy}}{dt} = -\frac{M_{xy}}{T_2}$$

T_2 is called the spin-spin relaxation time constant

Classical Description

- *NMR Pulse*
  - Applying the B_1 field for a specified duration (Pulse length or width)
  - Net Magnetization precesses about B_1 a defined angle (90º, 180º, etc)

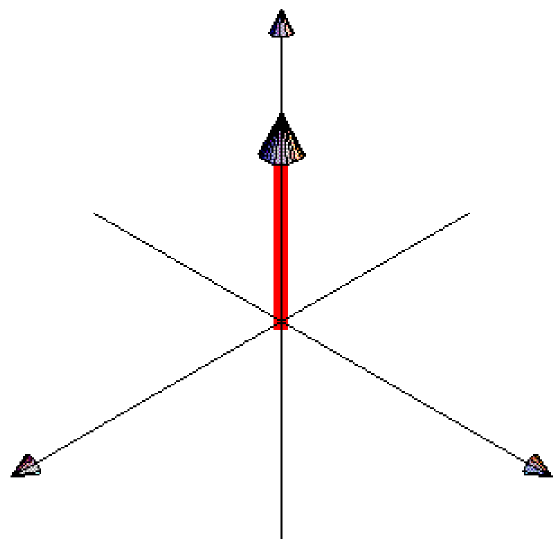

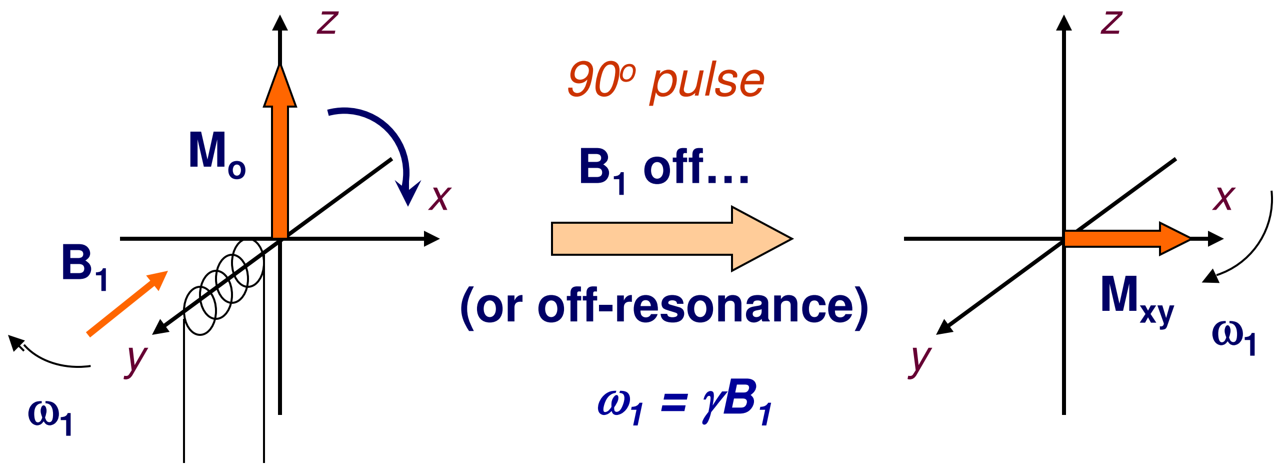

Relaxation of M_{xy} During Fourier Transform NMR

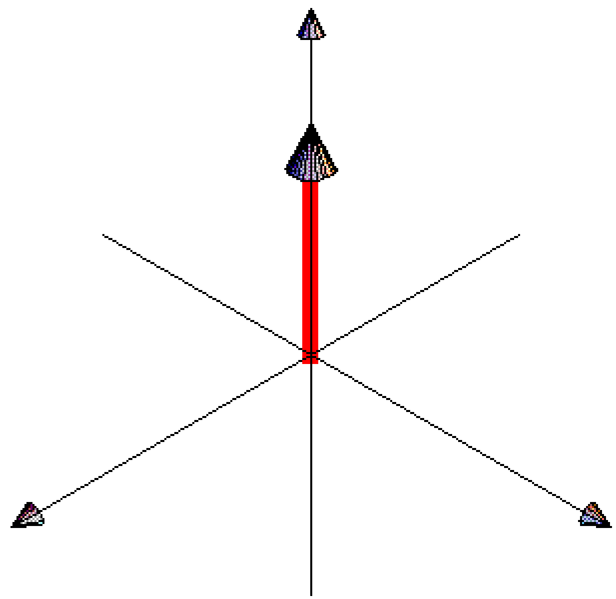

Responses Due to T_1 AND T_2

For liquids in porous media $T_1 >> T_2$

Classical Description

- *Observe NMR Signal*
  - **Remember**: a moving magnetic field perpendicular to a coil will induce a current in the coil.
  - The induced current monitors the nuclear precession in the X,Y plane

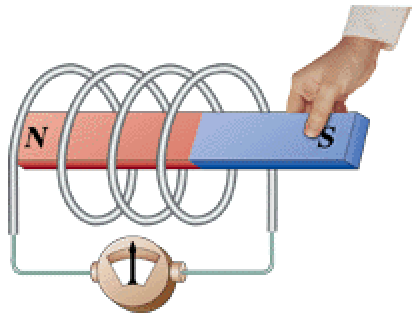

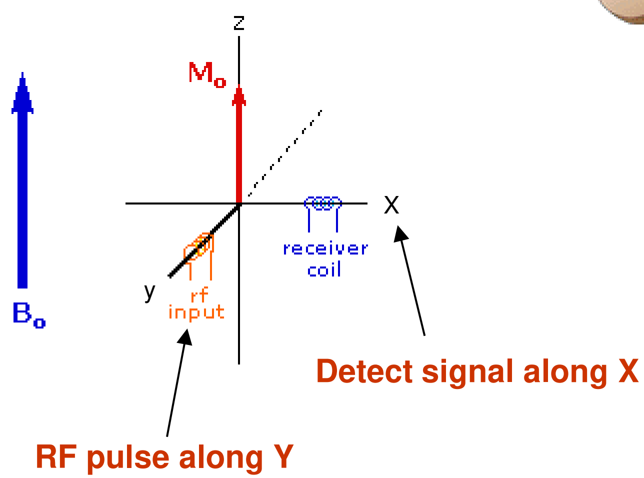

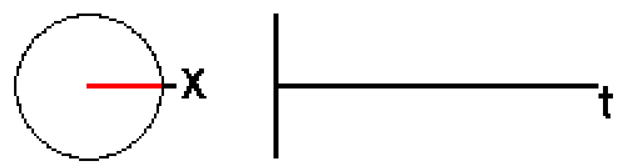

$$\nu = \gamma B_o / 2\pi$$

Experimental setup

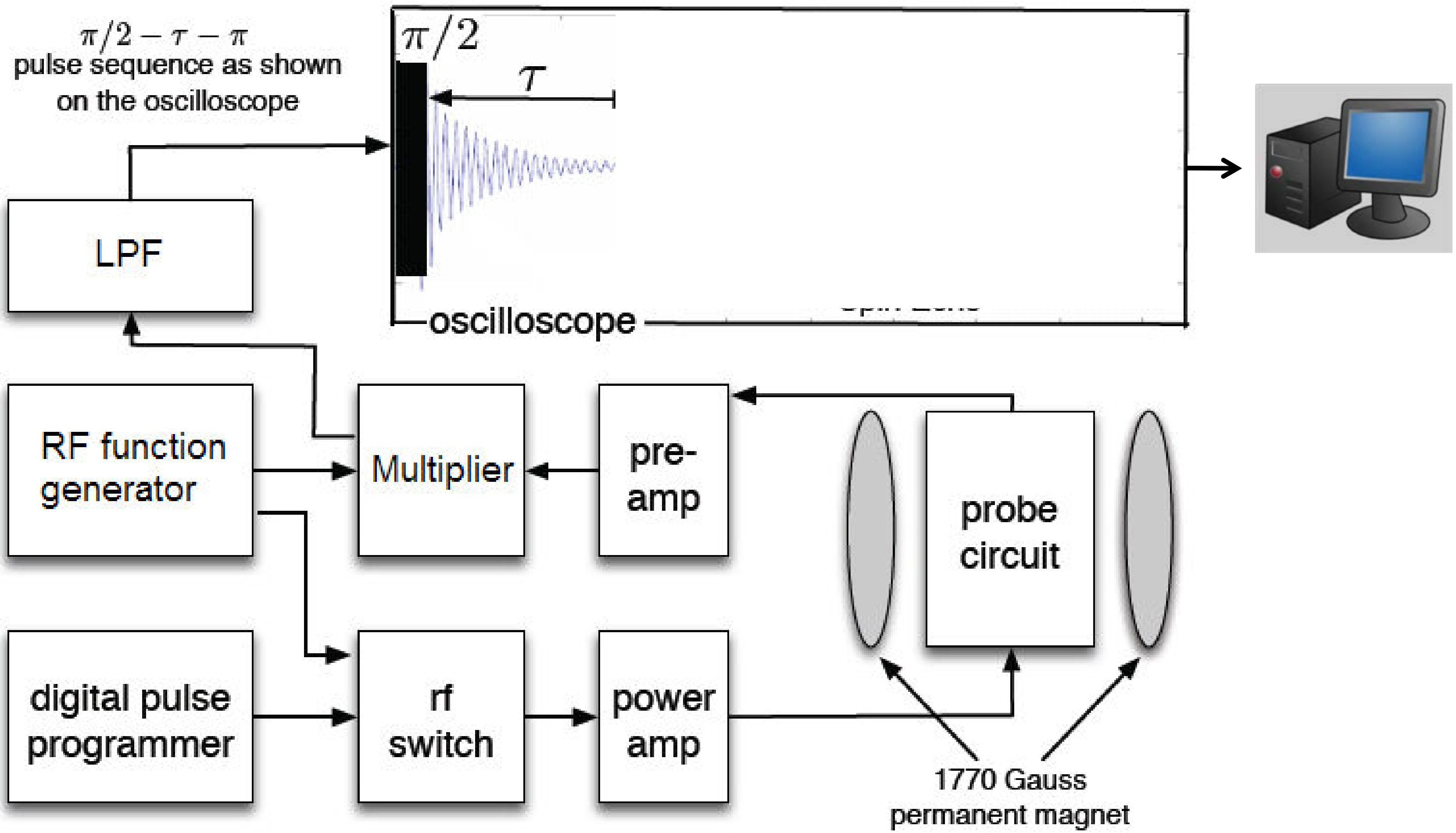

After 90^o pulse Free Induction Decay

The signals decay away due to interactions with the surroundings.

A free induction decay, FID, is the result.

Fourier transformation, FT, of this time domain signal produces a frequency domain signal.

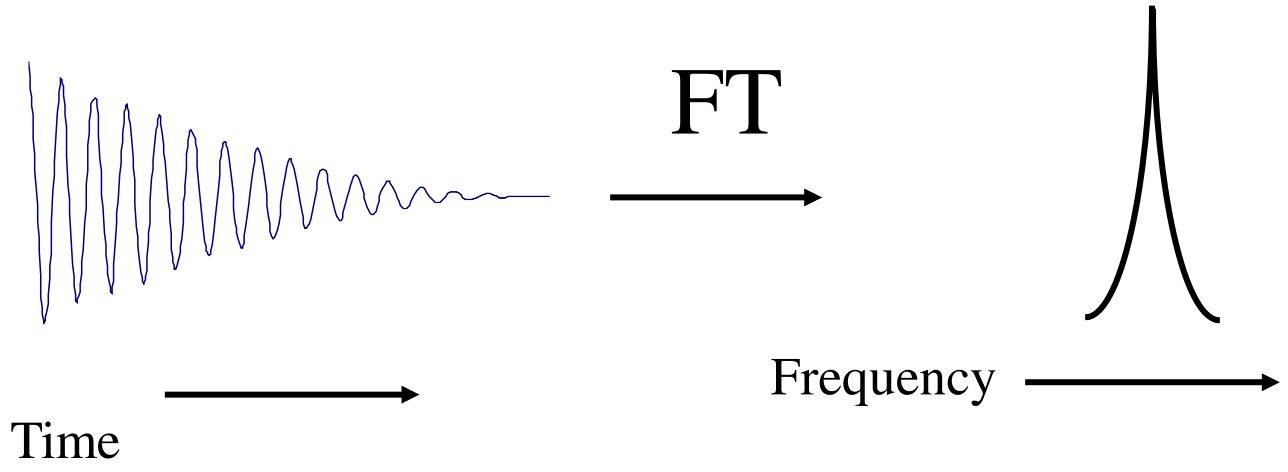

Free Induction Decay (FID)

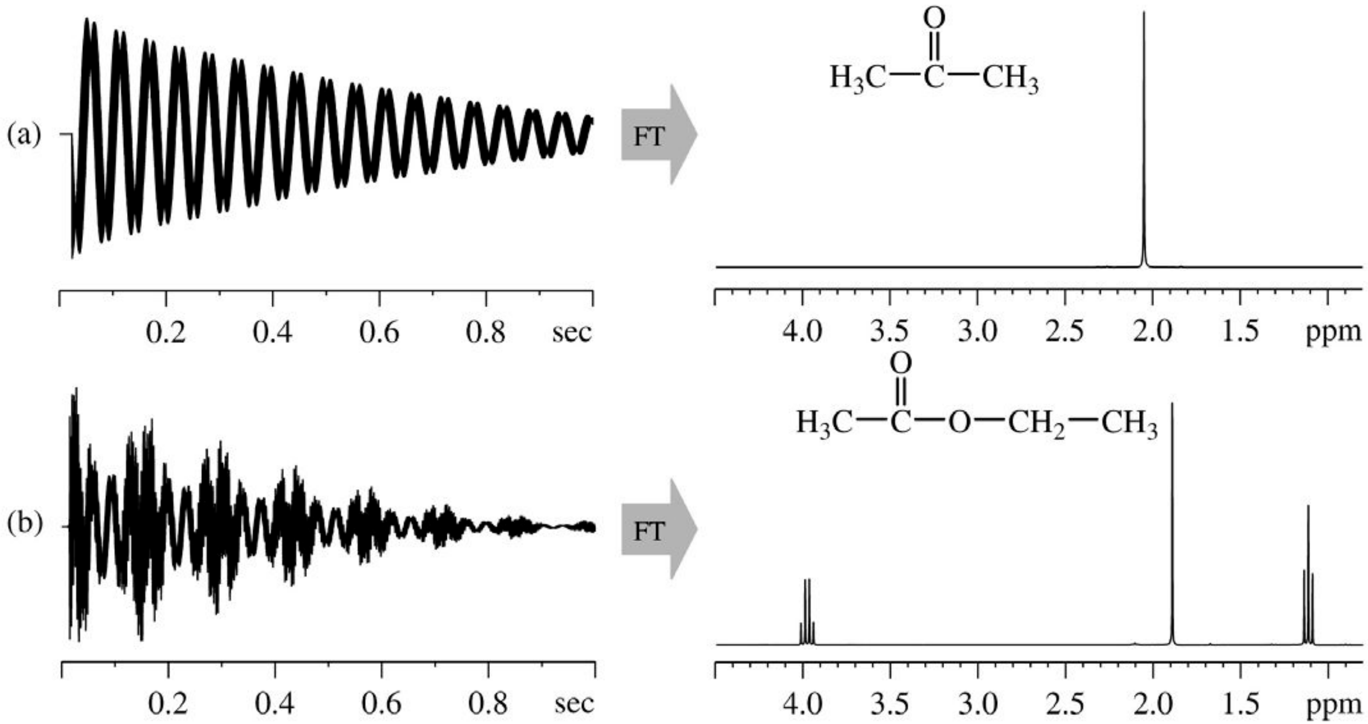

FID = the sum of all of the nuclei radiating absorbed rf as they return to the Ground State. The information in the FID is a function of time and must Be converted via Fourier Transform to the frequency domain to produce a Readable spectrum.

An NMR-based metabolomics study of pork from different crossbreeds and relation to sensory perception

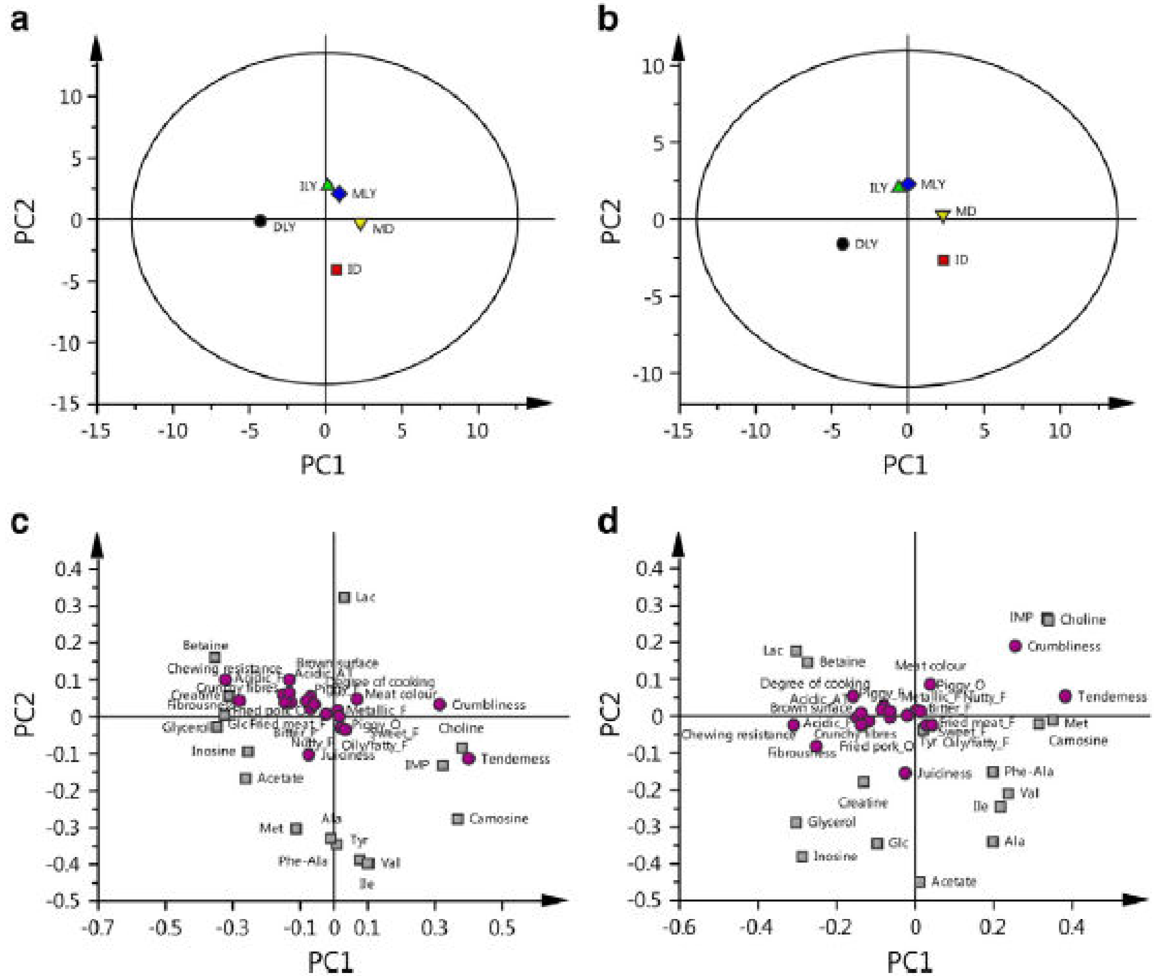

Fig. 3. PLS score (a and b) and loading (c and d) plots showing the means of the sensory profile and the polar metabolites from the meat extraction (a and c) and the freeze–thaw drip (b and d) from the five crossbreeds. For the metabolites from the meat extraction, the first two principal components (PC1 and PC2) explain 81 and 11% of the variance, respectively (c). Whereas for the metabolites from the freeze–thaw drip PC1 and PC2 explain 83 and 9% of the variance, respectively (d). "O", odour, "F", flavour, and "AT", aftertaste. Grey boxes show metabolites, and magenta circles show attributes assessed by the sensory panel. Abbreviations as in Table 2.

Review

Non-Destructive Spectroscopic Techniques and Multivariate Analysis for Assessment of Fat Quality in Pork and Pork Products: A Review

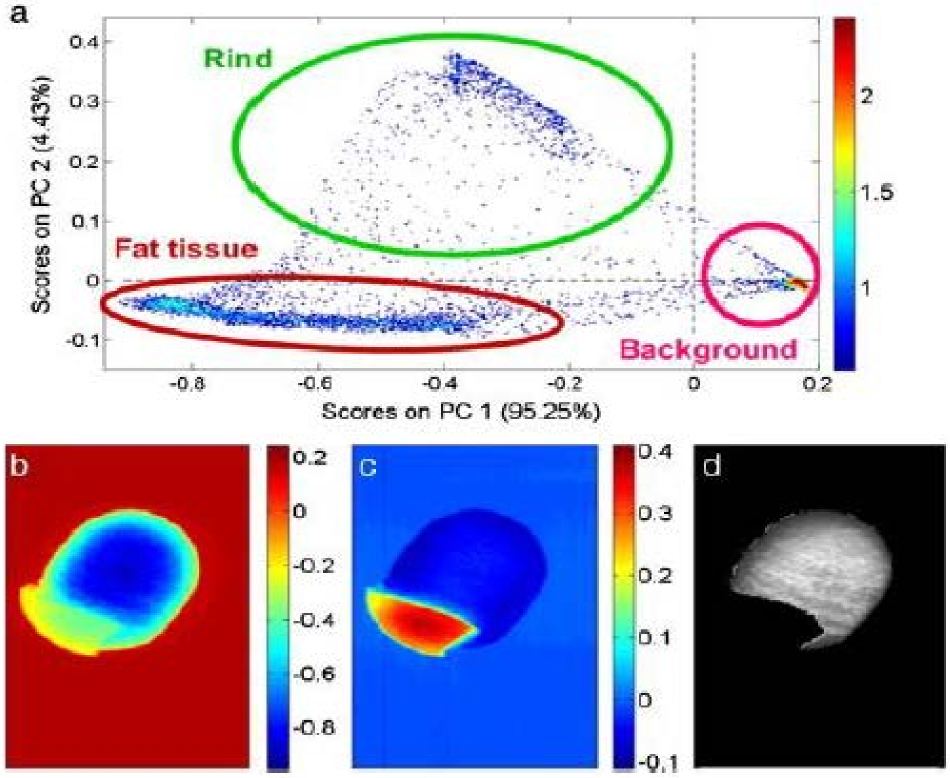

Figure 2. Classification of pork sample from the into rind, adipose tissue, and background (**a**); The background (**b**) and fat tissue (**c**) pixels. (**d**) is the gray image of the pork sample [82].

Introduction

NMR signal

Spectroscopy

T1-T2 relaxation

Diffusion

Imaging

Plastics

Conclusions

The big trick of NMR: Spin echo

- Inversion pulse after time τ $\rightarrow$ phase recovery at 2τ
- Corrects for dephasing due to static B inhomogeneities

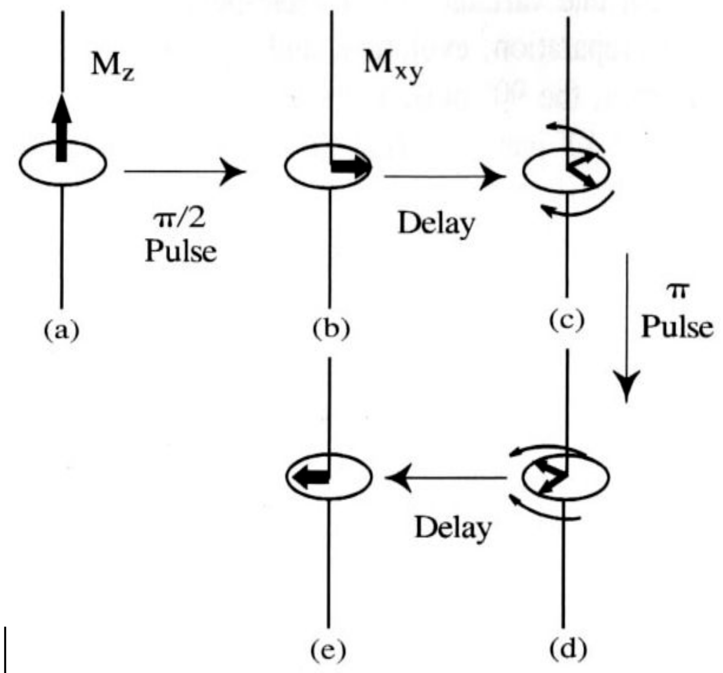

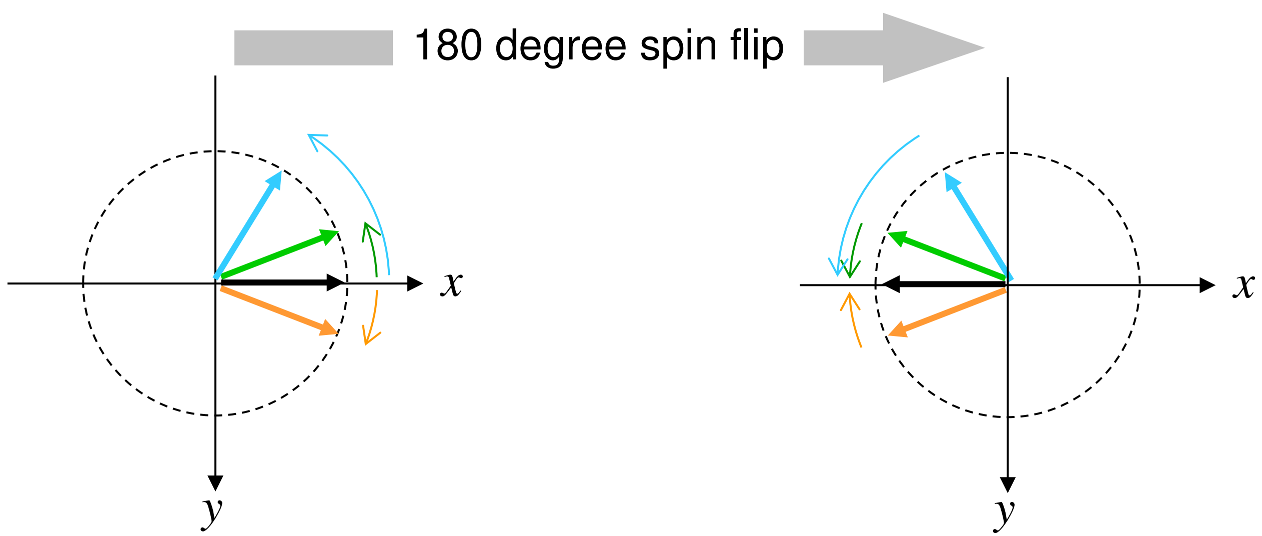

Experimental setup

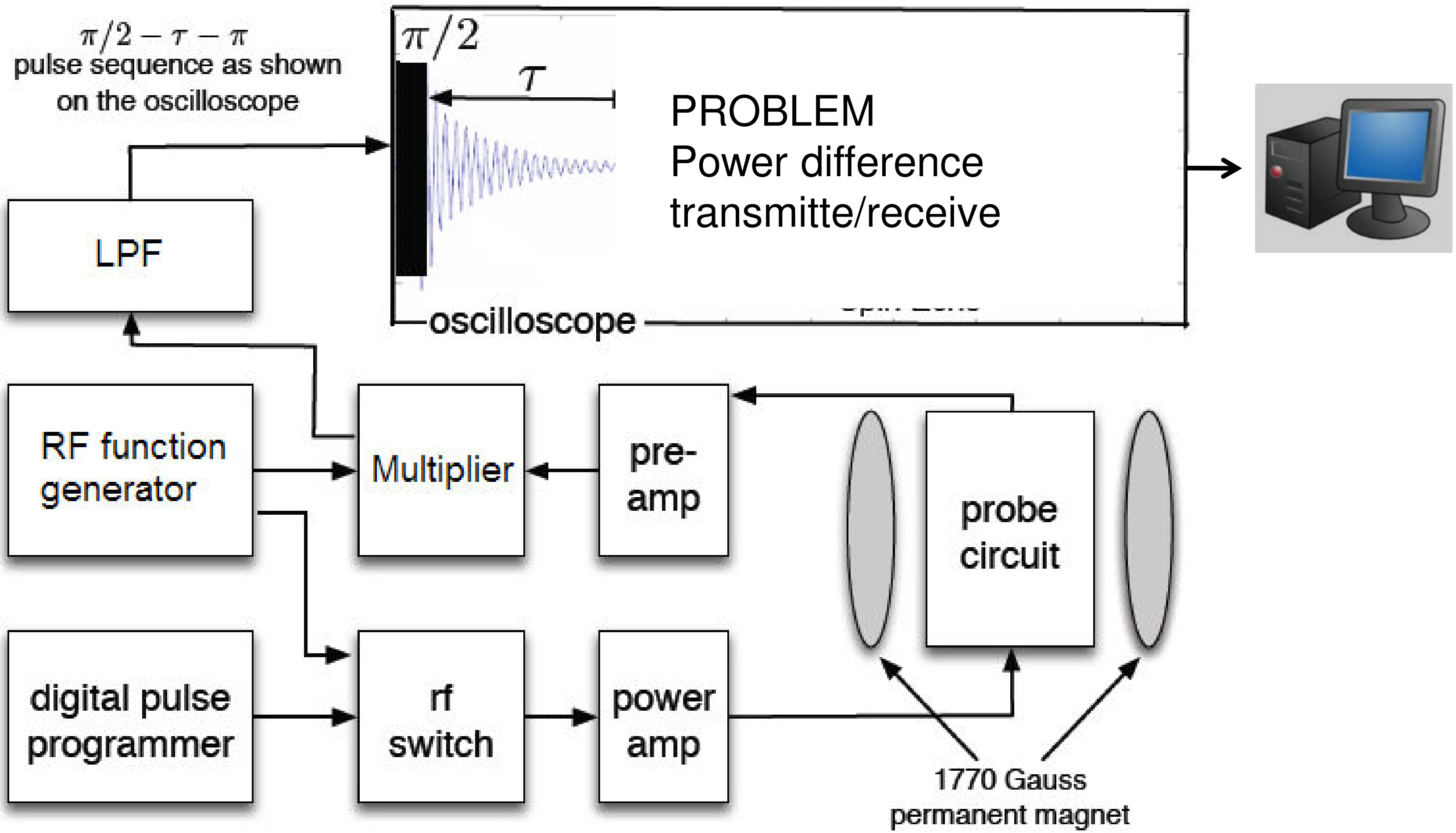

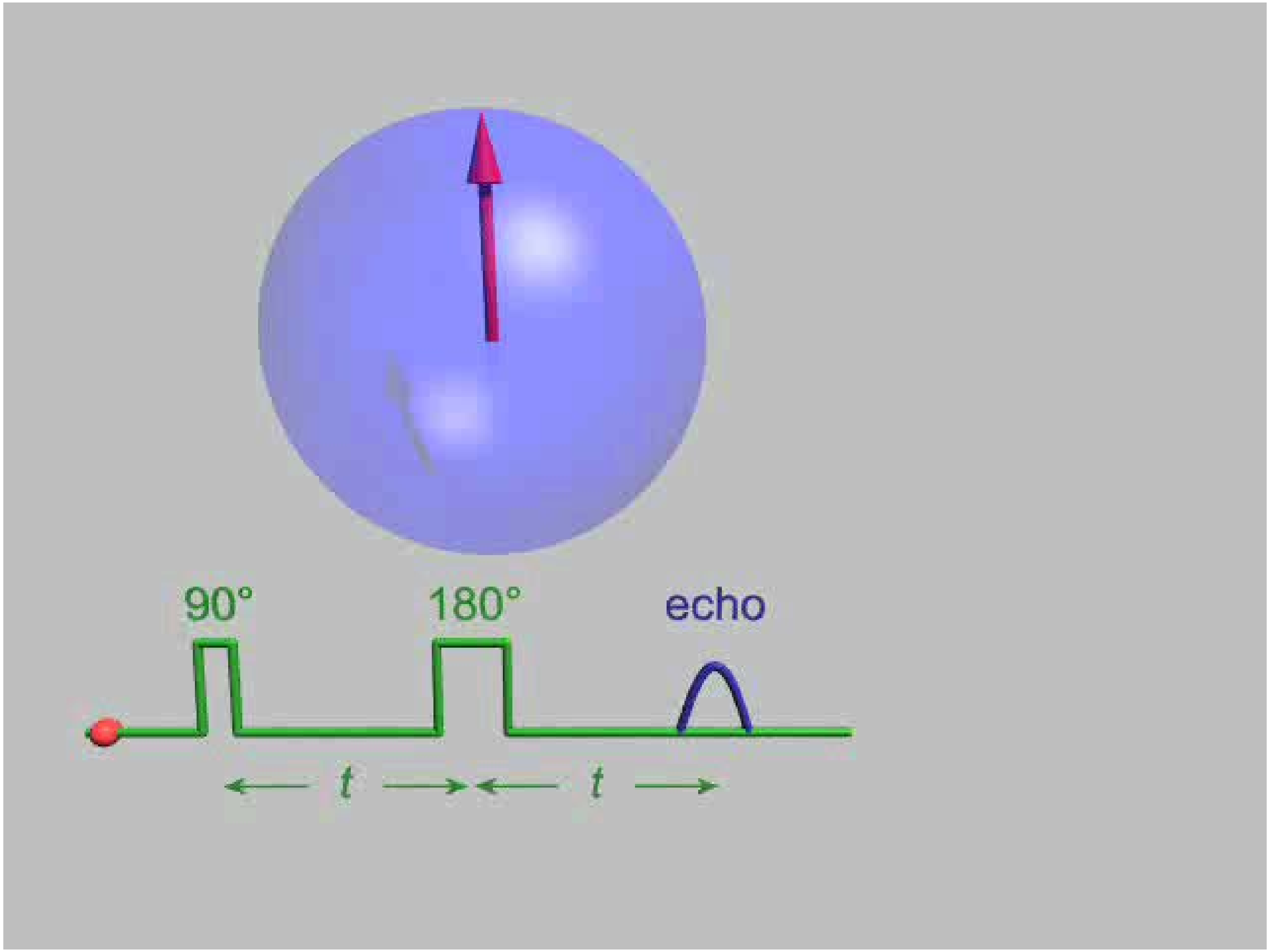
90°
180°
echo
t
t

Pulsed NMR signal (spin-echo experiment)

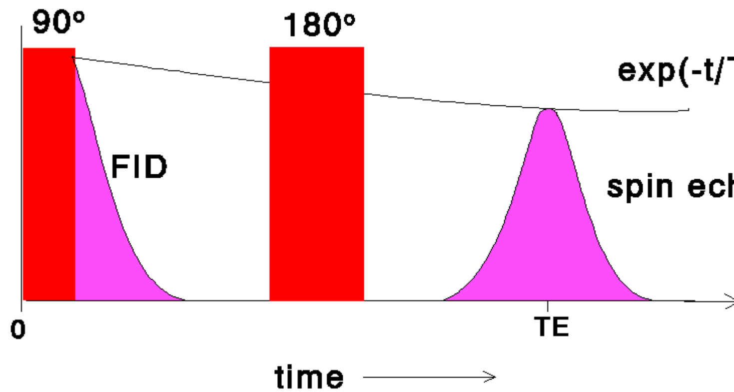

Information on pore water and ion distribution in pores

Amplitude spin-echo

$$S \sim G\rho \,[1-\exp(-TR/T_1)]\, \exp(-TE/T_2)$$

Signal proportional to moisture content or Na content

G = relative sensitivity (for ^{1}H G = 1, ^{23}Na = 0.1)

ρ = density of nuclei

T_1 = spin lattice relaxation

TR = repetition time experiment

T2 = spin-spin relaxation time

TE = spin-echo time

Na lower sensitivity longer measurement time

see, e.g., E.L. Hahn, Phys. Rev., 80, 580-594 (1950)

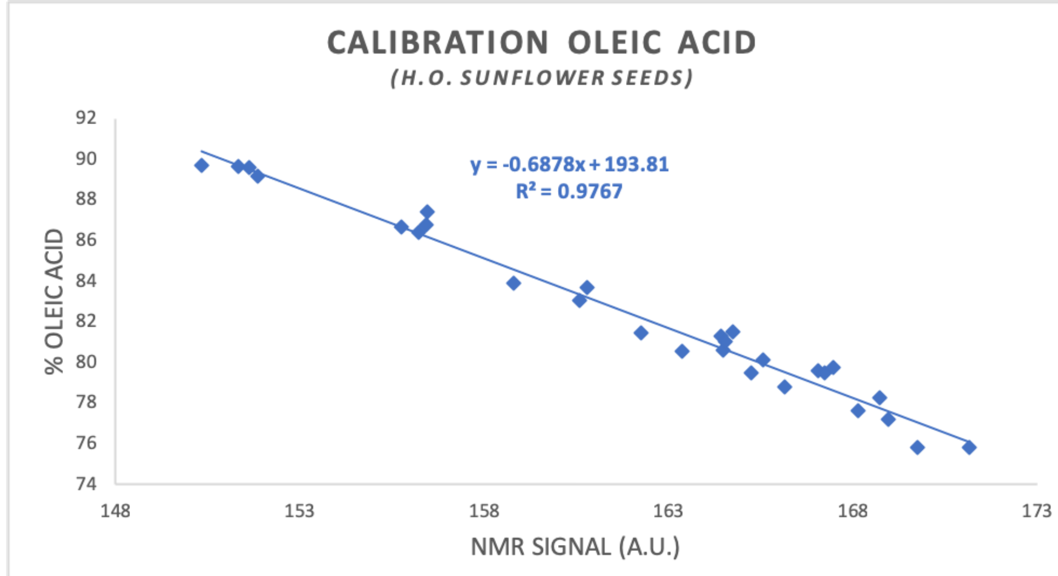

SLK-200-PEANUT

MAGNETIC RESONANCE ANALYZER NMR

BULK 27 CM³ & SINGLE SEED ANALYSIS

SIMULTANEOUS DETERMINATION

- **Oil**
- **Moisture**
- **Fatty acids**

· Fast and non-destructive measurement.

ACCURACY TABLES

MEASURING 27 cm³ OIL SEEDS			
	REPEATABILITY (Reliability 95%)	ACCURRACY (Reliability 95%)	MEASUREMENT TIME
OIL	± 0,06 %	± 1 %	4 Sec.
MOISTURE	± 0,07 %	± 0,6 %	4 Sec.
FATTY ACIDS (*)	± 0,50 %	± 2 %	20 Sec.
PROTEIN	± 0,2 %	± 0,7 %	12 Sec.

(*) OLEIC ACID, LINOLEIC ACID, PALMITIC ACID AND SATURATED FATTY ACIDS.

MEASURING SINGLE SEED % FATTY ACIDS (*)	
REPEATABILITY (Reliability 95%)	MEASUREMENT TIME
± 2,00 %	50 Sec.
± 1,00 %	150 Sec.

(*) DEVIATIONS DECREASE USING AVERAGES AS MUCH A LONGER MEASUREMENT.

Water relaxation

bulk water

mono exponential

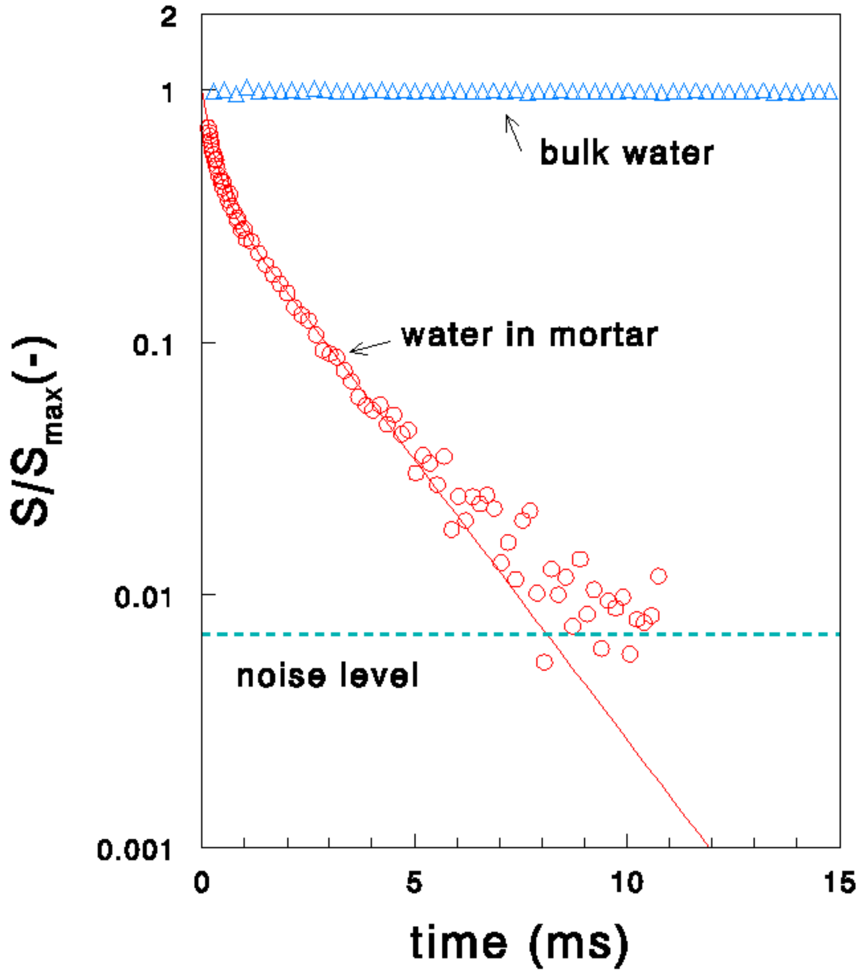

mortar

structure in T_2

WHY ?

Water in a pore

• Water molecules move due to self diffusion

(Brownian motion)

• Near the wall there is a fast surface relaxation

(no longer take part in experiment)

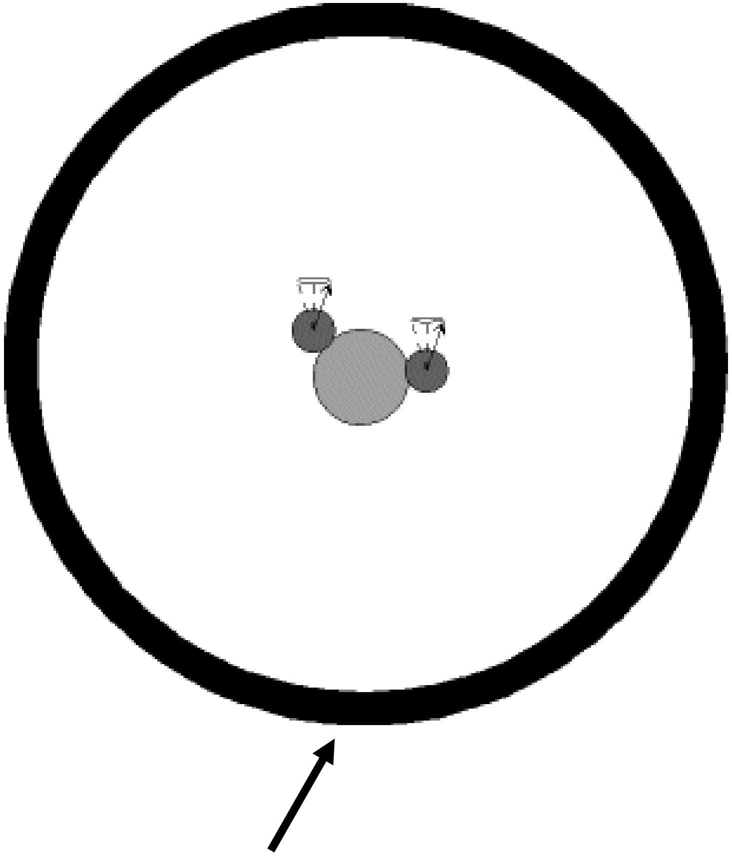

fast surface relaxation

Brownstein, Tarr *Phys Rev A* **19** 2446 1979 bulk water

water in pores

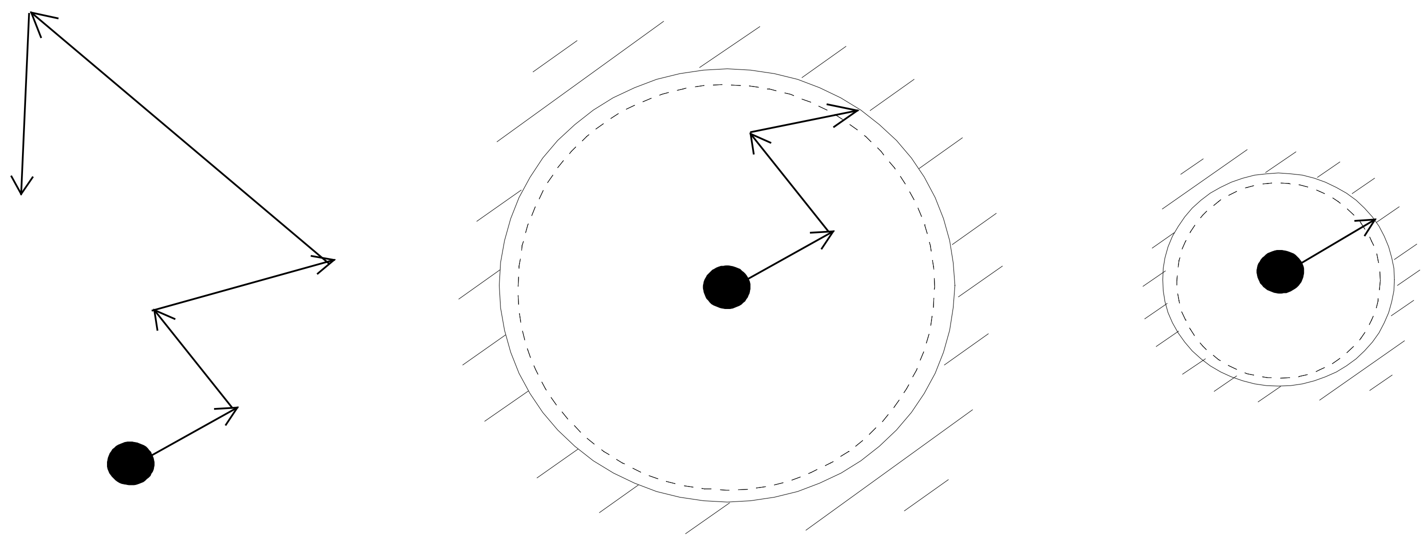

T_2 = large T_2 = medium T_2 = small

$$T_2 = \frac{V}{S}\frac{1}{\rho_2} \propto r_{pore}$$

where ρ_2 = surface relaxivity

Brownstein, Tarr *Phys Rev A* **19** 2446 1979

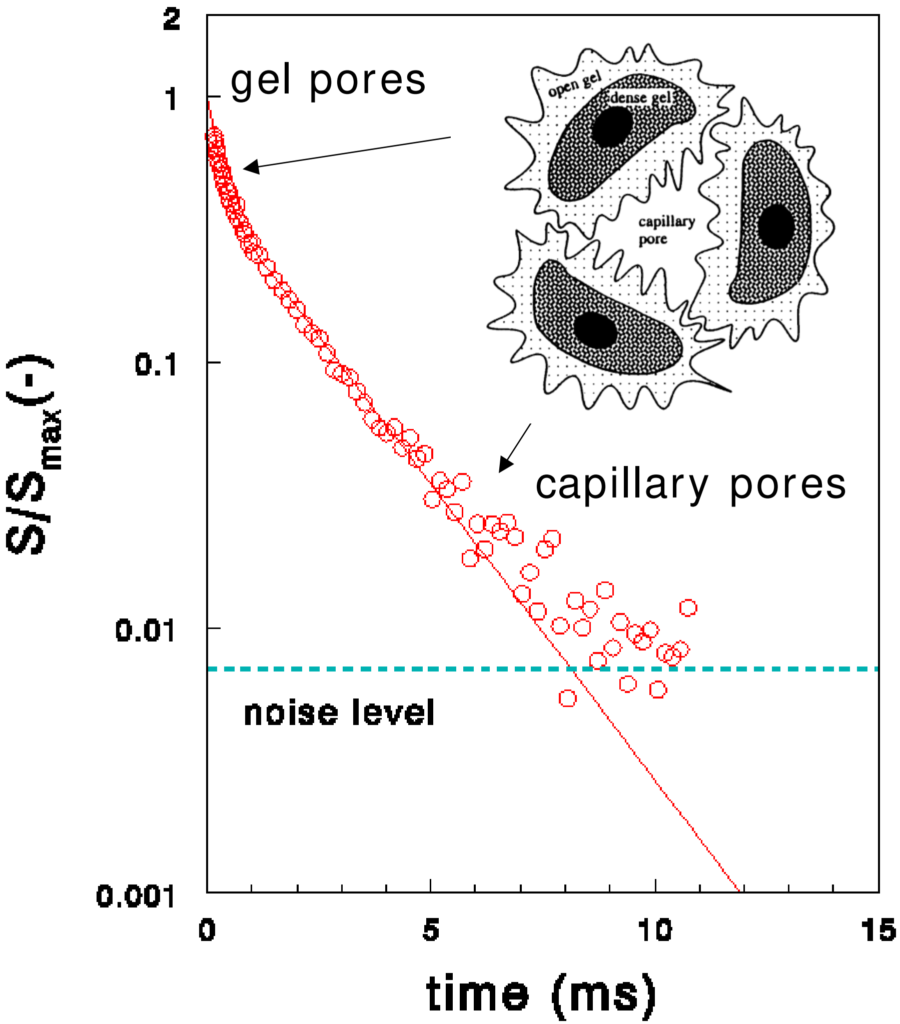

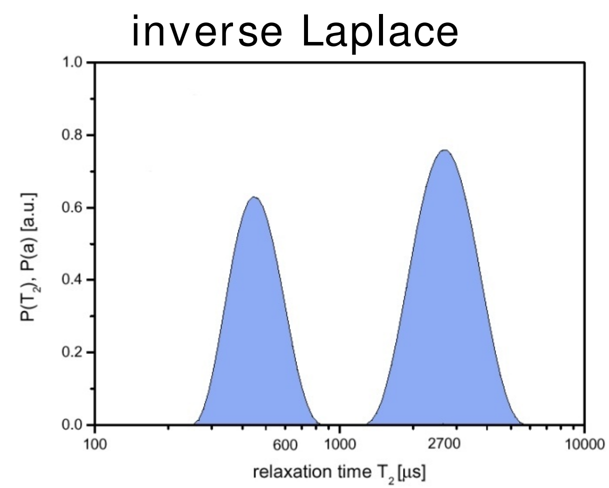

Probing pores in nanometer range

NMR relaxometry study of development of freeze damage in mandarin orange

Lu Zhang[a] and Michael J McCarthy[a,b*]

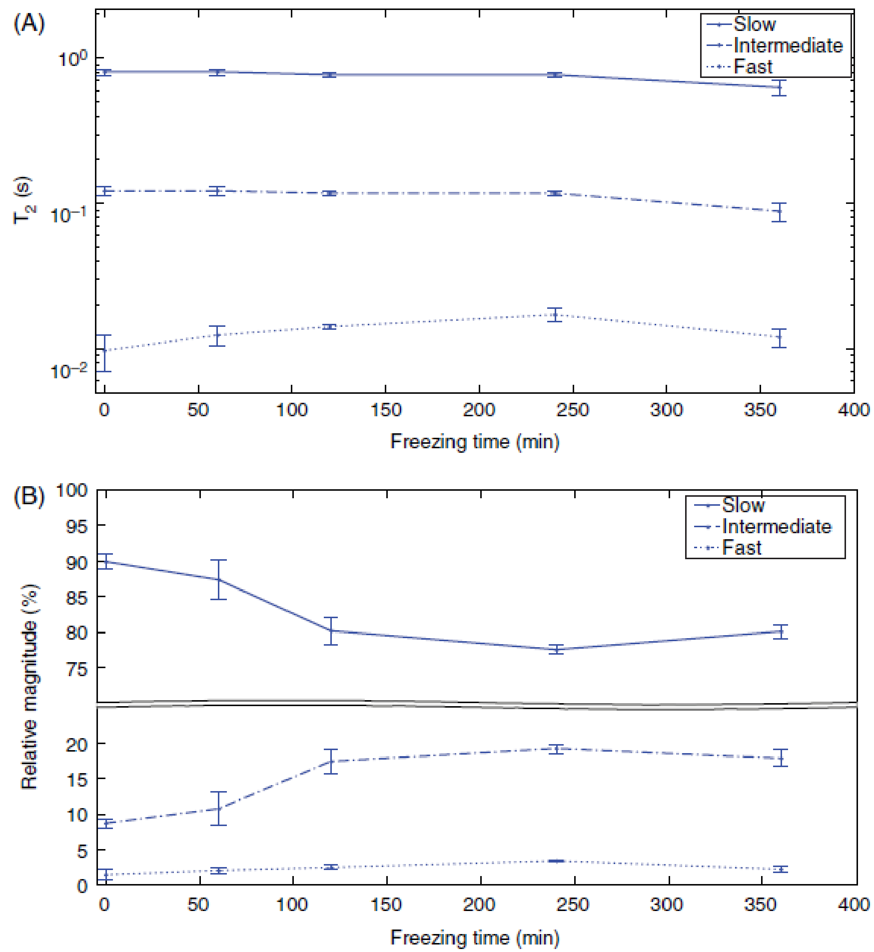

Figure 4. Changes in T_2 relaxation time (A) and relative magnitude (B) of the slow, intermediate and fast relaxation components as a function of freezing time at −20 °C.

Figure 3. Comparison of sterile (open circles) to unsterile (solid circles) T_1 values as a function of room temperature exposure time. The 95% confidence intervals corresponding to averaging over 15 samples are included in the plot.

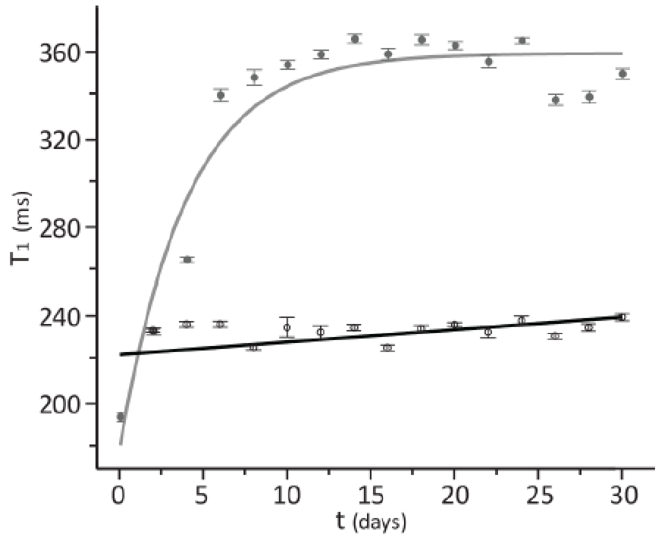

Table 1. NMR Relaxation Parameters for Tomato Samples.

	T < 5 °C		T > 25 °C		
	T_1 (ms)	**T_2 (ms)**	**T_1^{∞} (ms)**	**τ (days)**	**T_2 (ms)**
Sterile	217.3 ± 2.2	53.5 ± 1.4	234.8 ± 1.8	-	58.8 ± 1.0
Unsterile	199.4 ± 1.3	47.2 ± 0.9	349.0 ± 2.6	4.0 ± 1.8	57.0 ± 0.5

Figure 4. Example ^{1}H NMR spectra obtained with the single sided coil magnet for a 100 mL tomato paste sample without (**a**) and enclosed in (**b**) the aluminum lined tote material.

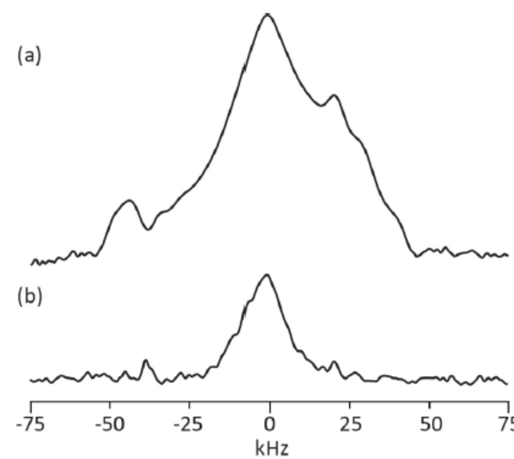

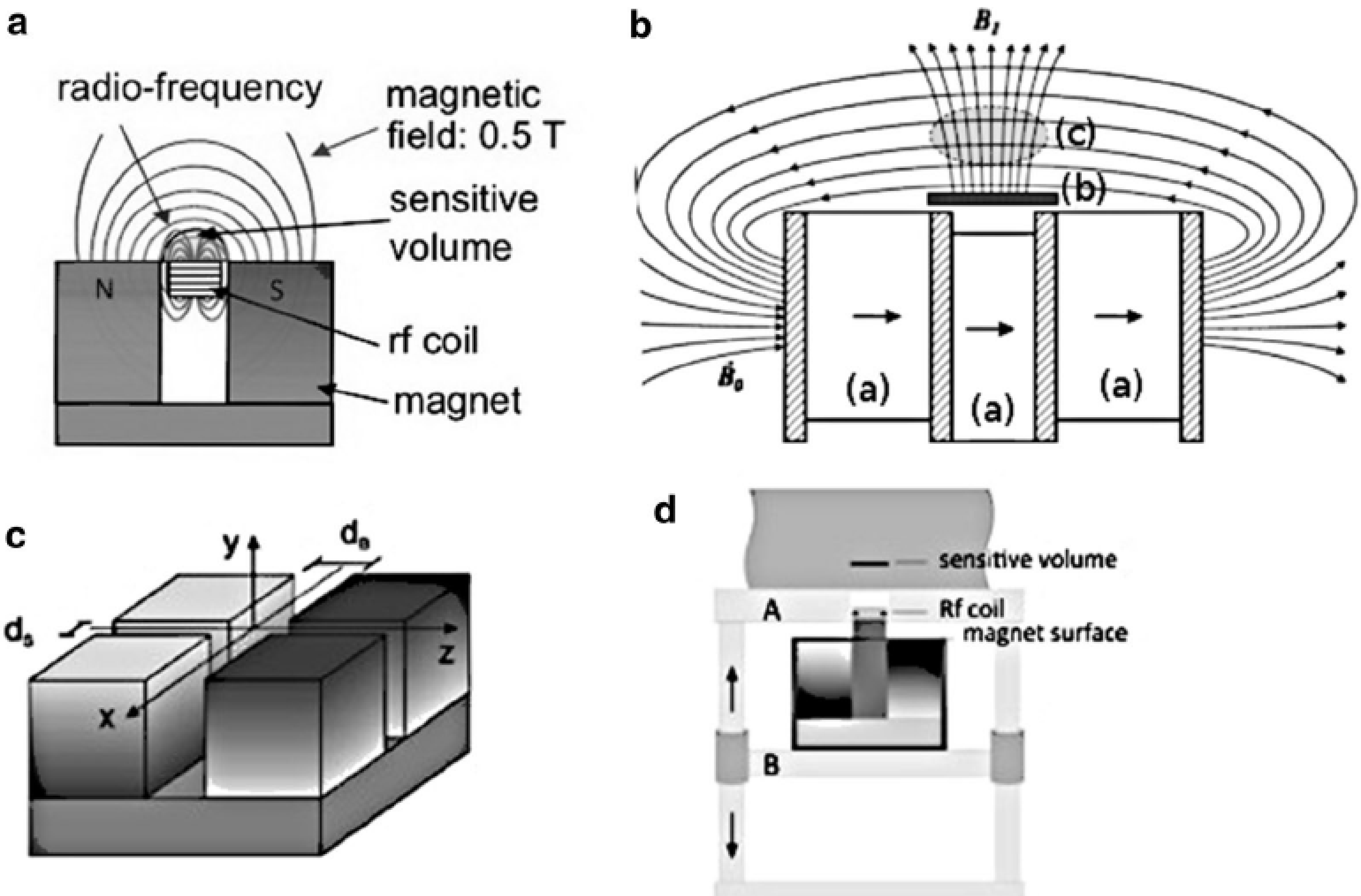

a
radio-frequency
magnetic
field: 0.5 T
sensitive
volume
N
S
rf coil
magnet
b
B_1
(c)
(b)
B_0
(a)
(a)
(a)
c
y
z
x
d
sensitive volume
A
Rf coil
magnet surface
B

NMR Detection of Tomato Paste Spoilage in 1000 Liter Metal Lined Totes

March 7, 2015 process nmr NMR, TD-NMR

Poster to be Presented at the 56th ENC, Asilomar CA, April 2015

NMR Detection of Tomato Paste Spoilage in 1,000 L, Metal Lined Totes

Michele Martin[1]; Paul Giammatteo[2]; Michael McCarthy[1]; Matthew Augustine[1]

[1]University of California, Davis, Davis, California; [2]Process NMR Associates, Danbury, CT

Abstract

Low field nuclear magnetic resonance (NMR) is used as a non-invasive method for detecting spoiled tomato paste. It is shown that the ^{1}H T_1 and T_2 relaxation times change as tomato paste spoils due to changes in viscosity and/or changes in the concentration of paramagnetic compounds. With the goal of developing a spoilage detector that can be used in a tomato processing facility, a γB_0 = 19.5 MHz single-sided handheld NMR instrument is used. Due to the dominance of diffusion on relaxation measurements made with the single sided instrument, the slope of the amplitude of a spin echo for three different delay times is used to provide a viscosity dependent parameter that permits the differentiation between pristine and spoiled tomatoes.

One-Sided NMR – Non-Invasive Analysis of Tomato Paste

Journal of the Science of Food and Agriculture *J Sci Food Agric* 88:2563–2567 (2008)

Rapid determination of the fat content in packaged dairy products by unilateral NMR

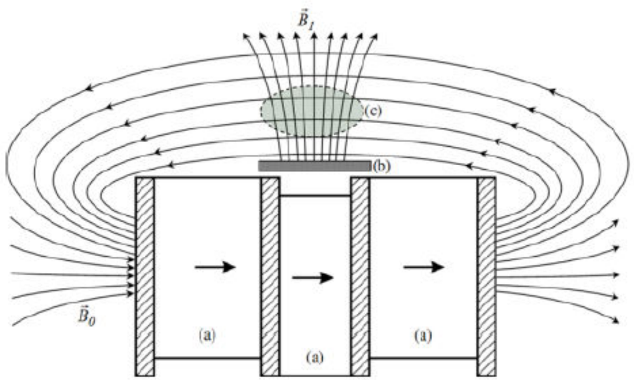

Figure 1. Schematic representation of the magnet array consisting of three block magnets (a). The sensitive spot (c) is located ~1 cm above the face of the magnet. The magnet spacings are optimised to produce a locally homogeneous field in this region creating a relatively large MR sensitive volume above the surface RF coil (b).

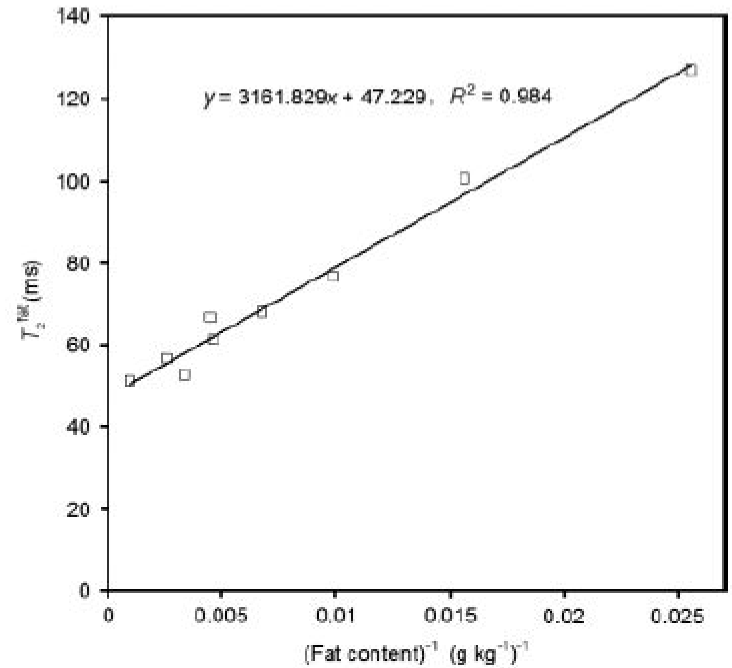

Figure 5. Transverse relaxation time of the fat component T_2^{fat} as a function of the inverse fat content for all studied samples.

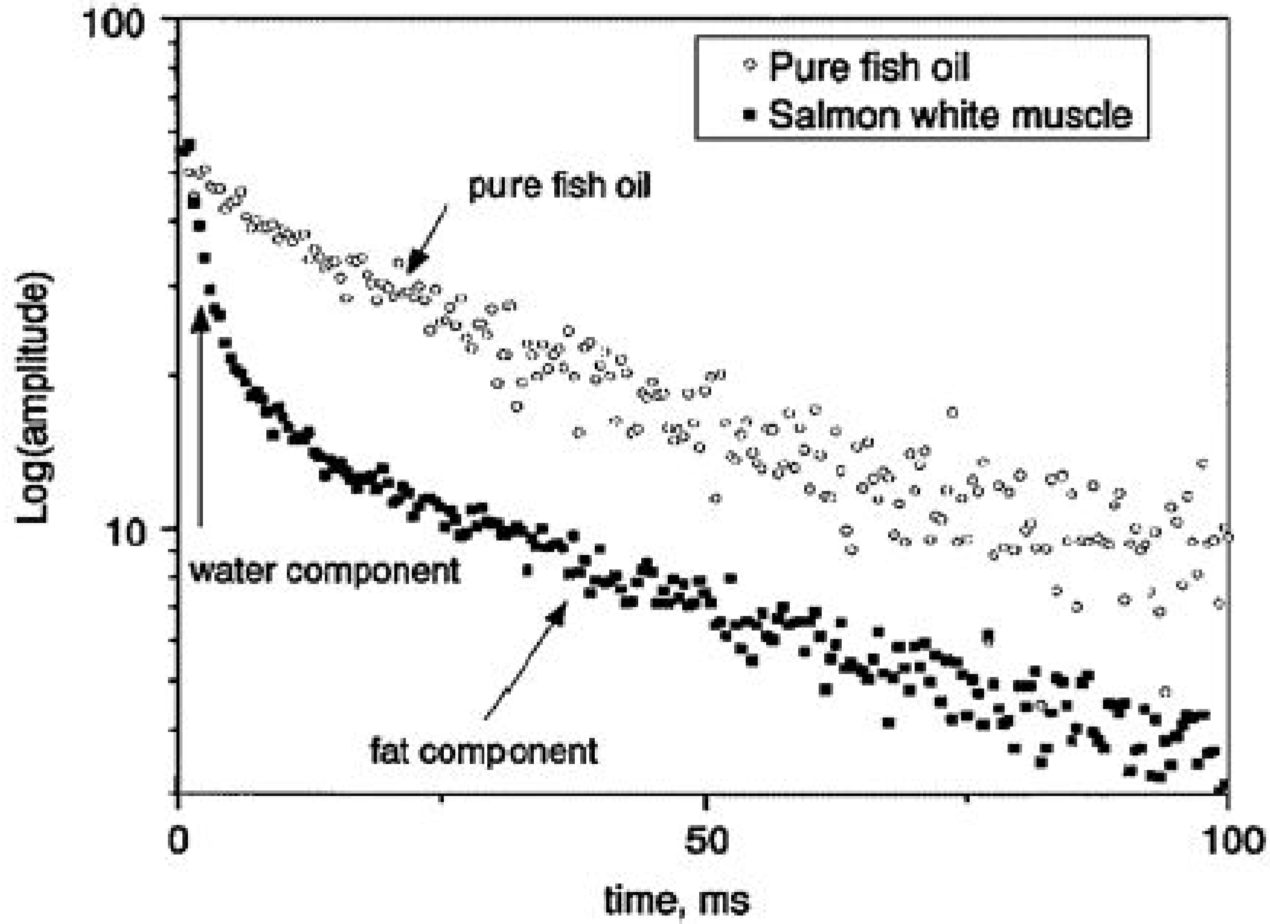

Fig. 4 Transverse relaxation curves of pure fish oil and Atlantic salmon white muscle measured at 4 °C using a single-sided NMR sensor. Reproduced with permission from [42]

Table 1 Reviews of portable NMR technologies and their applications in food science

Reference	Food	Focus	Year
Guthausen et al. [36]	Margarine; mayonnaise	Measurements of fat content	2004
Guthausen et al. [37]	Coffee cream	Water moisture and fat analysis in packaged products	2006
Martini et al. [40]	Vegetable oils	Solid fat content determination	2005
Pedersen et al. [41]	Vegetable oils	Measurements of fat content	2003
Haiduc et al. [42]	Fat emulsions	Microstructural quality of packaged food emulsion	2007
Stork et al. [44]	Bottled beverages	Determination of dissolved oxygen in unopened table waters	2001
Xu et al. [46]	Adulterated virgin olive oil	Detection of the adulteration of virgin olive oil in sealed bottles	2014
Pinter et al. [48]	Tomato paste	Monitoring of spoilage in tomato paste processing industry	2014
Veliyulin et al. [43]	Salmon	Fat content in live fish	2005
Veliyulin et al. [28]	Dairy products	Measurements of fat content in packaged dairy products	2008
Capitani et al. [49]	Kiwifruit	Water status as a function of season	2010
Capitani et al. [50]	Kiwifruit	Monitoring of development and ripening	2013
Capitani et al. [51]	Blueberry	Monitoring of shelf life	2014
Adiletta et al. [52]	Pear	Monitoring of drying process	2015

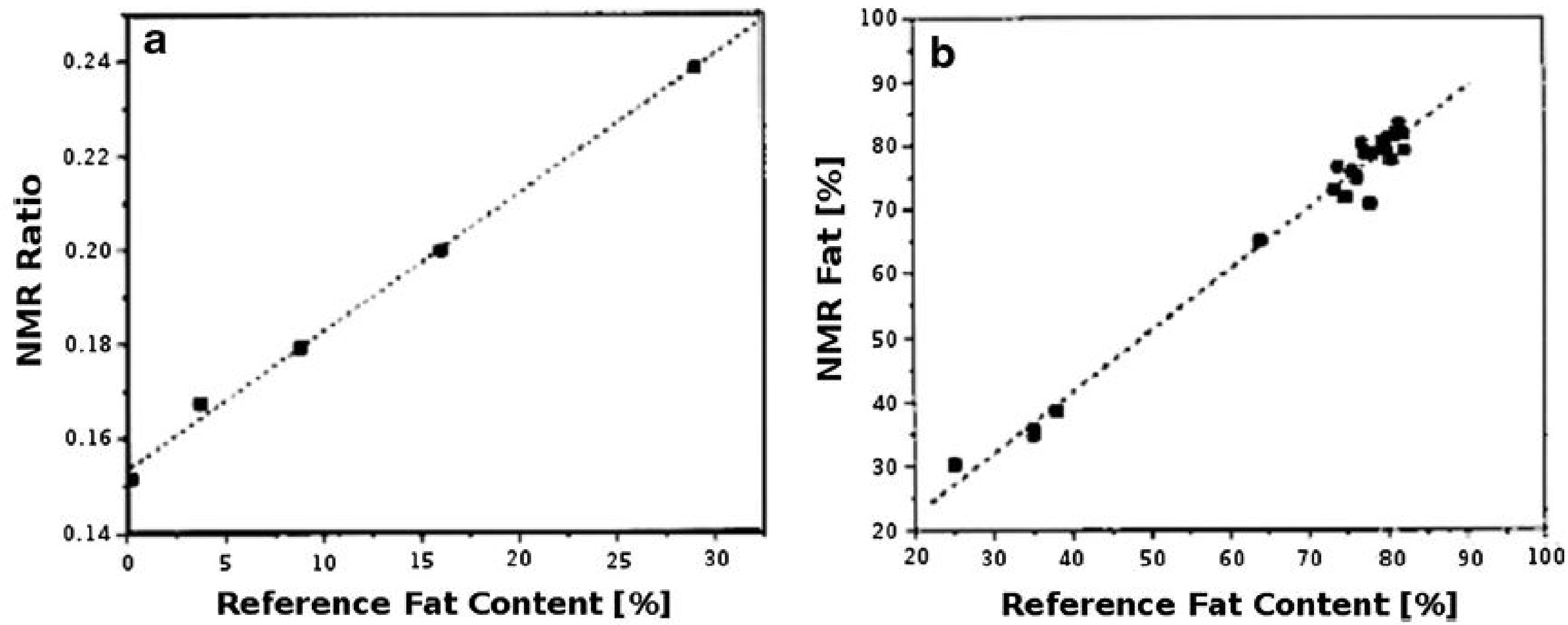

Fig. 2 **a** Correlation of the NMR ratio with the reference fat content of coffee creams. **b** Correlation diagram for measurements on mayonnaises and margarines with the reference fat content. Reproduced with permission from [34]

Bruker works with Unilever to analyse droplet size distribution

By Joseph James Whitworth
11-May-2016 - Last updated on 12-May-2016 at 09:49 GMT

Picture: Bruker. The minspec G-Var droplet size analyzer

Bruker has launched a method for fast determination of droplet size distribution in food emulsions based on collaboration with Unilever.

Influence of the season on the relationships between NMR transverse relaxation data and water-holding capacity of turkey breast meat

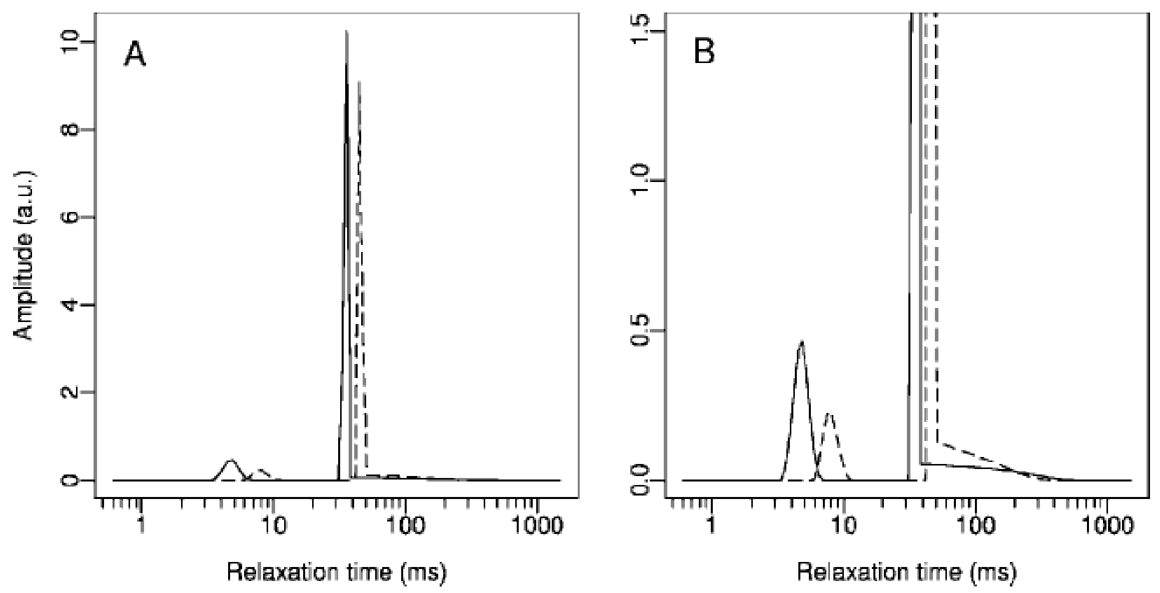

Figure 2. UPEN[16] distributions of transverse relaxation times obtained from the average summer (solid line) and winter (broken line) CPMG relaxation curves of turkey meat. Panel B is an expansion of panel A showing the long relaxation tail due to extracellular water.

Introduction

NMR signal

Spectroscopy

T1-T2 relaxation

Diffusion

Imaging

Plastics

Conclusions

For short time + diffusion dominated

$\omega = \gamma B \rightarrow \quad \phi = \text{Integral}(\gamma B\, dt)$

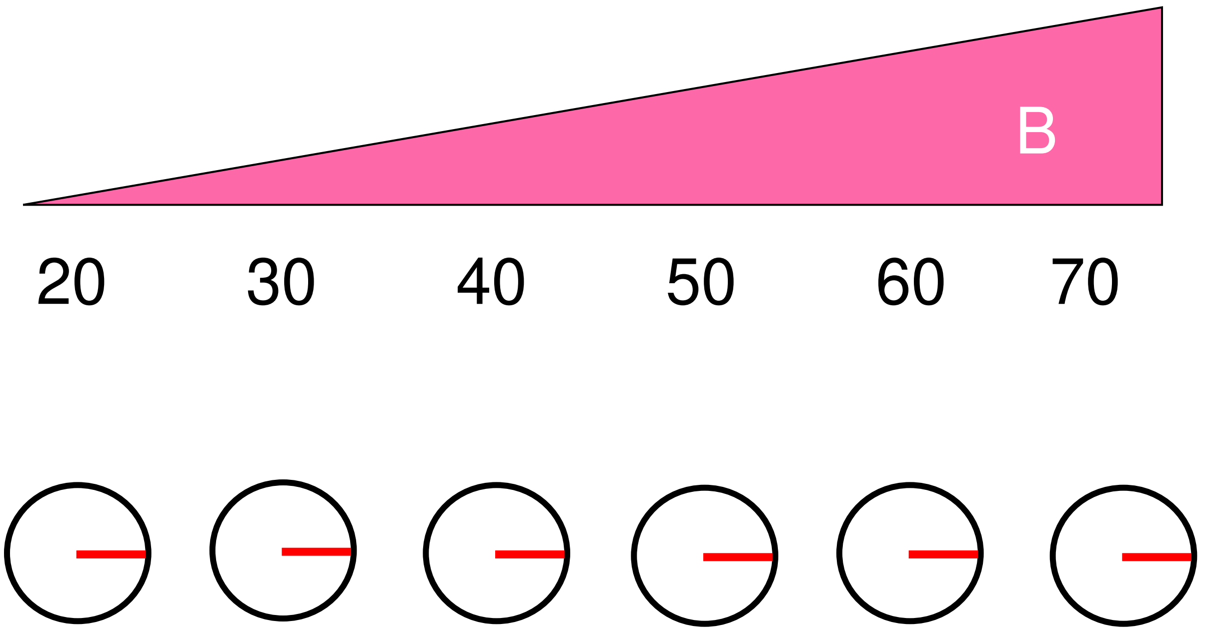

Bound water

Bound water

$\omega=\gamma B \rightarrow -\phi = -$ Integral (γ B dt)

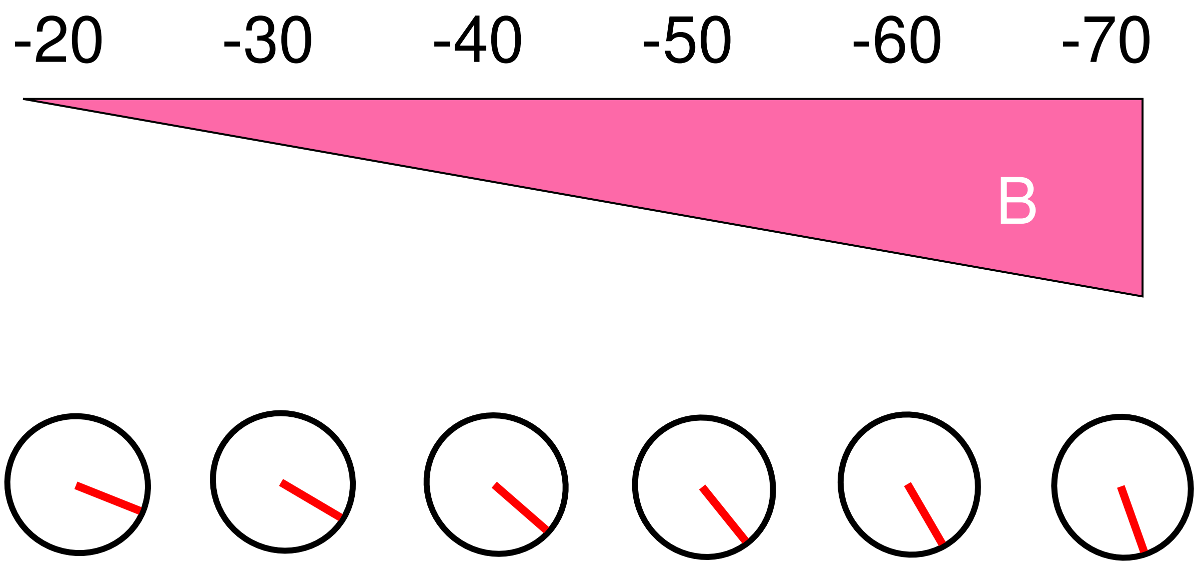

Bound water

Bound water

wait for a short time Δ....

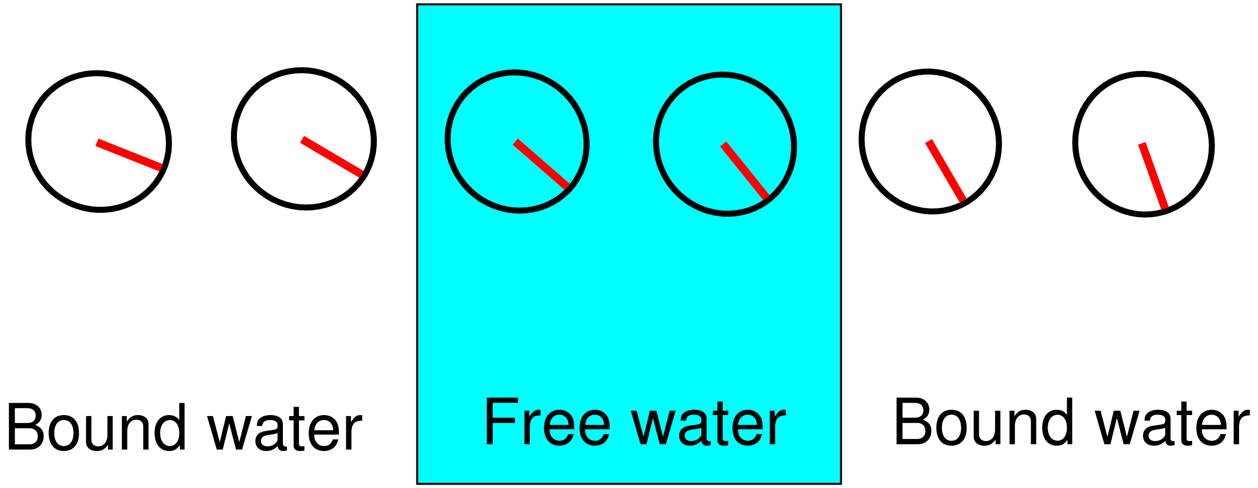

$\omega = \gamma B \rightarrow -\phi = -\text{Integral}(\gamma B\, dt)$

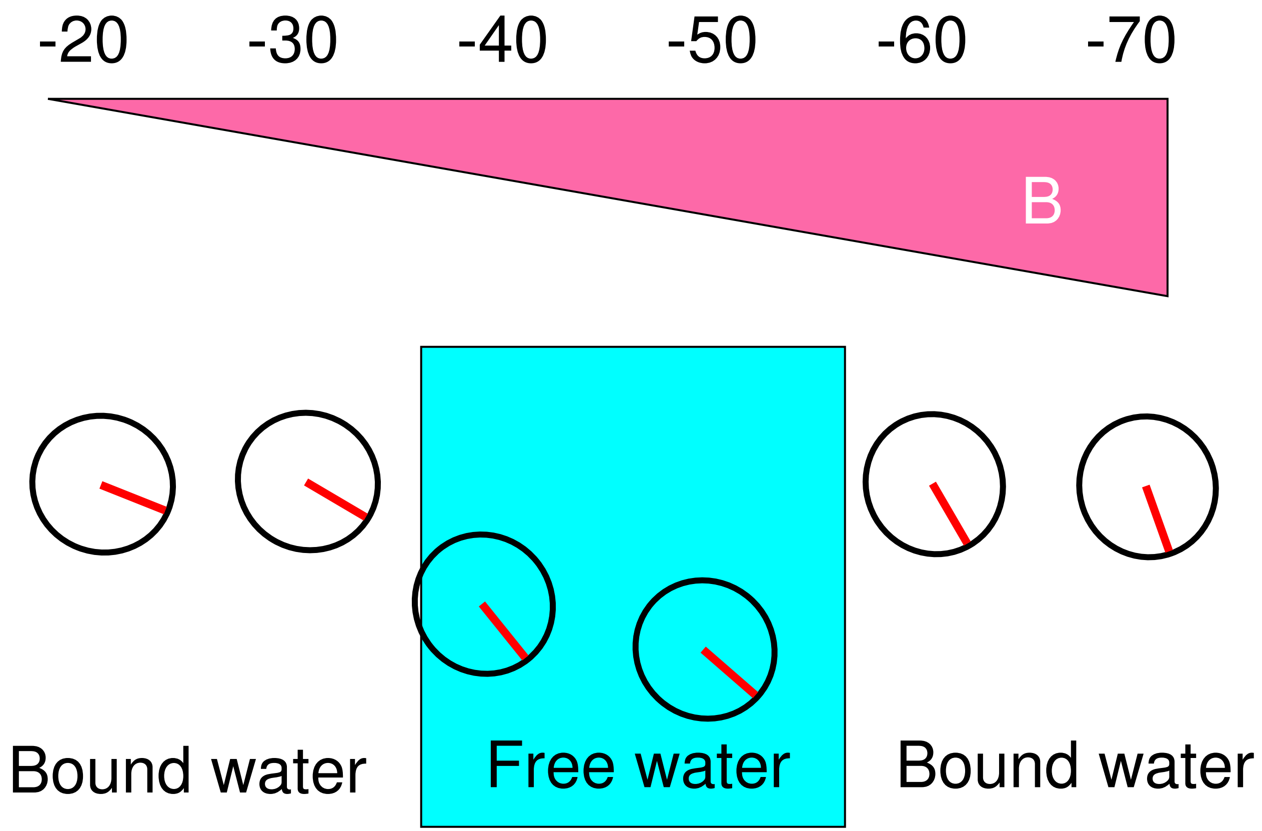

Diffusion → phase incoherence → $S/S_0 = \exp(-b D)$

COMBINE : one measurement both diffusion + poresize distribution

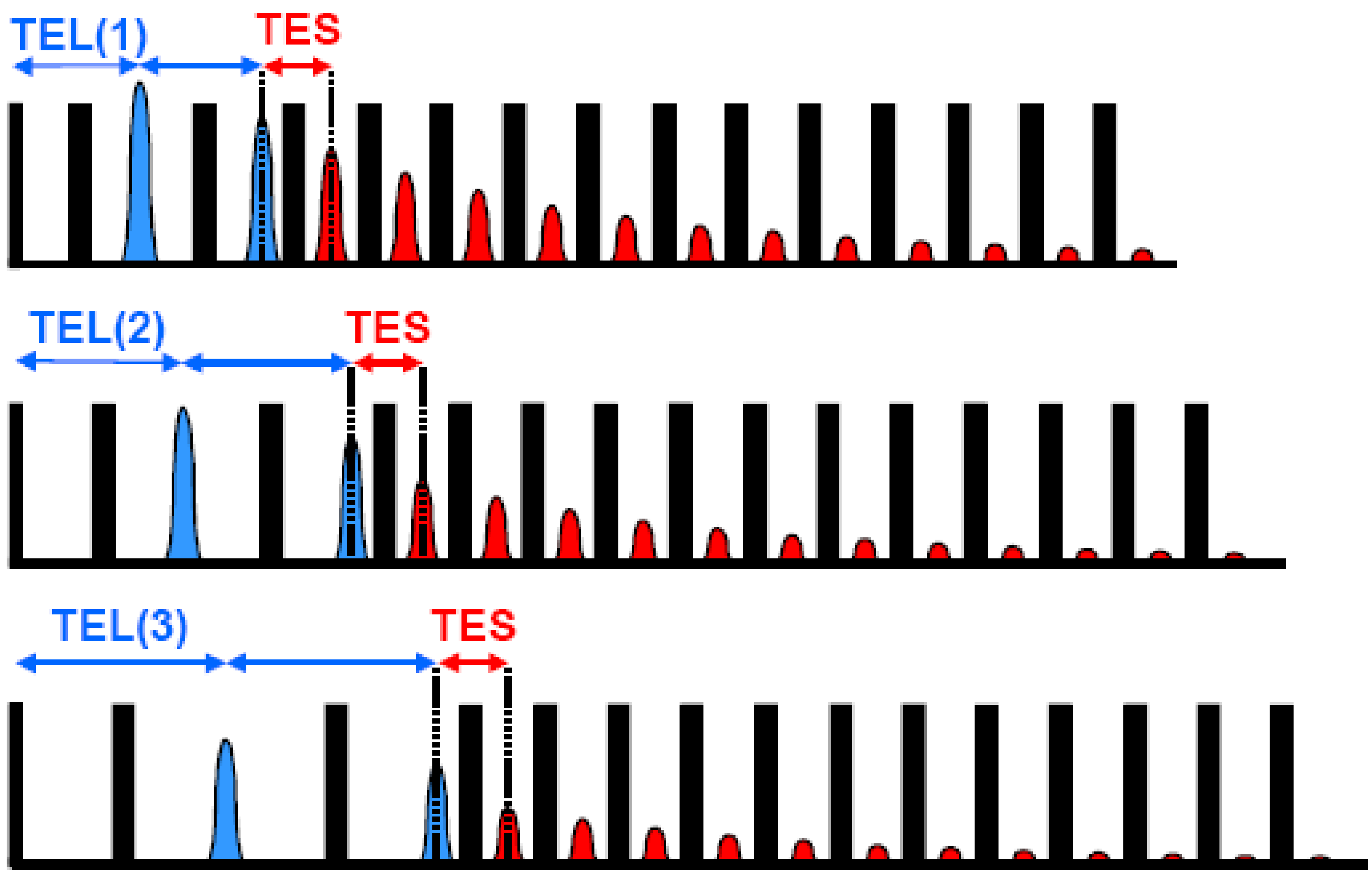

diffusion

Pore distribution

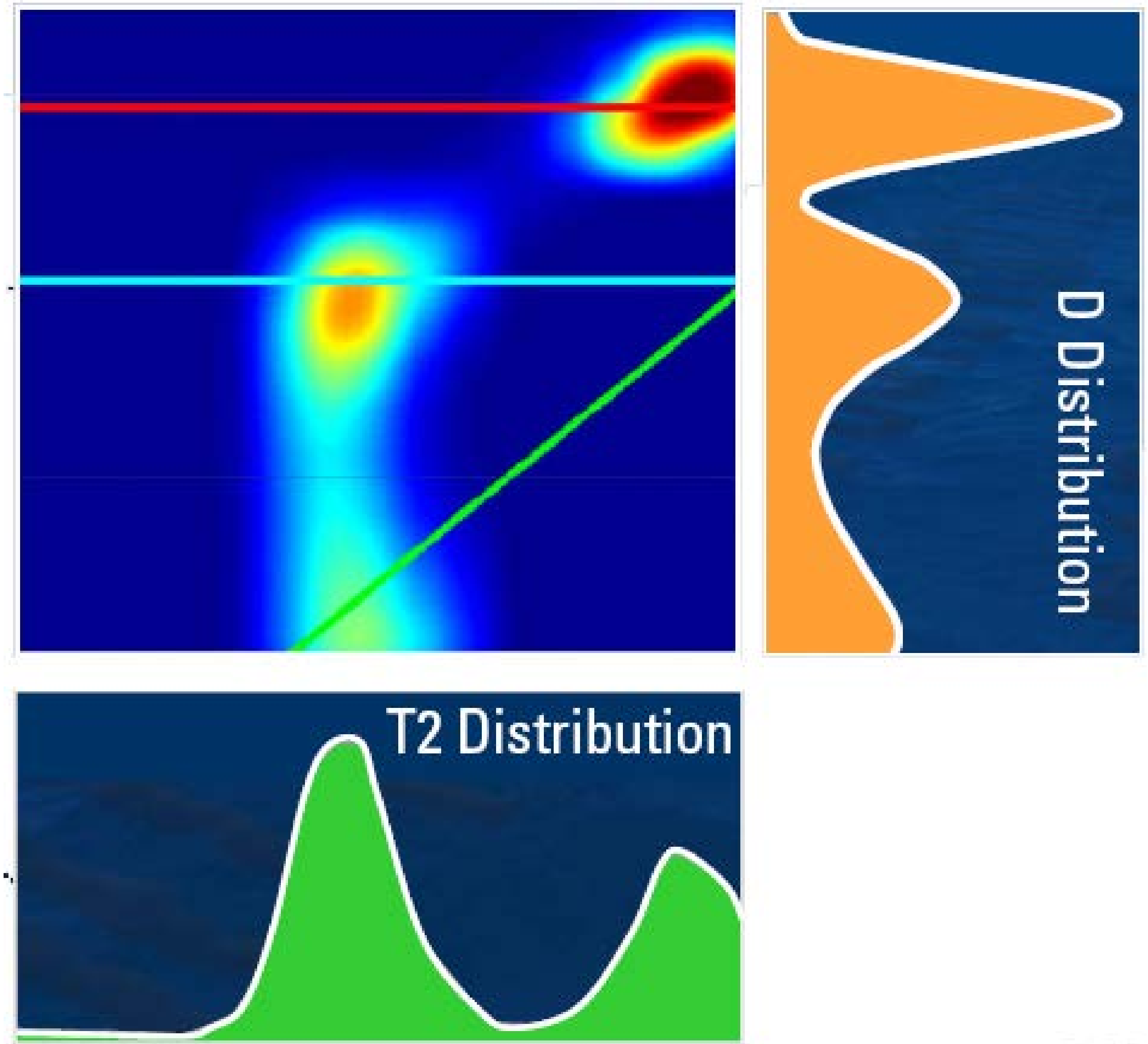
D Distribution
T2 Distribution

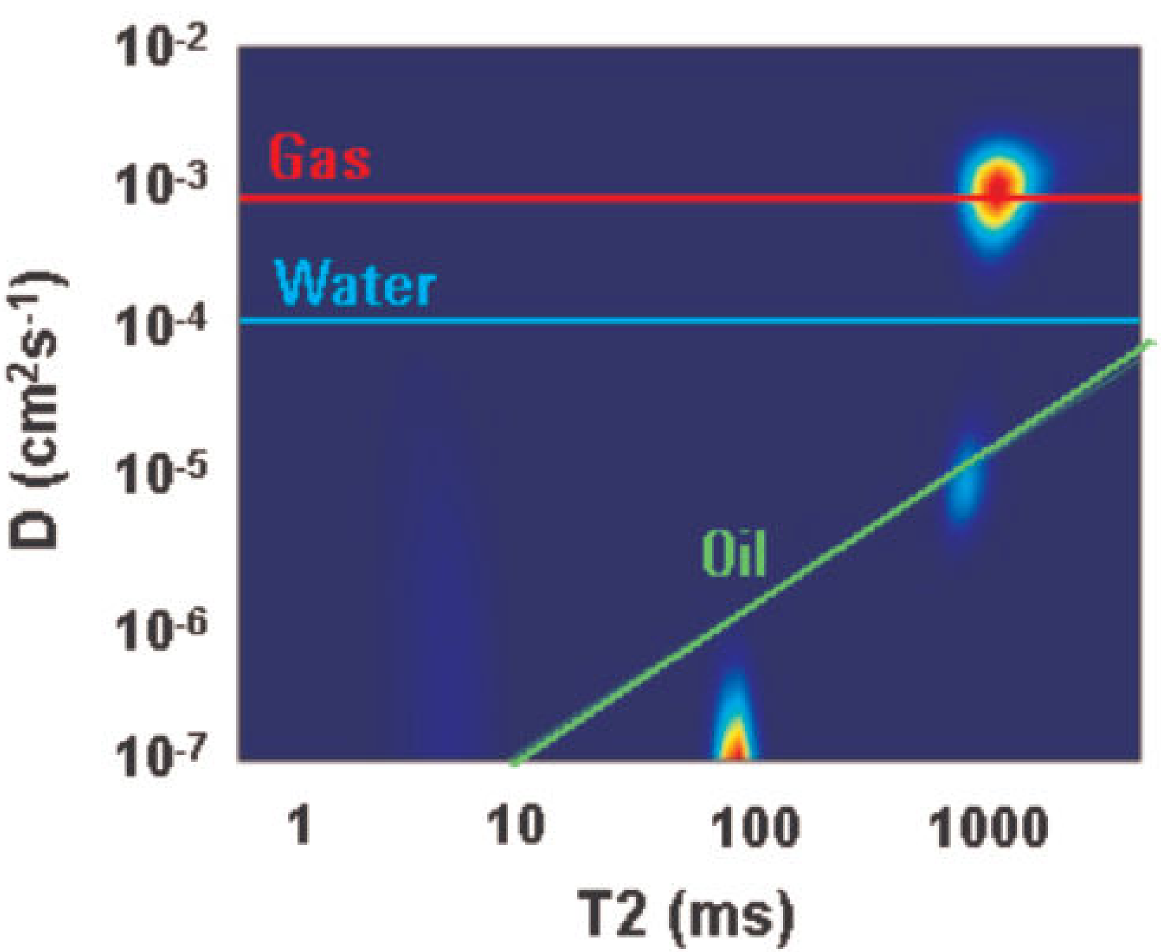

D-T_2 map from a gas-bearing sand in a North Sea well drilled with OBM. The data were acquired as a station log using the CMR tool. The bright color peaks correspond to different fluids. The overlay lines represent the ideal responses of water, oil, and gas.

Inside out NMR

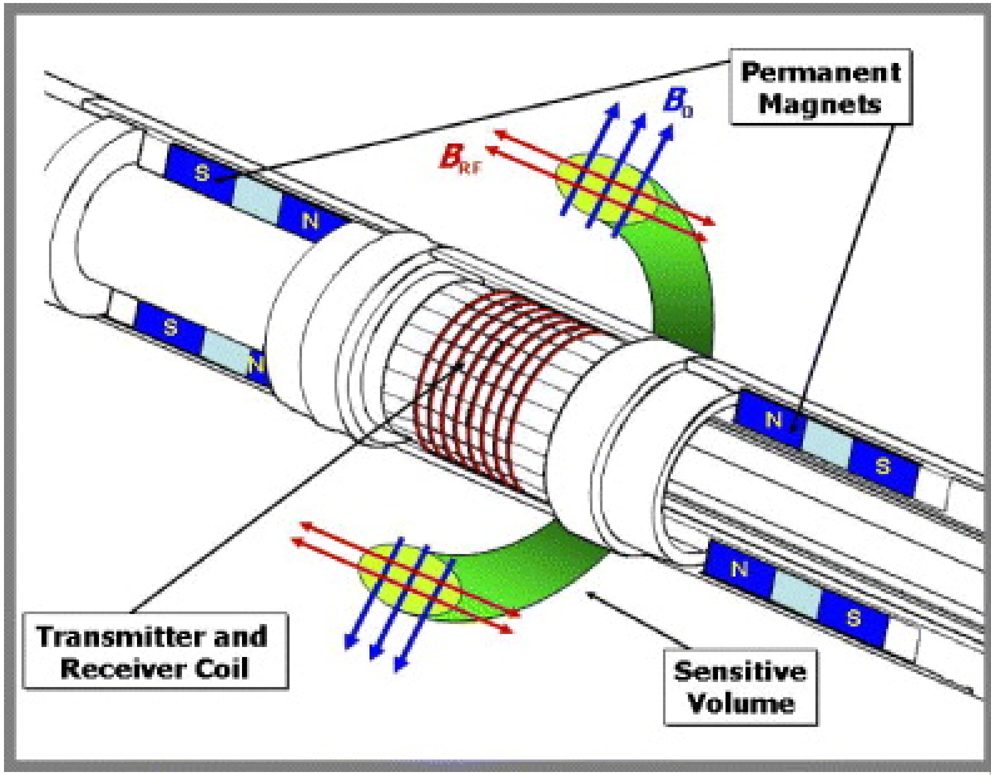

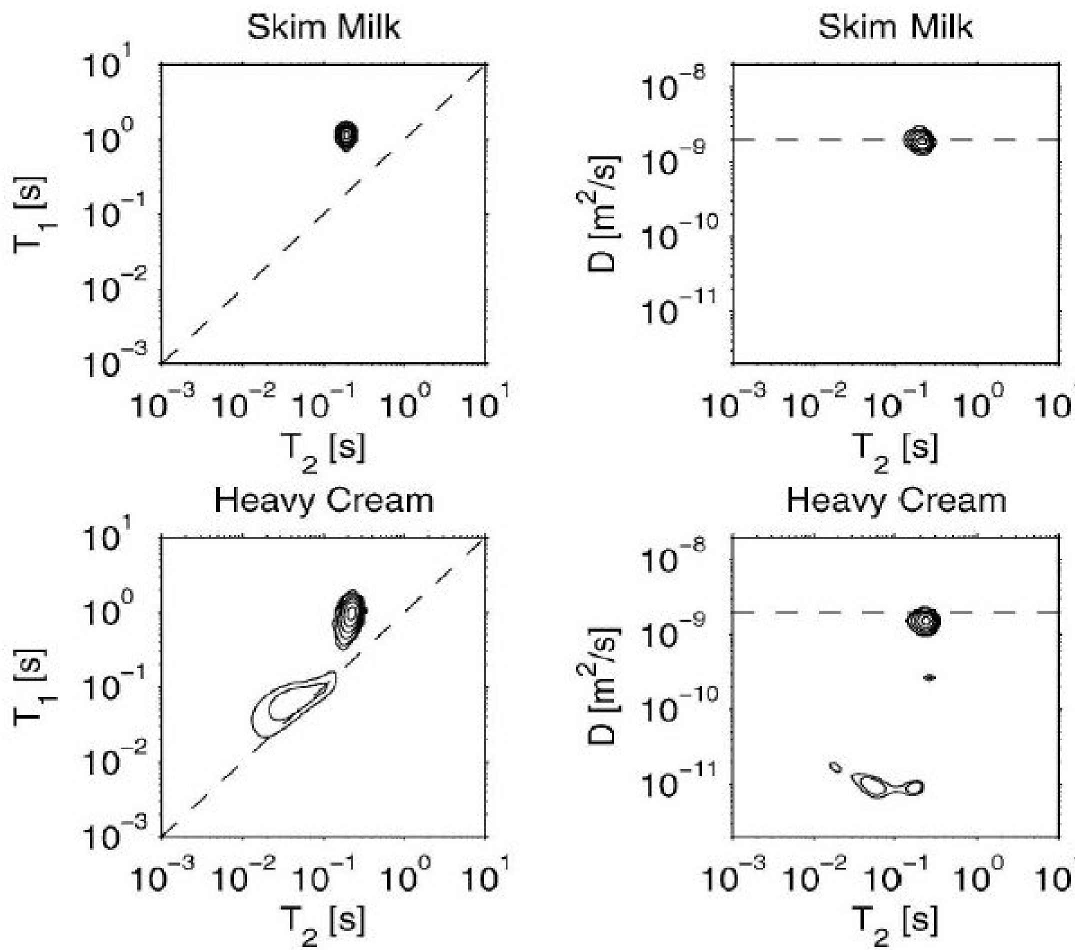

Figure 6. Comparison of T_1–T_2 distribution functions (left) and D–T_2 distribution functions (right) measured on four different dairy products: skim milk, heavy cream. The dashed lines in the T_1–T_2 distribution functions indicate T_1=T_2, whereas in the D–T_2 distribution functions, they indicate the diffusion coefficient of water. Contour lines are shown at 10, 30, 50, 70, and 90% of maximum values in each panel. For the samples of heavy cream and Brie, we show in addition the 5% line.

Introduction

NMR signal

Spectroscopy

T1-T2 relaxation

Diffusion

Imaging

Plastics

Conclusions

Magnetic Resonance Imaging

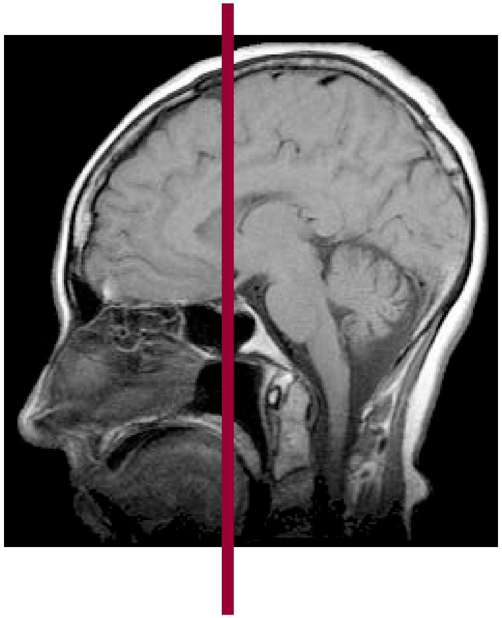

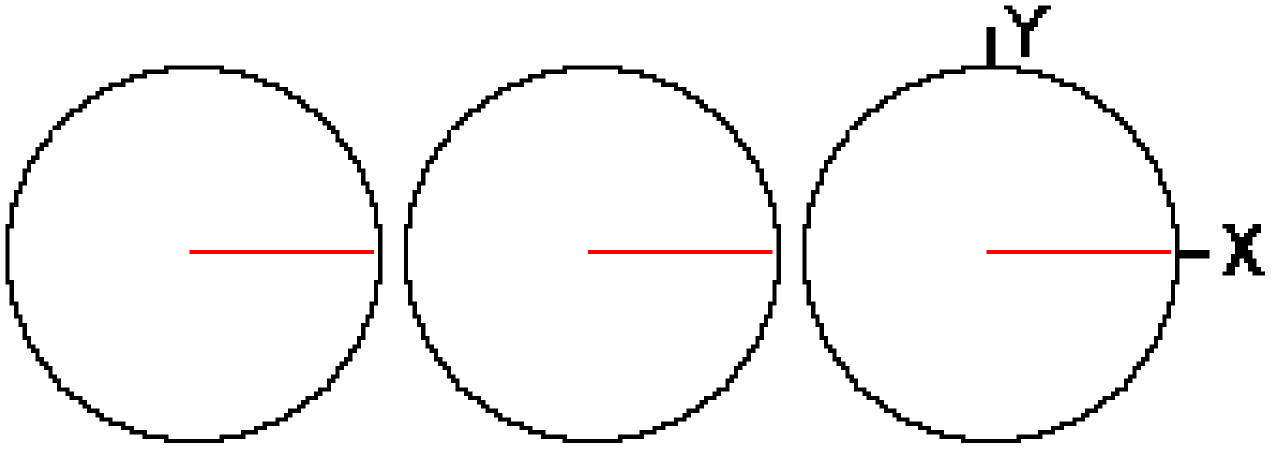
Y
X

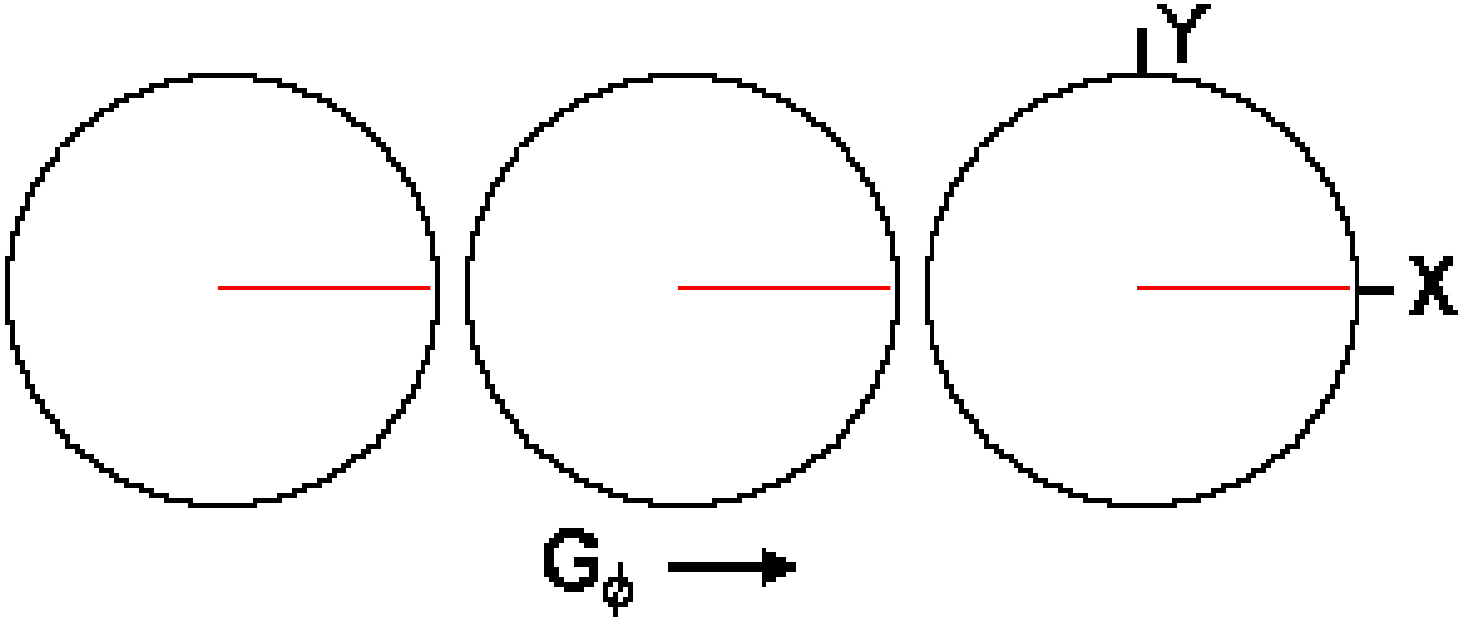

Frequency encoding

Spatial Encoding of the MR Signal

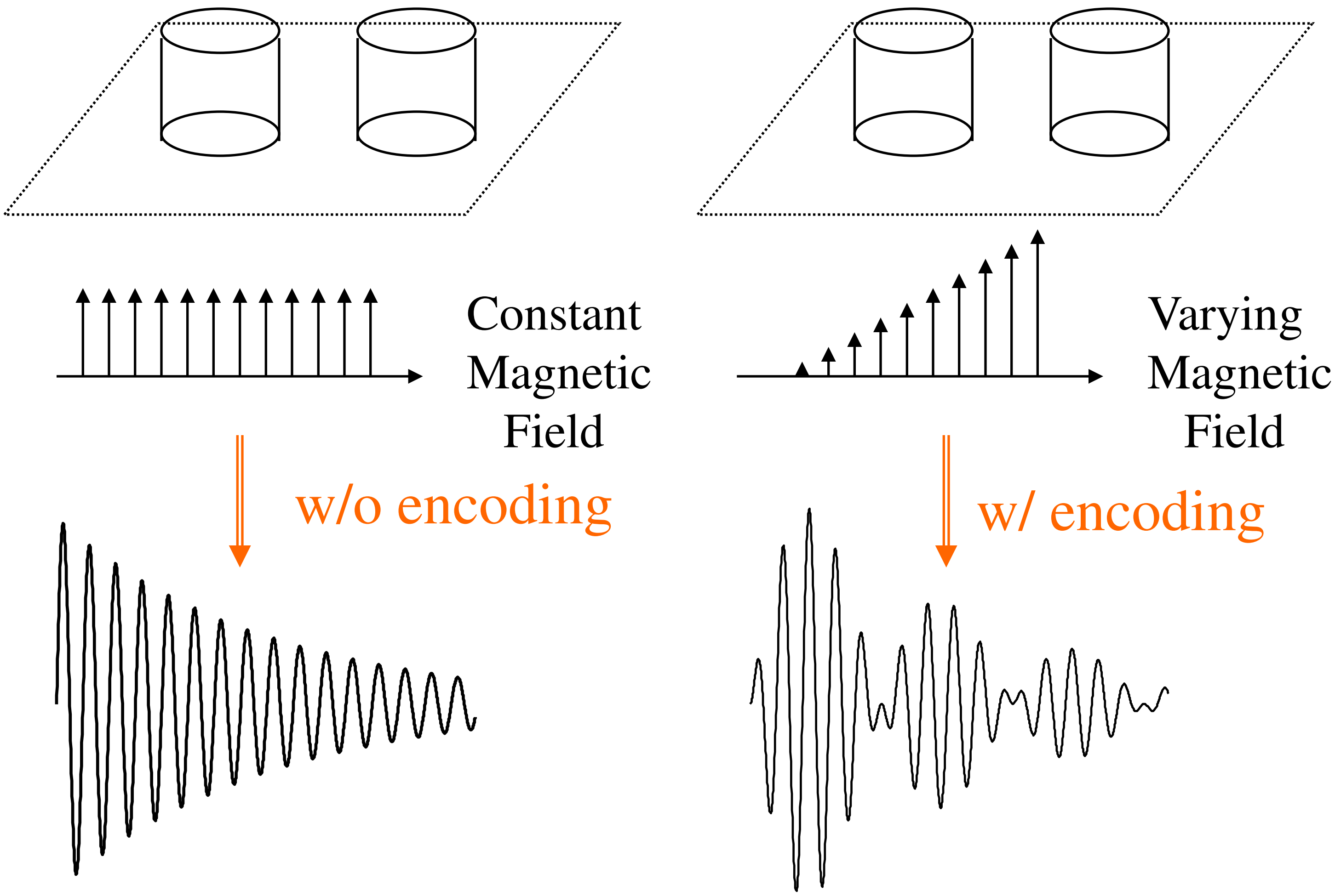

Spatial Encoding of the MR Signal

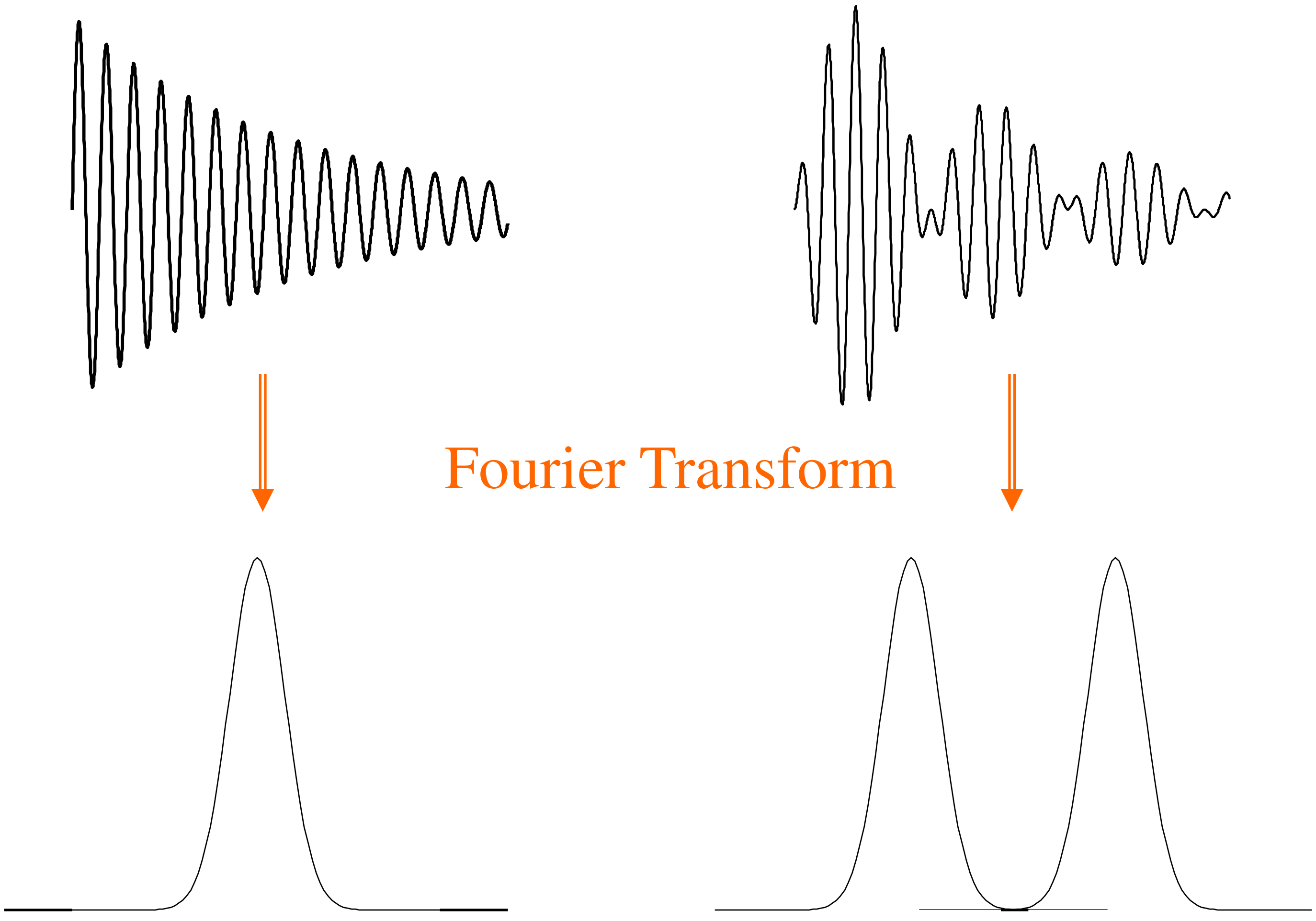

Backward projection

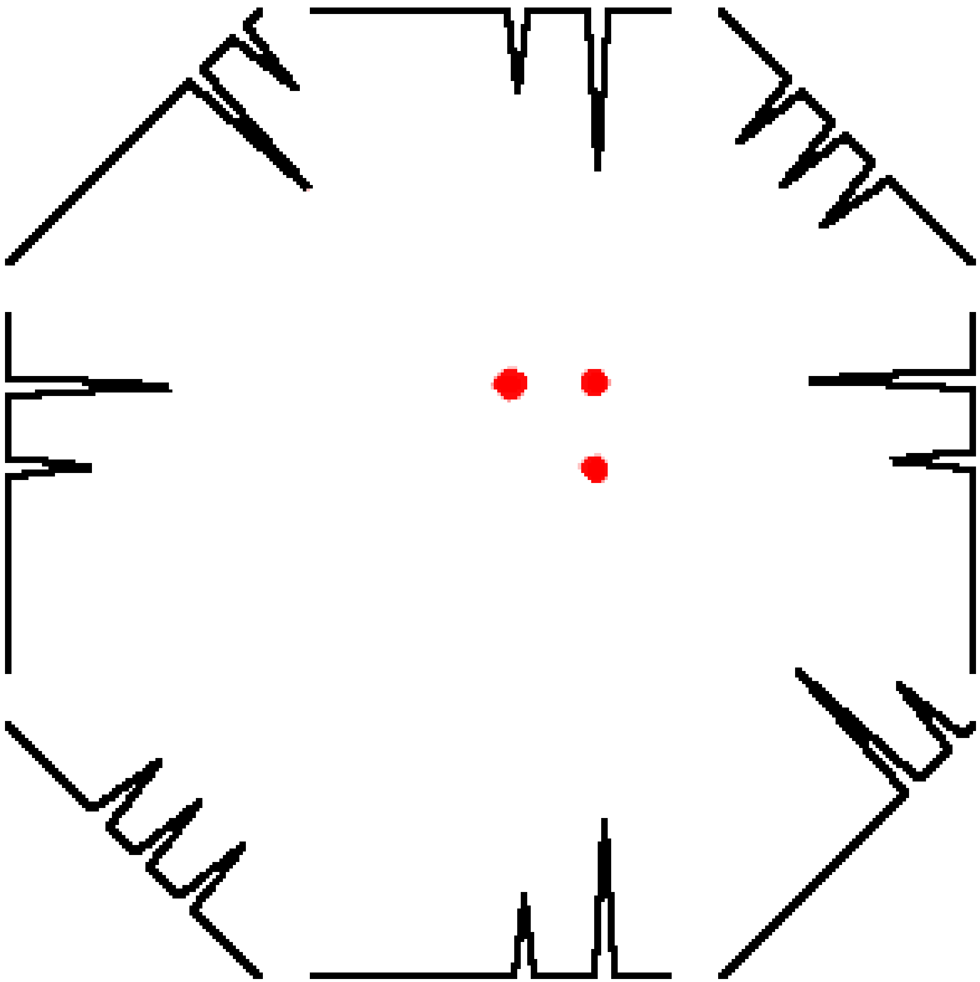

3D imaging: http://www.cis.rit.edu/htbooks/mri/

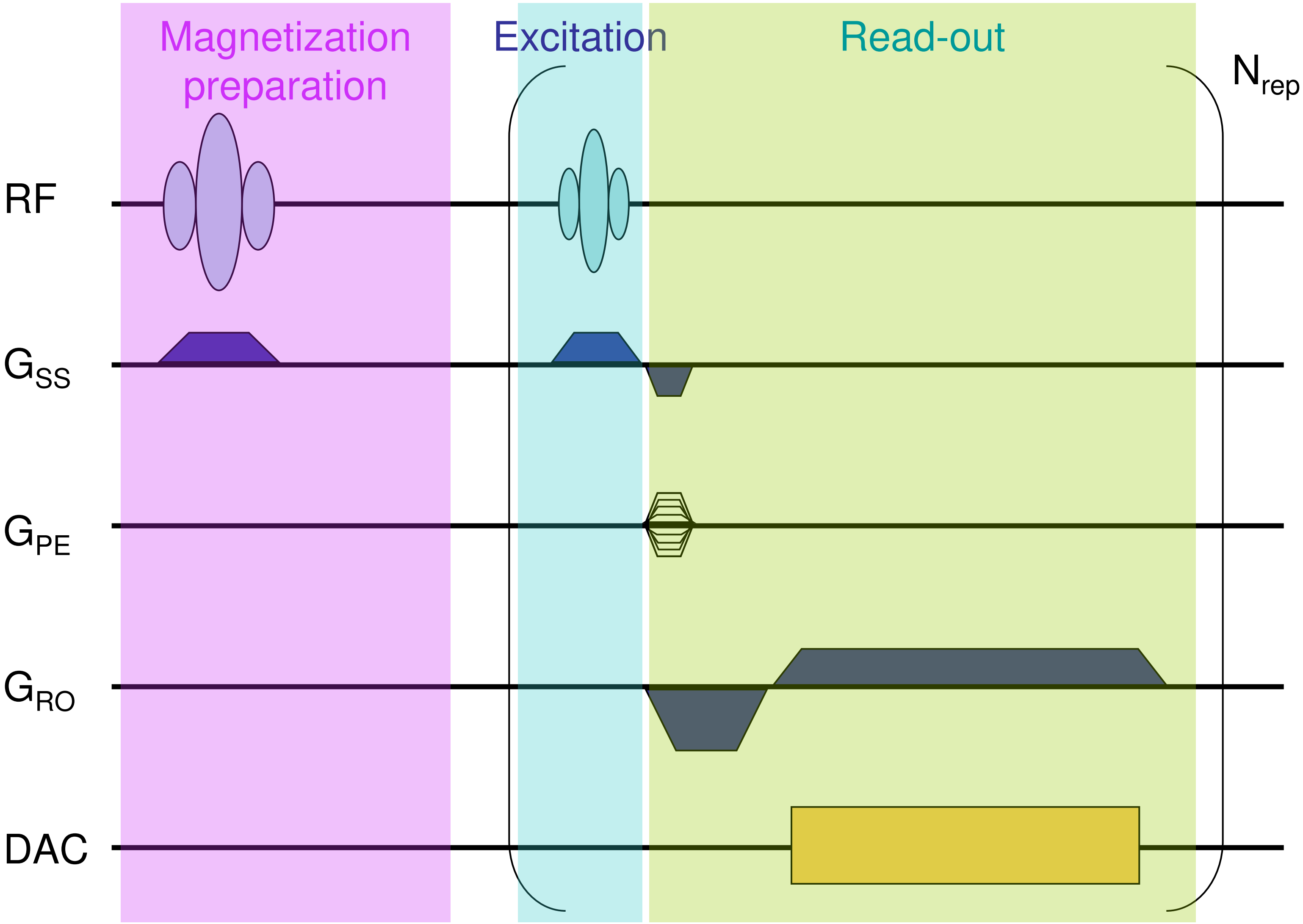

NEED SWITCHING GRADIENT COILS

Water relaxation

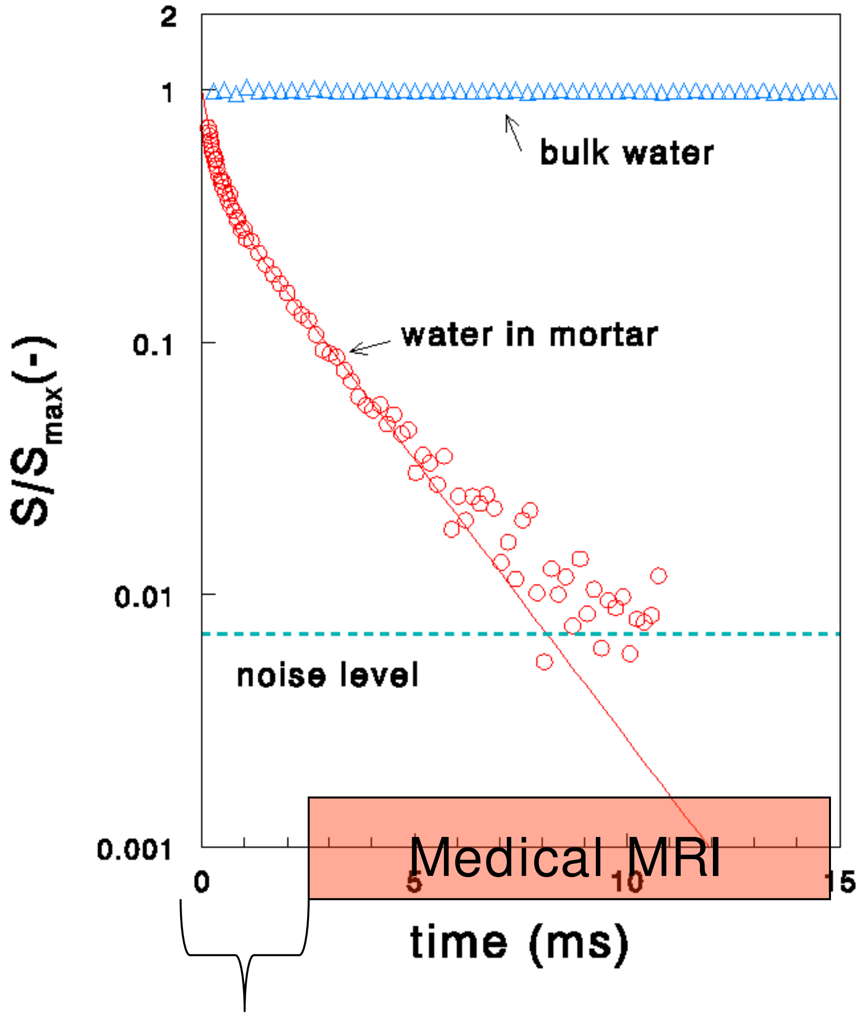

Window of materials you can not see, e.g., plastics etc

Pulsed NMR signal (spin-echo experiment)

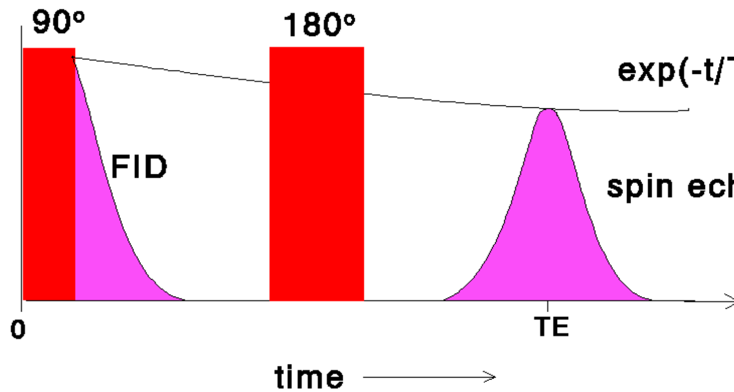

Information on pore water and ion distribution in pores

Amplitude spin-echo

$$S \sim G\rho\,[1-\exp(-TR/T_1)]\,\exp(-TE/T_2)$$

G = relative sensitivity (for ^{1}H G= 1, ^{23}Na= 0.1)

ρ = density of nuclei

T_1 = spin lattice relaxation

TR = repetition time experiment

T2 = spin-spin relaxation time

TE = spin-echo time

Signal proportional to moisture content or Na content

Na lower sensitivity longer measurement time

see,e.g.,E.L. Hahn,Phys. Rev., 80, 580-594 (1950)

High Field System – Industrial System 1.0 Tesla

No external field

Industrial grade

Large volume

1 Tesla Field Strength

High performance

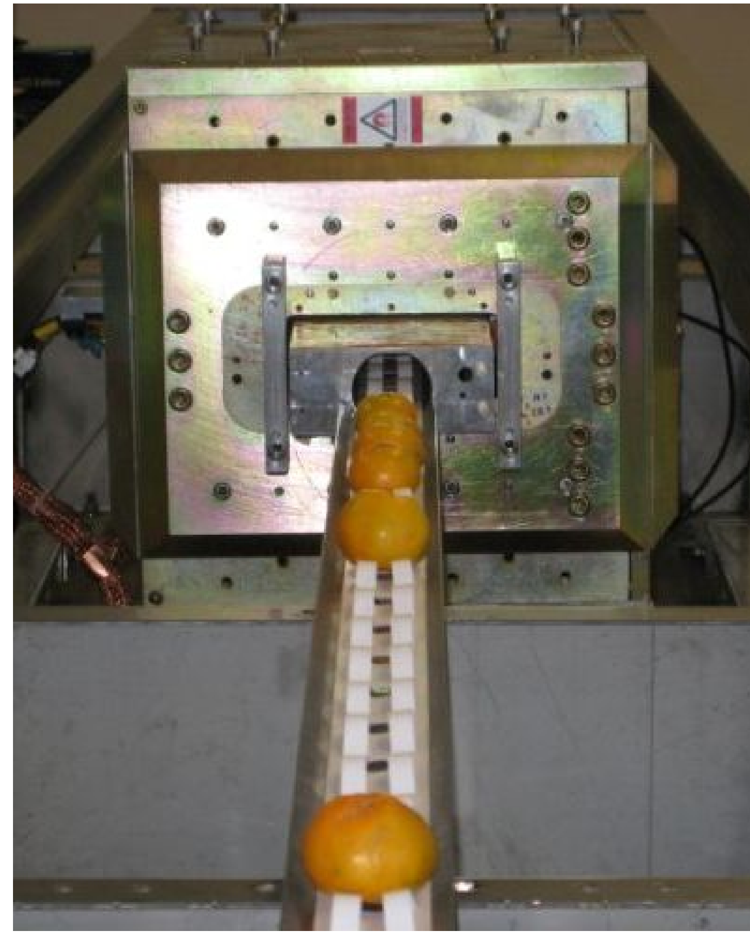

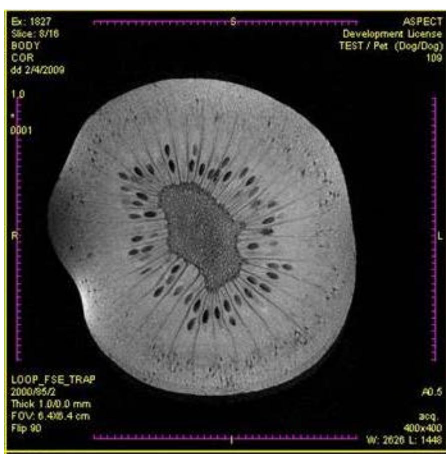

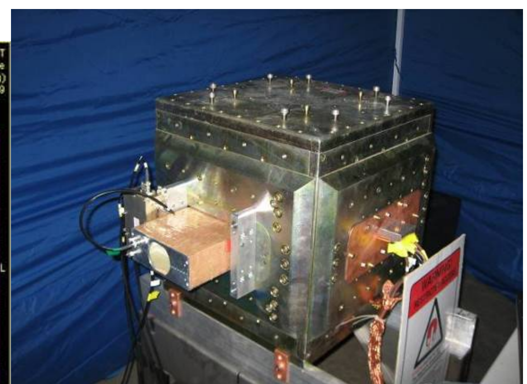

Photos courtesy of ASPeCT Magnet Technologies Ltd.
www.aspect-mr.com

Advanced in-line sensors for sorting fruit

Using a Partial Least Squares-Discriminant Analysis applied to MRI data it is predicted that yields for the process can be increased by approximately 10%

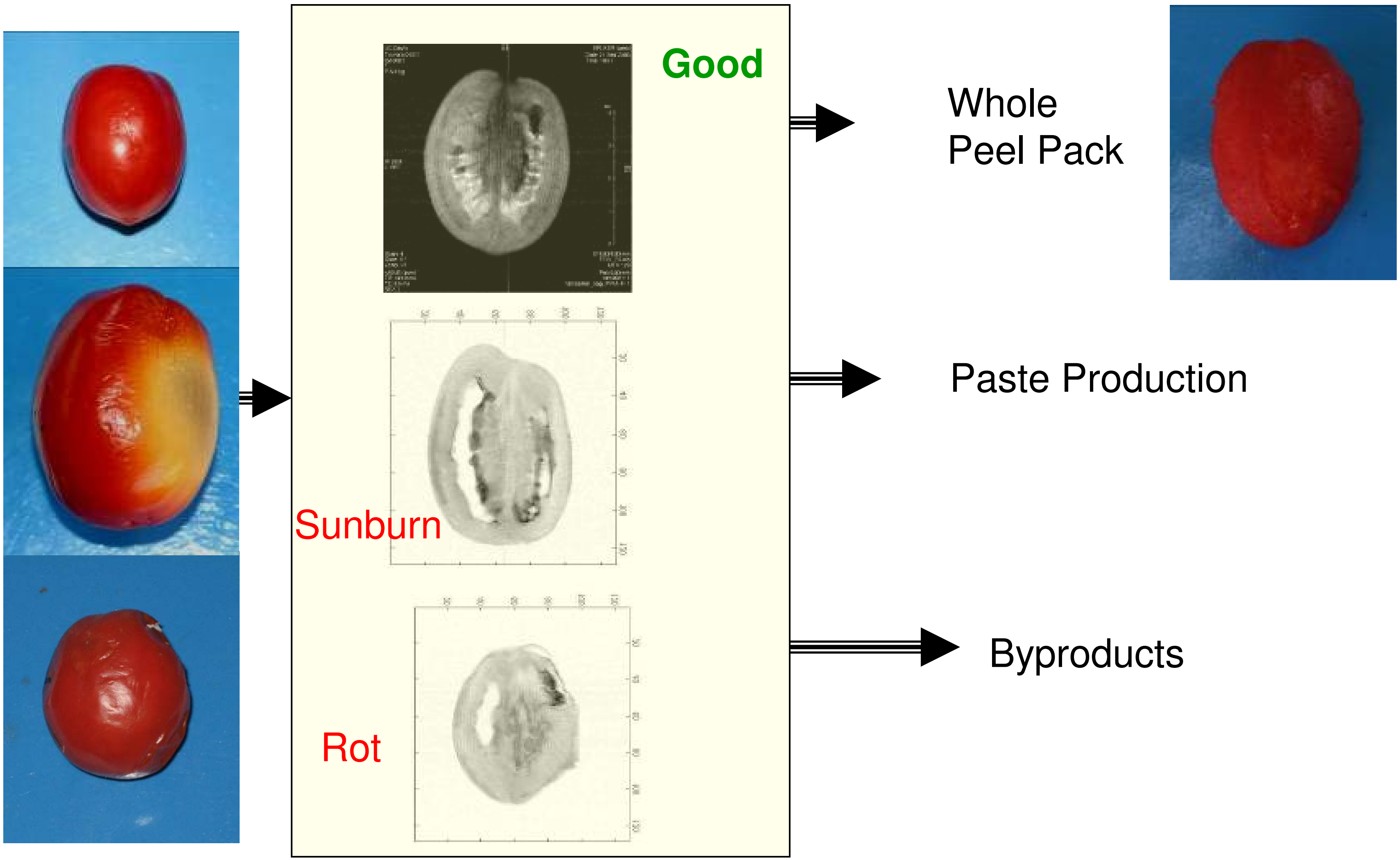

Magnetic Resonance Imaging

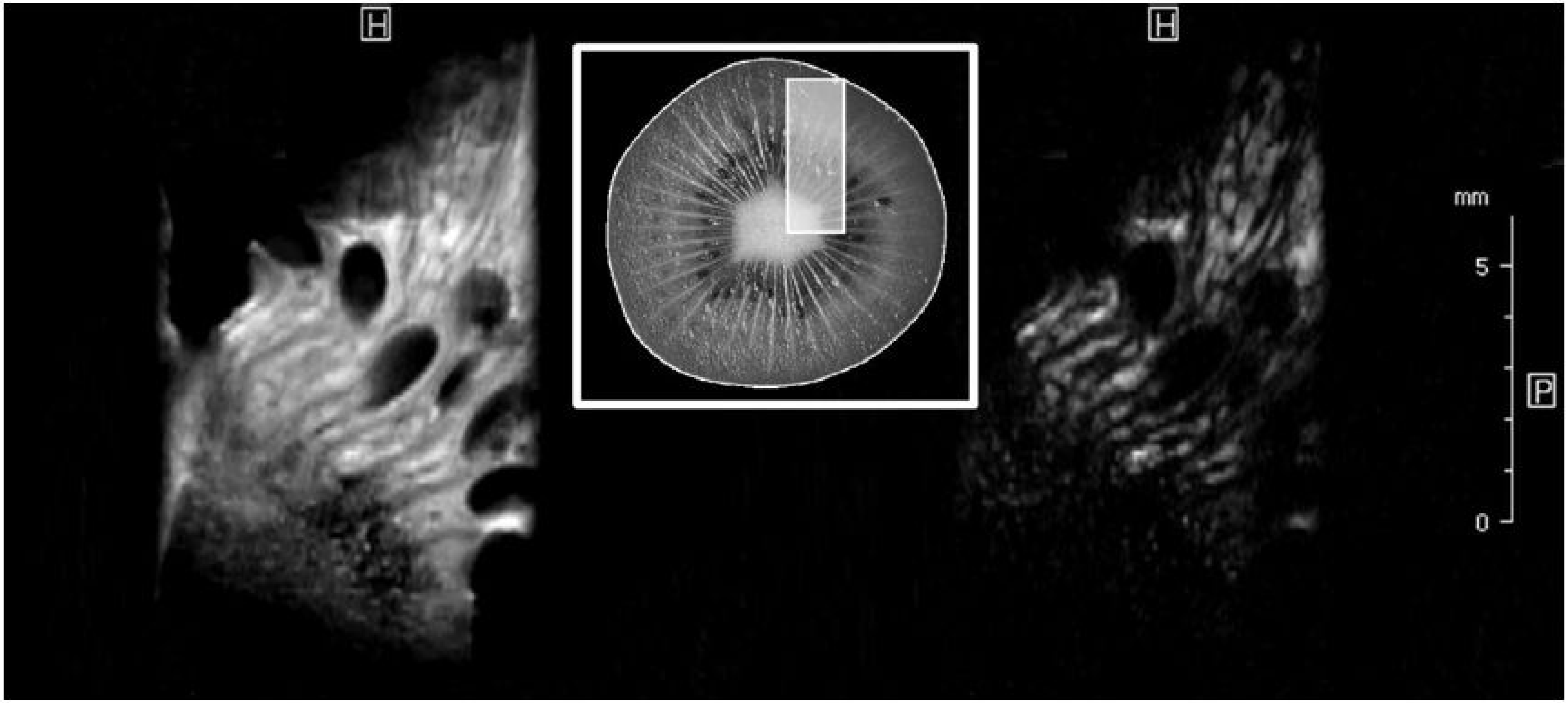

Figure 10. Spin density (left-hand) and T_2-weighted (right-hand) axial MR images of a kiwifruit (*Actinidia chinensis*). The MR images refer to the fruit region included in the orange rectangle of the central reference image. The application of a spin-spin modulation (total spin-echo delay of 150 ms) permitted to suppress the columella tissue and highlight the fruit pulp (Unpublished data).

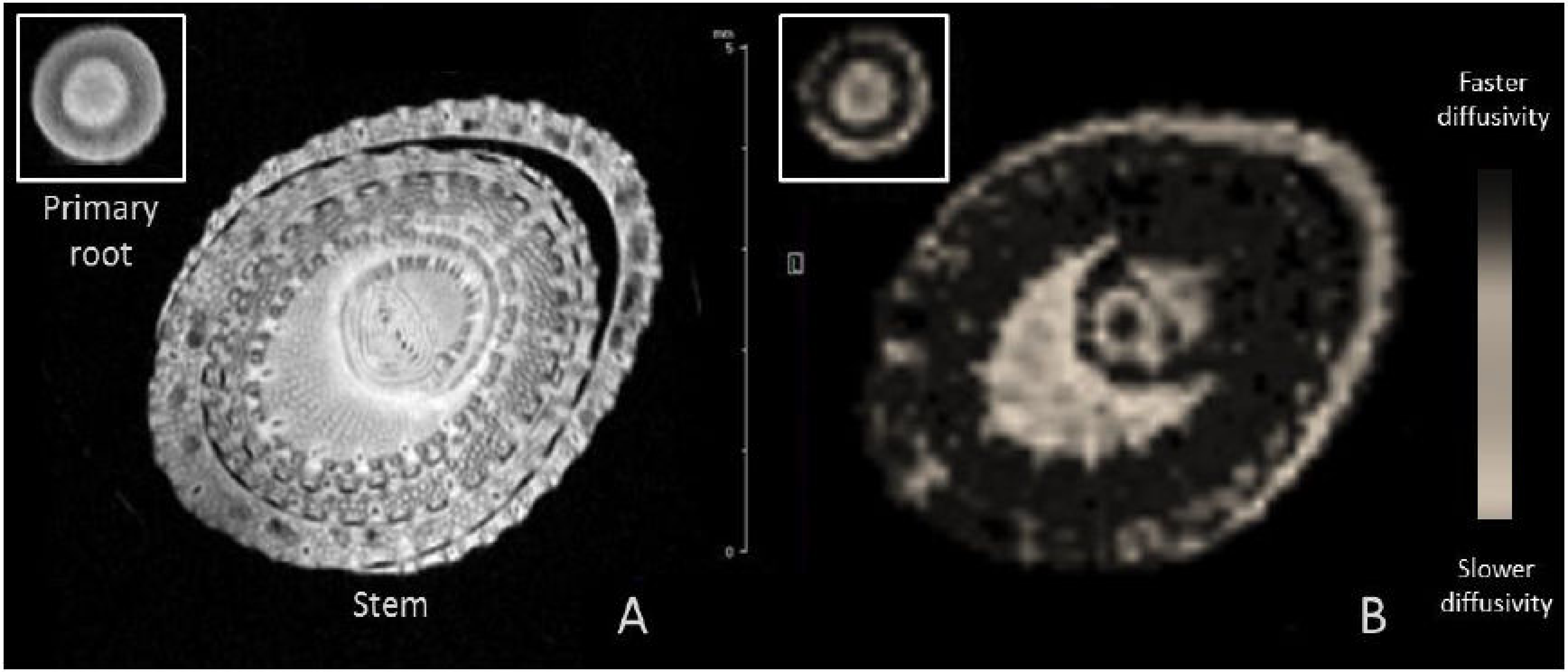

Figure 11. Spin density (A) and diffusion-based parametric (B) axial MR images of both stem and primary root of a young maize plant (*Zea mays*). The colors associated to the latter image are modulated as a function of diffusivity and permit to identify its spatial variability within maize plant tissues (Unpublished data).

http://www.spinlock.com.ar/

Figure 5. Halbach magnet for flow analysis with pre-polarizer magnet (Colnago et al., 2014).

Detection of Pits in Olives Under Motion by Nuclear Magnetic Resonance

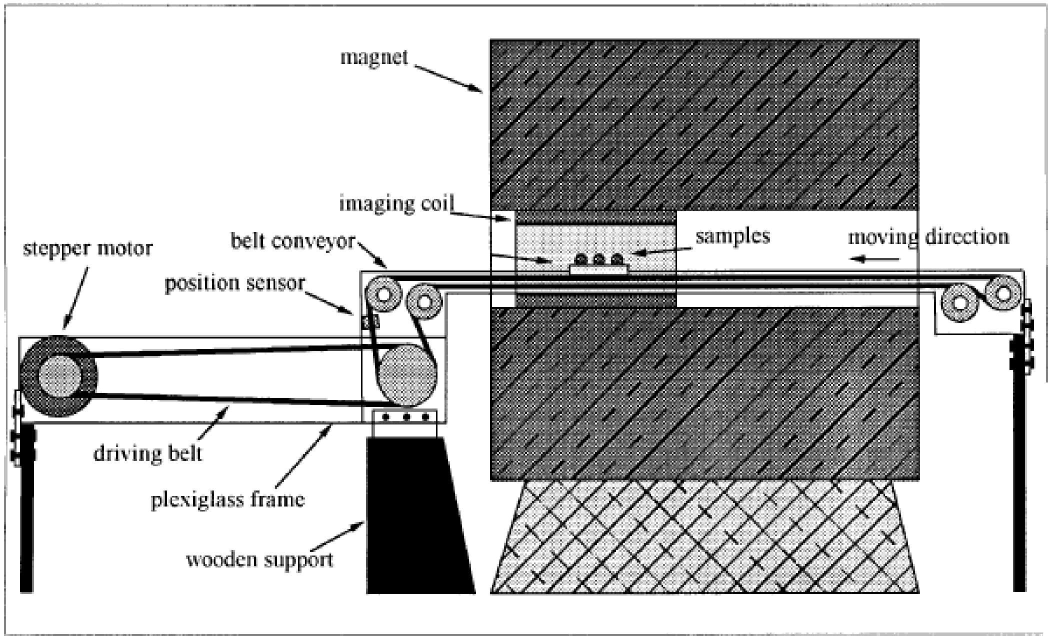

Fig 1. NMR sensor with a conveying system for non-destructive detection of internal quality attribute

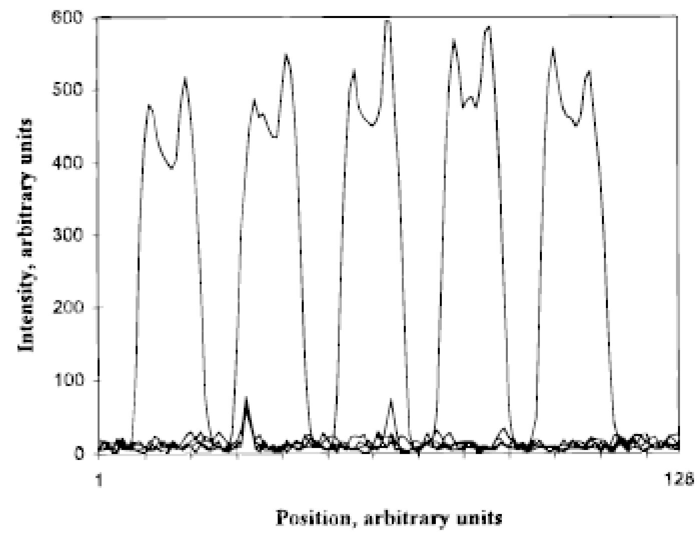

Fig 3. Projections of a single olive at rest in five different positions (25 mm apart) in the imaging coil. The five projections were superimposed on each other for illustration purposes.

MRI technique detects the properties of packaged meats

April 4, 2018, Spanish Foundation for Science and Technology (FECYT)

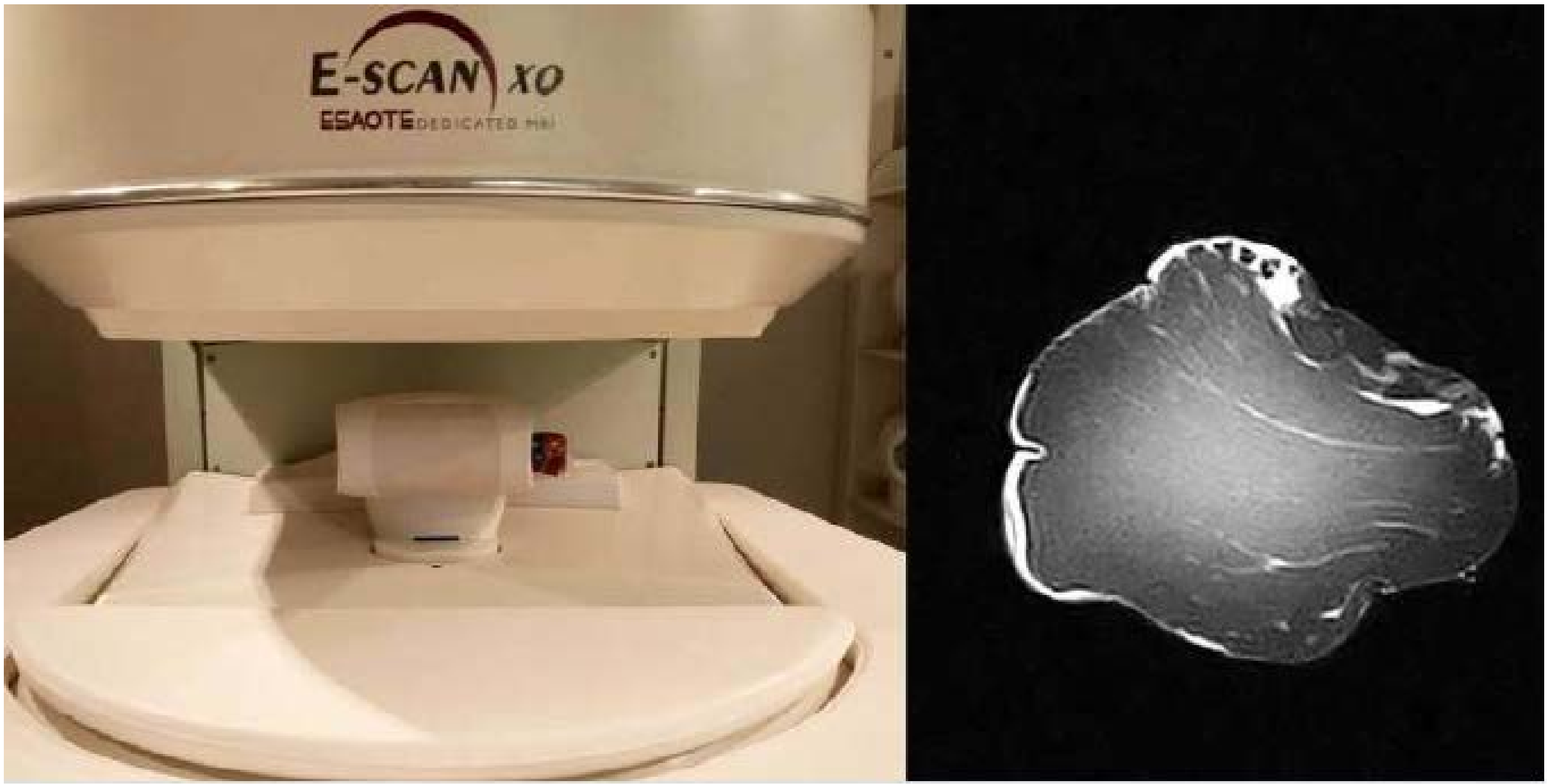

b

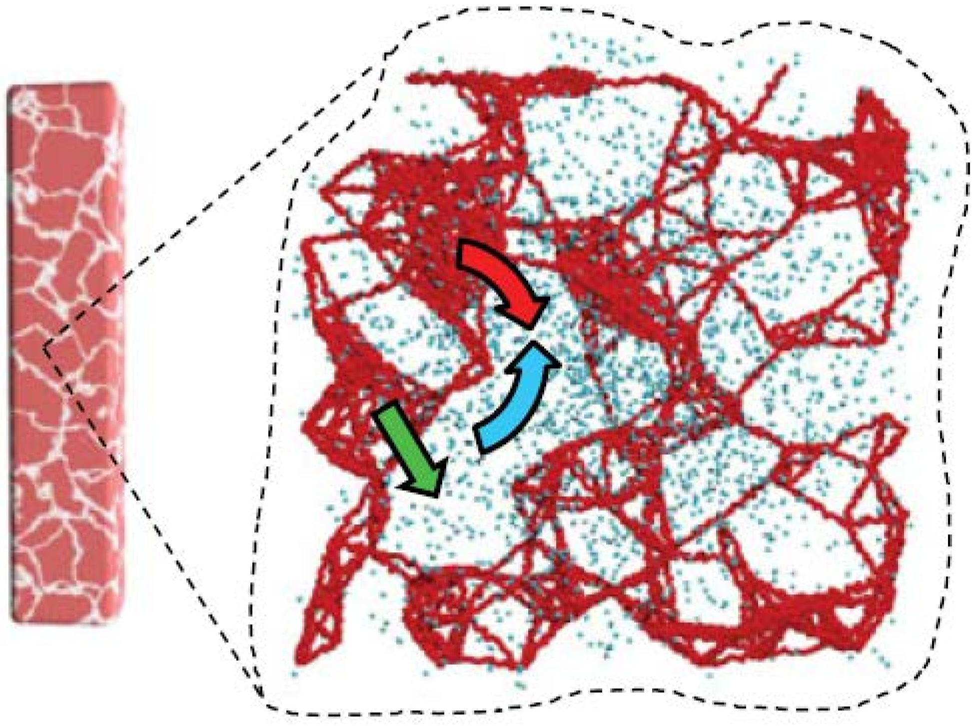

Figure 1. (a) Schematic drawing of the experimental setup where a sample was inserted first into the FFC-relaxometer and then into the high-field NMR system. (b) Illustration of water/protein microenvironment in meat tissue. The arrows indicate proton magnetization exchange between free (blue arrow) and restricted (red arrow) magnetization pools as well as nitrogen–proton interaction (green arrow).

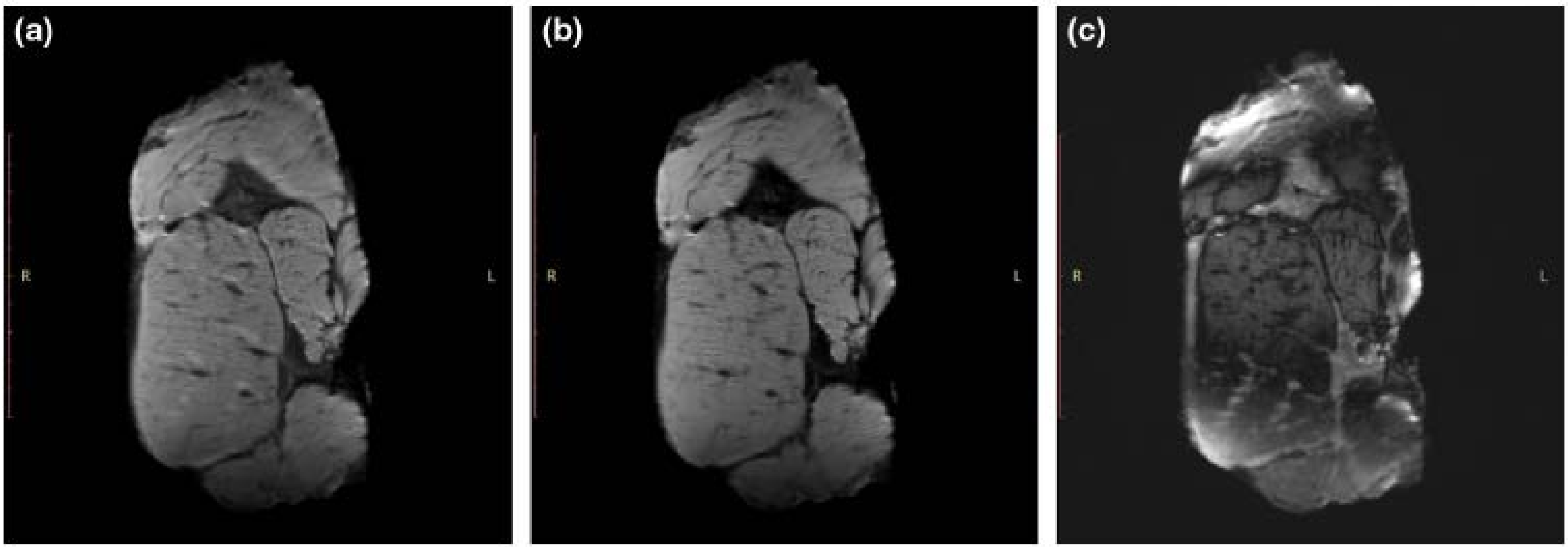

Fig. 11 MR images of fresh meat taken with the sequences. **a** Spin echo, **b** fat suppression spin echo and **c** water suppression spin echo

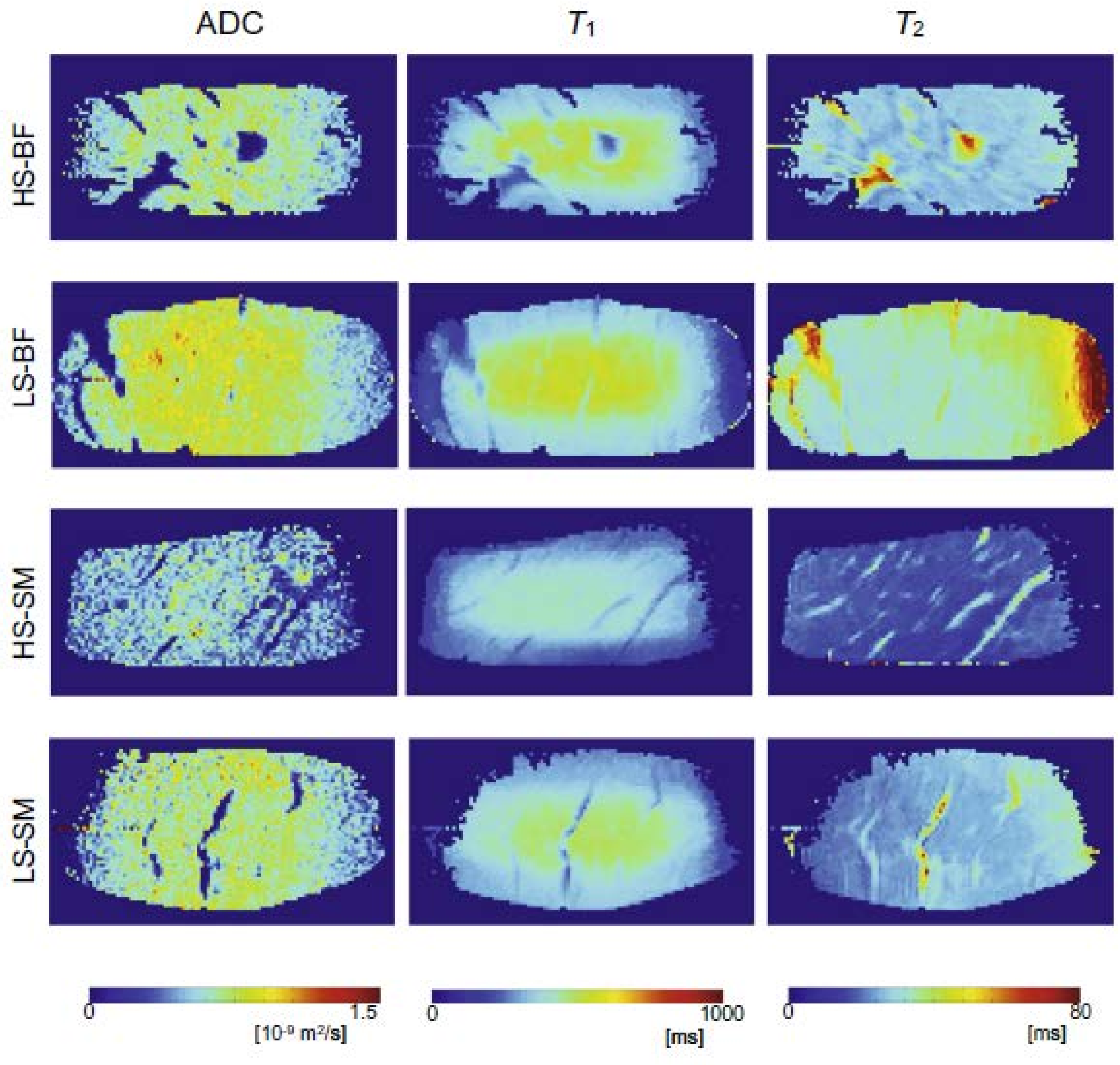

Fig. 2. Central-slice maps of ADC, T_1 and T_2 for the four examined ham sample groups (HS-BF, LS-BF, HS-SM and LS-SM). The maps were obtained by fitting Eqs. (1)–(3) to DWI, IR and CPMG experimental data.

Dynamic MRI and Thermal Simulation To Interpret Deformation and Water Transfer in Meat during Heating

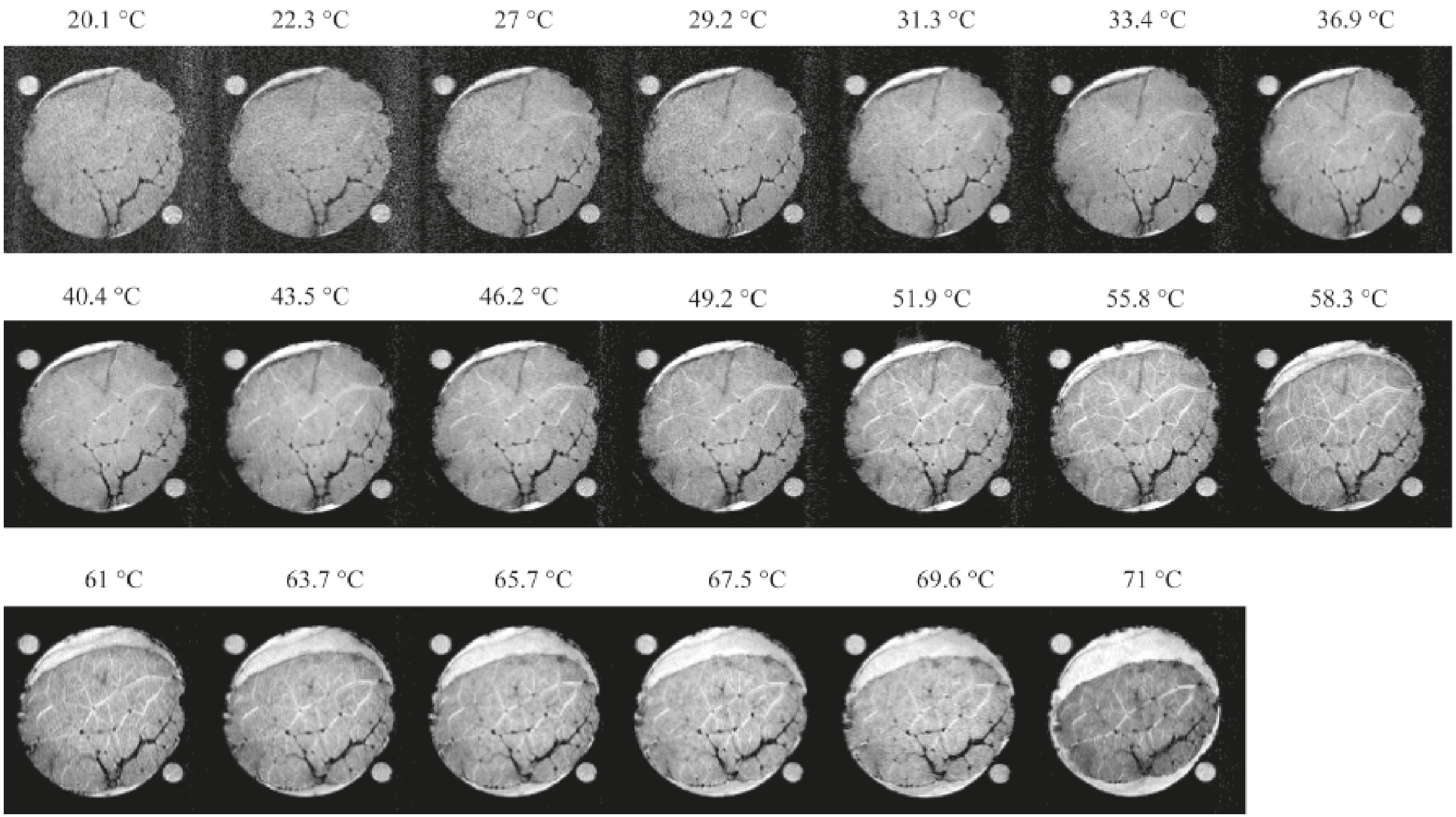

Figure 7. NMR images of the deformation in the central section of the sample. The gray scale windowing has been adjusted to compensate for degraded SNR. The values displayed are means of simulated temperatures in this central section.

Non-invasive measurement of body and carcass composition in livestock by Computer Tomography, Dual Energy X-Ray Absorptiometry, Magnetic Resonance Imaging, and Ultrasound Scanning

Armin M. Scholz (LMU Munich, Germany)
Lutz Bünger (SRUC Edinburgh, Great Britain)
Jørgen Kongsro (Norsvin Hamar, Norway)
Ulrich Baulain (FLI Mariensee, Germany)
Alva D. Mitchell (USDA Beltsville, USA)

[1]H Magnetic Resonance Imaging

→ automatic, semi-automatic or manual segmentation into muscle, fat or bone volumes

→ no “unique” signal intensities

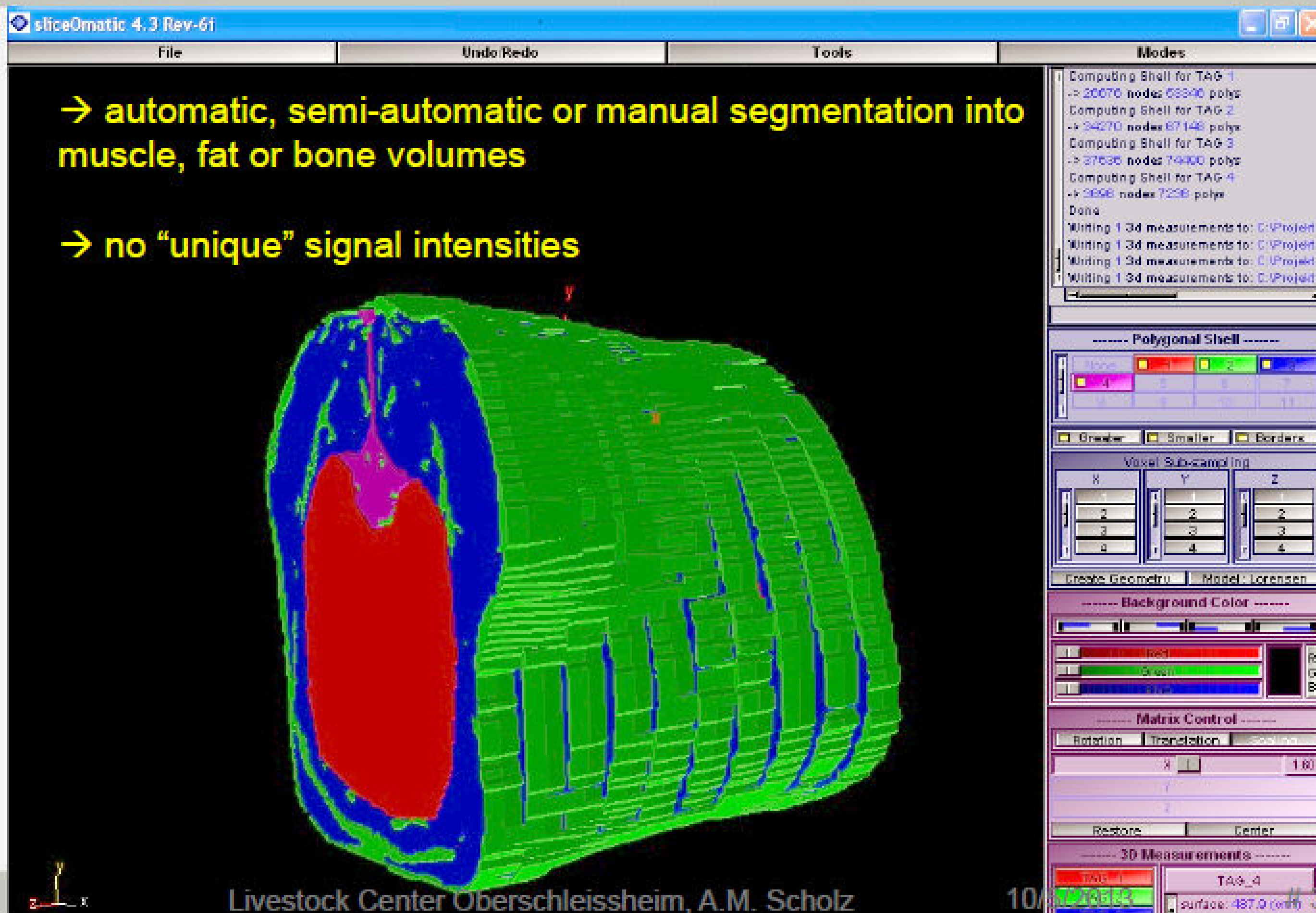

LUDWIG-MAXIMILIANS-UNIVERSITÄT MÜNCHEN

^{1}H Magnetic Resonance Imaging

in vivo *carcass*

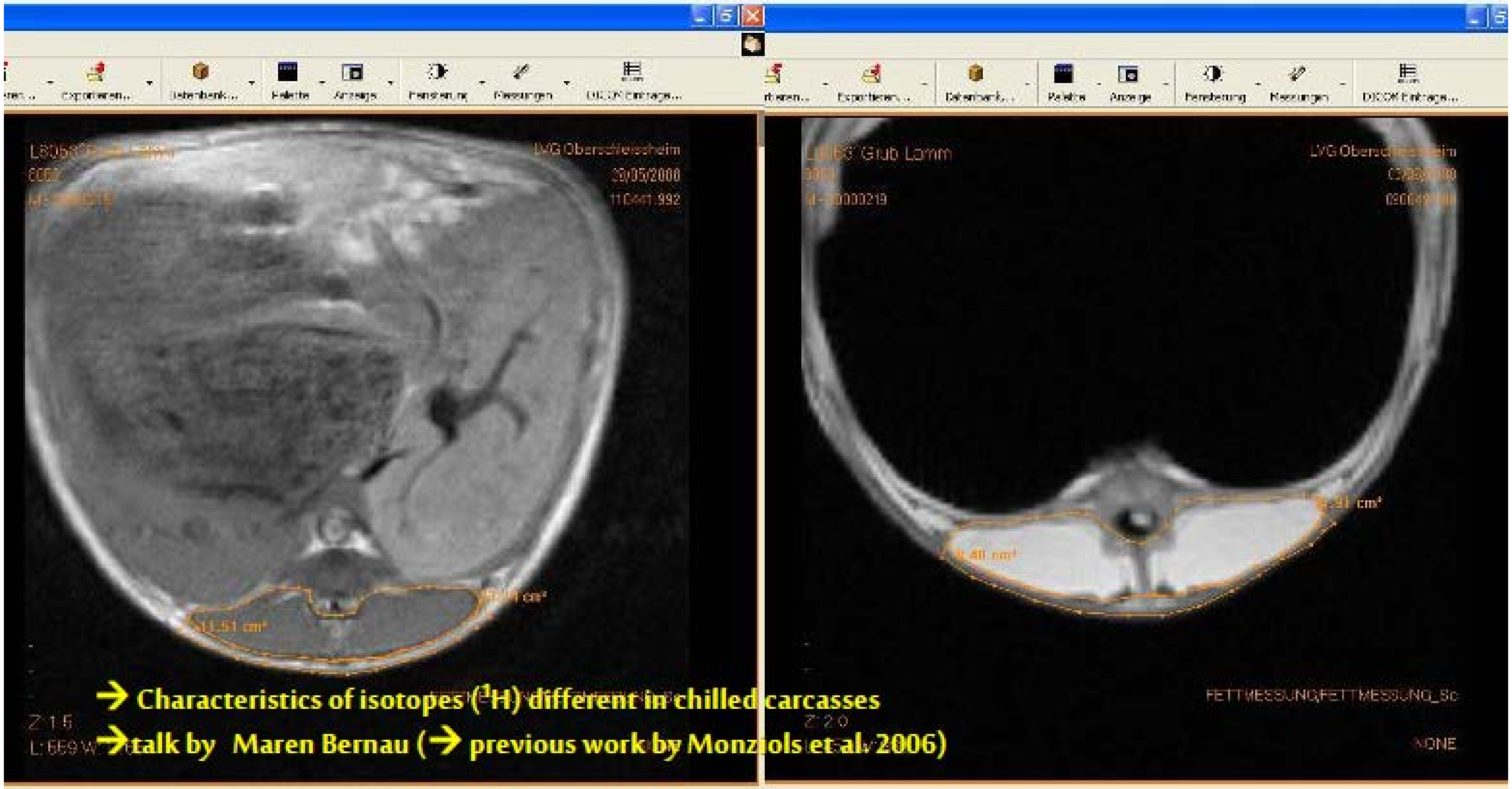

→ Characteristics of isotopes (^{1}H) different in chilled carcasses

→ talk by Maren Bernau (→ previous work by Monziols et al. 2006)

T1 weighted sequence

Conclusion for imaging methods (generally)

Kallweit 1993:

"There are advantages and disadvantages of individual systems in their present state.

The rapid progress in technical development may lead to further improvements in the future."

→ 20 years later: Nothing has changed !

Introduction

NMR signal

Spectroscopy

T1-T2 relaxation

Diffusion

Imaging

Plastics

Conclusions

hamburger

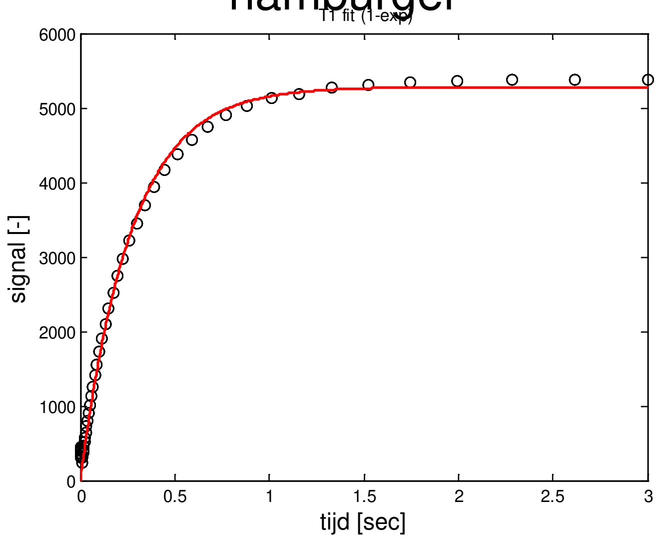

T_1~300 ms

$$S \sim G\rho\,[1-\exp(-TR/T_1)]\,\exp(-TE/T_2)$$

T_1~100 ms

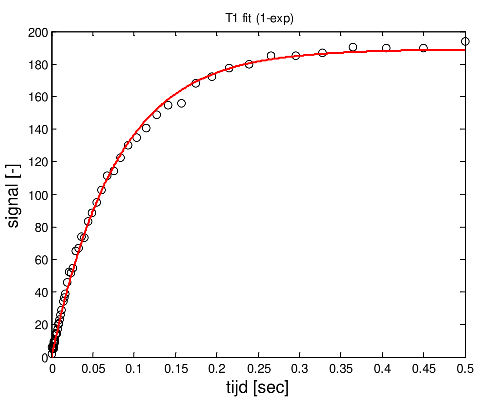

handschoen

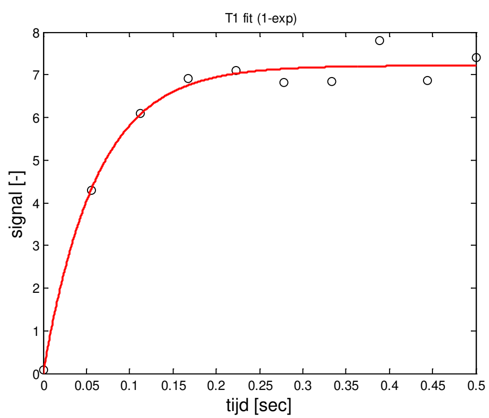

POM

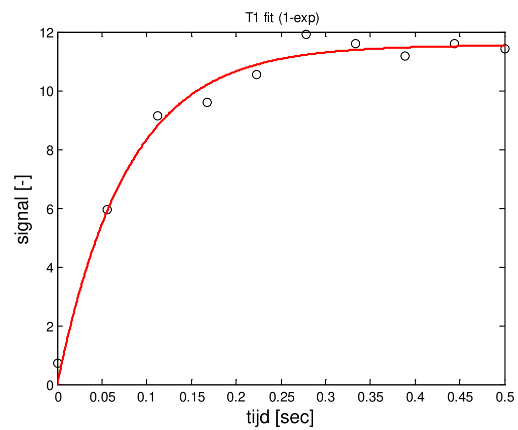

PE

handschoen

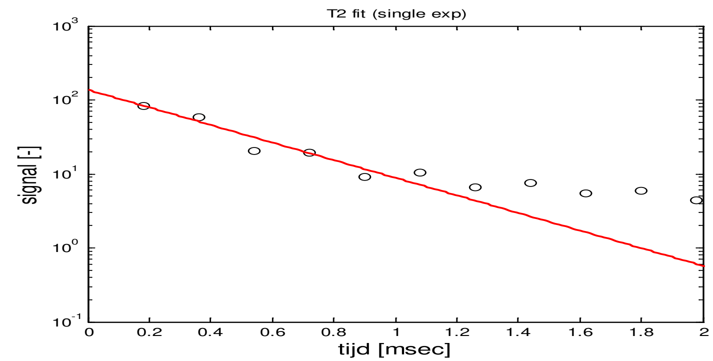

hamburger

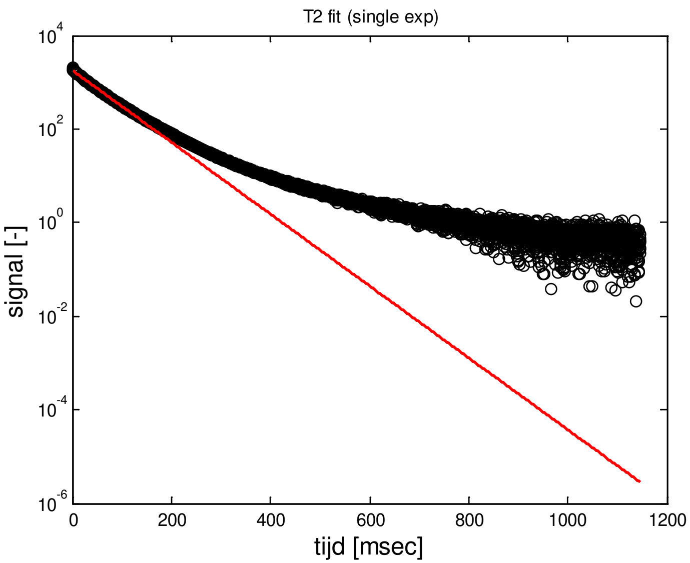

POM

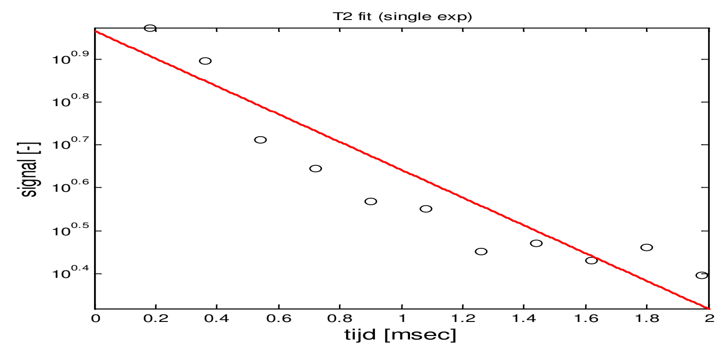

PE

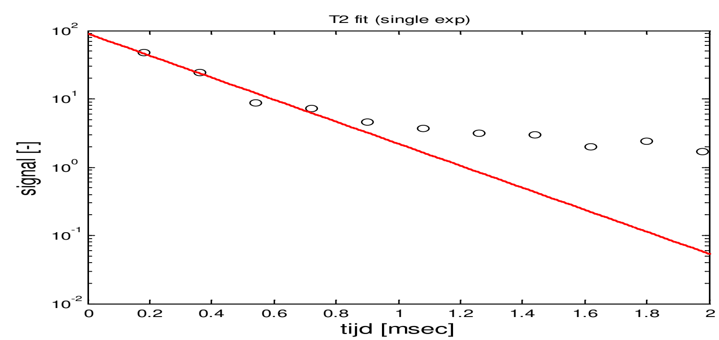

Hamburger ~ >50 ms

Plastics ~ 1 a 2 ms

$$S \sim G\rho \, [1-\exp(-TR/T_1)] \, \exp(-TE/T_2)$$

Diffusion influence

hamburger

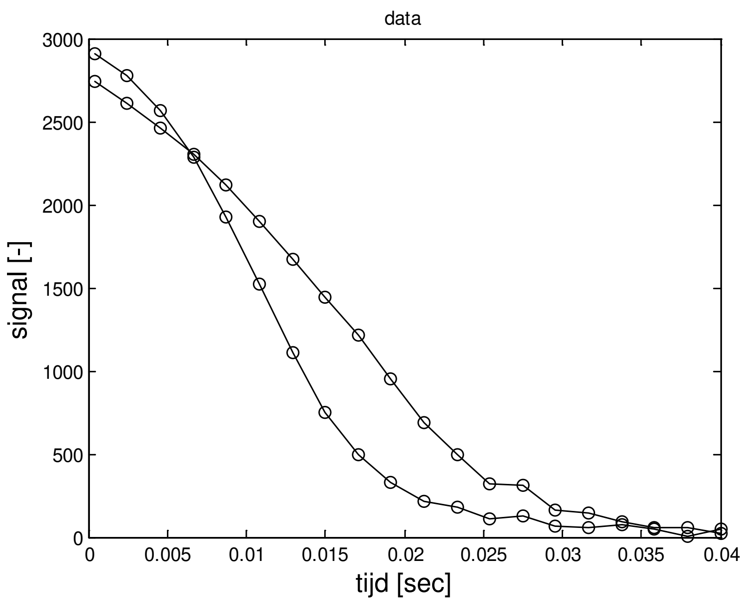

handschoen

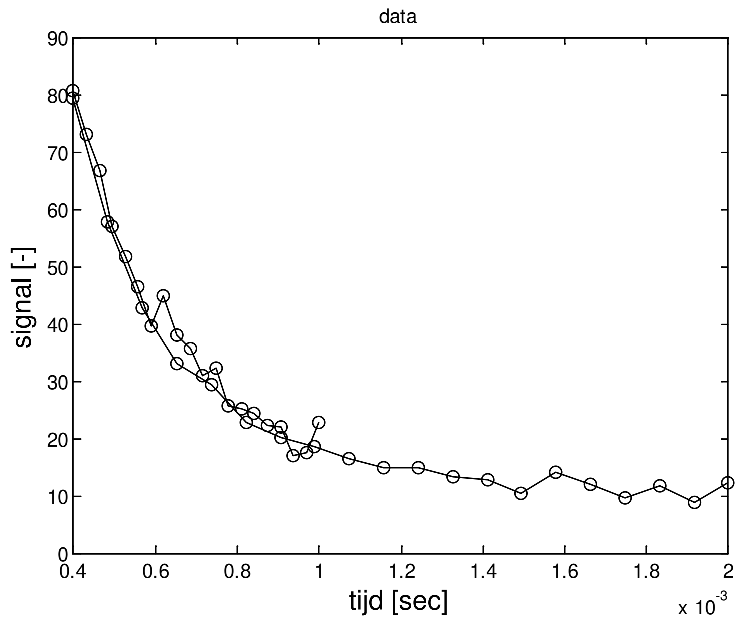

Theoretical

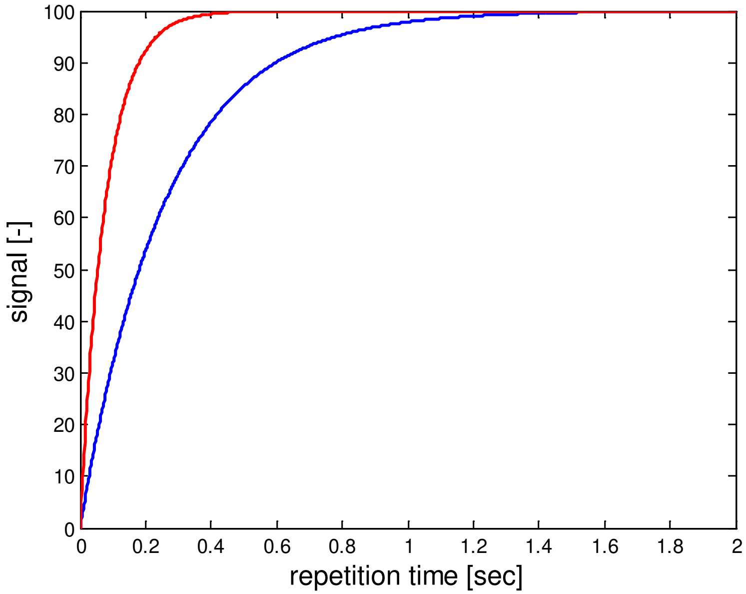

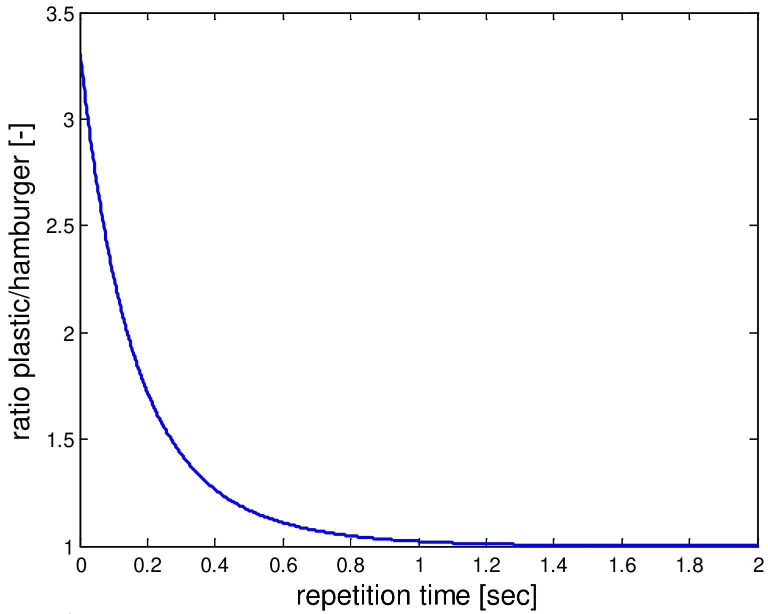

Not enough difference, i.e., 10.000 in order to find small pieces

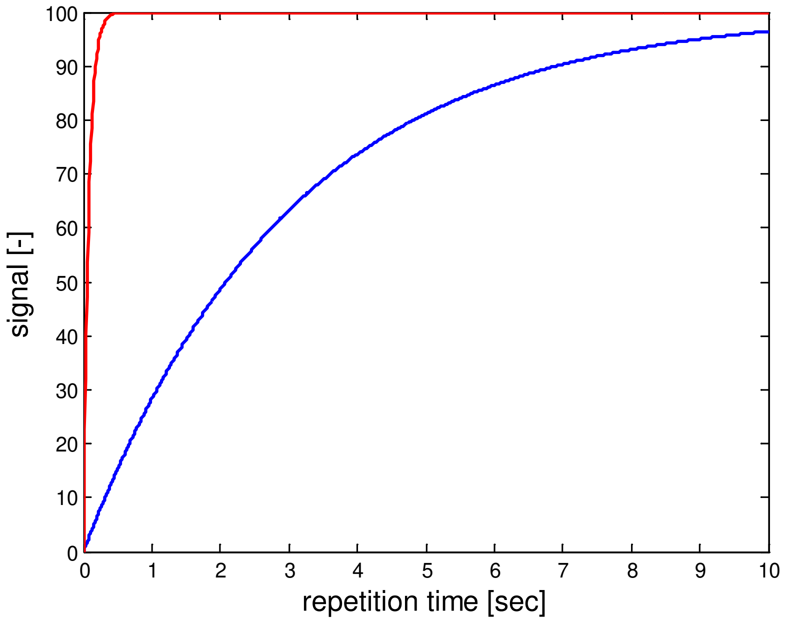

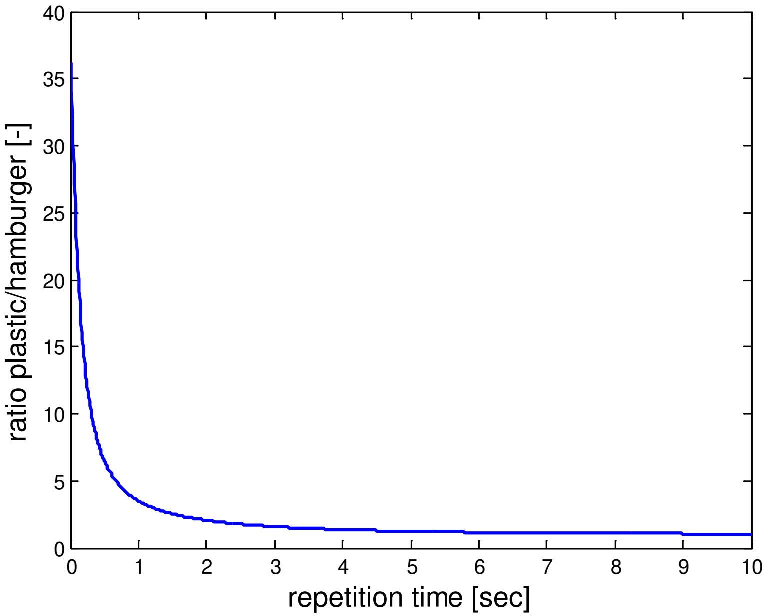

Example
Plastic + water

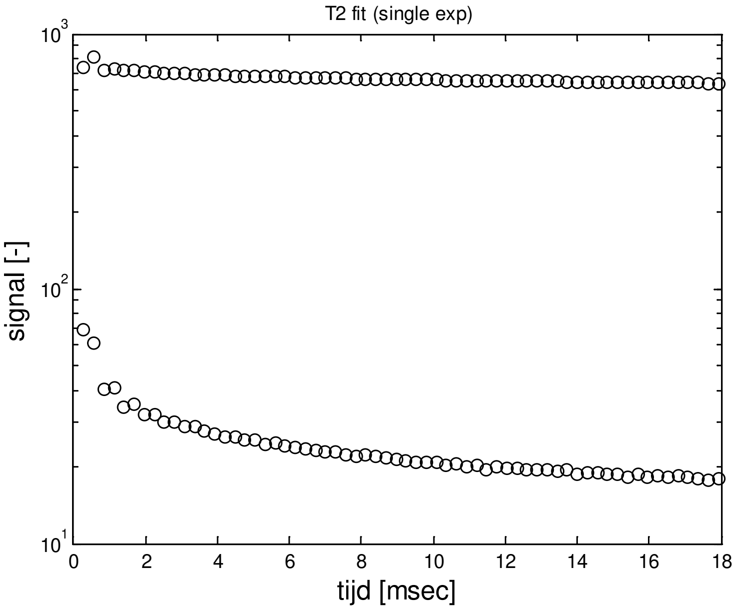

Introduction

NMR signal

Spectroscopy

T1-T2 relaxation

Diffusion

Imaging

Plastics

Conclusions

Conclusions

- Plastic gives NMR signal
- Can not generate specific signal only due to plastic
- Will be inverse, i.e., no signal where plastic is
  - (or glas, bones etc)
  - Enough time > super technique

- At this moment still too much research instrument, which large promise (if costs go down)

- Additional NMR problems
  - Magnetization time on conveyor (too short or super high field)
  - High homogeneity
  - Safety

TABLE 2 Applications of noninvasive techniques for detecting foreign bodies

Mode	Food products	Foreign bodies	References
X-ray	Loaf of bread, a hamburger steak, nd cabbage	Steel screws, aluminum rivets, staples, aluminum foil, glass and plastic fragments	(Morita et al., 2003)
	Chili soup	Metals and bone fragments	(Chen et al., 2005)
	Instant ramen, macaroni, and spaghetti	Stainless steel, Teflon, aluminum, rubber, glass, and ceramics	(Kwon et al., 2008)
	Fish fillets	Bones	(Mery et al., 2011)
	Minced meat, cultured sour cream product	Glass, paper, a ladybug, a cigarette butt, and a fly	(Nielsen et al., 2013)
	Food jar	Glass fragments	(Lu & Peng, 2013)
	Bakery product and powder seasoning	Glass fragment and metal particles	(Niemeyer, 2015)
	Milk powder, minced meat	Polyethylene plastic, hay powder, and hollow cylinder	(Li et al., 2015)
	Cheese, minced milk, wheat bread	Glass, metal, wood, insects, plastic, rubber, and stones	(Einarsdóttir et al., 2016)
Thermal Imaging	Raisins, nuts, almonds	Wooden sticks and stones	(Meinlschmidt & Maergner, 2002)
	Raisins, almonds, nuts	Wooden sticks, stone, metal, and cardboard	(Ginesu, Giusto, Märgner, & Meinlschmidt, 2004)
	Chocolate bar	Stone, plastic, and glass fragments	(Bukowska-Belniak, Leśniak, Kiełkowski, & Michalski, 2010)
	Biscuits	Stone, glass, plastic, wood, paper, and textile fiber	(Senni et al., 2014)
Near-infrared (NIR) spectroscopy	Blueberries	Leaves, twigs, and stones	(Tsuta et al., 2006)
	Dough, cheese, doughnut, meat	Coin, glass ball, and rubber	(Pallav, Diamond, et al., 2009)
	Blueberries	Leaves and stems	(Sugiyama et al., 2010)
	Ham slice and chocolate	Hairs and insects	(Tashima et al., 2013)
	Ham slice, fish, and chicken wing sticks	Wooden sticks and bones	(Phetchalern et al., 2014)
	Shell and pulp	Walnut	(Jiang et al., 2007)
	Chicken breast fillets	Bone fragments	(Yoon et al., 2008)
	Semolina	Insect fragments	(Bhuvaneswari et al., 2011)
	Pork steaks	Polyethylene terephthalate, poly-ethylene, metal, insects, and bone	(Díaz, Cervera, Fenollosa, Ávila, & Belenguer, 2011)
Hyperspectral imaging (HSI)	Grains	Plastic shards, glass beads, and rubber fragments	(Gowen & O'Donnell, 2013)
Ultrasonic	Marmalade and cheese product	Bone, glass, steel, and wood	(Hæeggström & Luukkala, 2001)
	Bottled beverages	Metal, glass, and plastic pieces	(Zhao et al., 2003)
	Bottled beverages	Glass fragment	(Zhao et al., 2006)
	Deboned chicken	Bone fragment	(Correia et al., 2008)
	Cheese	Plastic pieces	(Leemans & Destain, 2009)
	Canned food	Rock and aluminum plate	(Meftah & Mohd Azimin, 2012)
	Cheese and poultry product	Metal rod, metal, and glass fragment	(Cho & Irudayaraj, 2003)
	Canned beverages	Copper and aluminum rods	(Ho et al., 2007)
	Cheese	Wood, rubber, and glass	(Pallav, Hutchins, & Gan, 2009)
Terahertz	Chocolate	Stone, glass, and plastic fragments	(Jördens & Koch, 2008)
	Flour sample	Aluminum foil, metallic cubes, cubic stones, grasshopper, and mealworms	(Kim et al., 2012)
	Noodle	Aluminium, granite, and insects	(Lee et al., 2012)
	Crackers product	Dried fish and metal fragment	(Han et al., 2012)
	Instant noodles	Crickets species	(Ok et al., 2012)
	Powdered milk	Insect, polymer, and metals	(Ok et al., 2014)
	Powdered milk	Metal razor and rubber fragments	(Lee & Lee, 2014)
	Powder	Teflon and Polyvinyl chloride (PVC)	(Ikari et al., 2014)
	Chocolate product	Caterpillar	(Yu et al., 2015)

Designing sensors to detect foreign bodies in food

March 31, 2017, Elhuyar Fundazioa

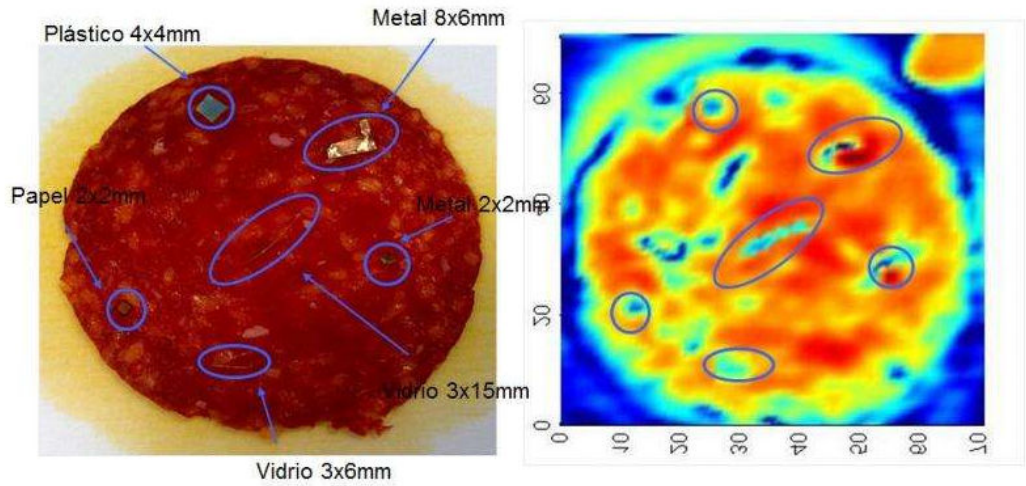

Image obtained with this technology in which there can be seen, on a slice of sausage, plastics, metals and splinters of glass of different sizes and shapes. Credit: Elhuyar Fundazioa

Researchers at the NUP/UPNA-Public University of Navarre and the Navarre-based company Anteral S.L. have designed a novel system of sensors to improve quality control in the food sector and based on terahertz technology. These devices enable foreign bodies, such as metals, paper, insects, plastic or glass to be detected in food along a production line, and pathogenic microorganisms to be identified in real time.

These devices are based on terahertz technology, a band in the electromagnetic spectrum located between the microwaves and infrared waves. This terahertz band is the last unexplored region of the electromagnetic spectrum owing to the difficulty in generating and detecting waves of this type. Yet one of the fields in which terahertz offer huge technological potential is in the sensing of substances and materials. This is due to the fact that nearly all the molecules display a characteristic footprint on this band and this allows them to be distinguished and identified.

"Seeing" inside substances

"Terahertz radiation is capable of penetrating a huge range of objects and substances, so they make it possible to 'see' what is inside them," explained Juan Carlos Iriarte. "In the same way, the reflection of terahertz waves varies according to the material or body they impact upon, and this provides images depending on the power and phase of the wave received."

Questions ?